NOVEL SYNTHESIS METHODS FOR PREPARATION OF CERIA ABRASIVES FOR CHEMICAL MECHANICAL PLANARIZATION APPLICATIONS IN SEMICONDUCTOR PROCESSING

By

OH MYOUNG HWAN

A DISSERTATION PRESENTED TO THE GRADUATE SCHOOL
OF THE UNIVERSITY OF FLORIDA IN PARTIAL FULFILLMENT
OF THE REQUIREMENTS FOR THE DEGREE OF
DOCTOR OF PHILOSOPHY

UNIVERSITY OF FLORIDA

2010

To my lovely wife, Minyoung and daughter, Yujin

ACKNOWLEDGMENTS

I am sincerely appreciative of my advisors, family members, colleagues, and friends whose support made it possible for me to complete my doctoral studies and research.

At this time, I would like to take a moment to acknowledge my professor, Dr. Rajiv K. Singh for challenging and guiding me through this research and for always being present as a mentor in science and in life. His support, guidance, caring, and patience allowed me to complete this research and to grow as a scientist. Also, I would like to acknowledge my committee, Dr. Stephen Pearton, Dr. David Norton, Dr. Hassan El-Shall, and Dr. Chang-Won Park, for their advice and support. In addition, special thanks are extended to the faculty and staff at the Particle Engineering Research Center and Major Analytical Instrumentation Center, especially Dr. Valentine Craciun, Eric Lambers, and Kerry Siebein for always preparing my samples to exact specification and for providing access to their instrumentation.

I am deeply indebted to my family members for all their help which have truly made it possible for me to reach my goals and obtain my dreams. I would like to thank my grandmother, Dalwha Choi, for her life lessons and encouragement. I would especially like to thank father and mother, Bonggeun Oh, and Jungsoon Yoo, for their great love and full support for me. I would also like to thank my father-in-law and mother-in-law, Soonbong Jang and Hyeonsook Lee, from the bottom of my heart for generous love and encouragement. I thank my brother, Kyounghwan Oh, for his deep affection for Yujin. I extend special thanks to brother-in-law and his family, Junsoo Jang, Yeonok Park, Uin Jang, Soyun Jang. Additionally, I would like to acknowledge to president of LG Chem Research Park and Director of Corporate R&D center, Dr. Jin-

Nyoung Yoo and Dr. Junguk Choi. I could not have done this without their full support and trust.

I also thank my past and present group members, Sejin Kim, Taekon Kim, Jaeseok Lee, Sushant Gupta, Aniruddh Khanna, Balasundaram Kannan, Jungbae Lee, and Jinhyung Lee, for their contributions to this research with valuable discussion and my old and present friends, Jinuk Kim, Sanghyun Eom, Chanwoo Lee, Donghyun Kim, Kangtaek Lee, Inkook Jun, Donghwa Lee, Kyeongwon Kim, Sungwon Choi, Jihun Choi, dongjo Oh, Byungwook Lee, Seonhoo Kim, Sangjun Lee, Dongwoo Song, Minki Hong, Myonghwa Lee who not only helped and encouraged me in this research but also made my graduate study years lots of fun in Gainesville. I would also like to thank Heesung Yoon for his helpful research discussion.

I express my most sincere appreciation to my wife and daughter, Minyoung and Yujin, whose endless love, encouragement and support made me the person I am today.

TABLE OF CONTENTS

page

ACKNOWLEDGMENTS 4

LIST OF TABLES 11

LIST OF FIGURES 12

LIST OF ABBREVIATIONS 17

ABSTRACT 20

CHAPTER

1 INTRODUCTION 22

Research Rationale 22
Scope of the Research 24

2 LITERATURE REVIEW 28

Chemical Mechanical Planarization (CMP) 28
CMP Process 28
CMP Slurry 29
CMP of Dielectrics 30
Oxide CMP 30
Process of oxide CMP 30
Mechanism of oxide CMP 31
Relationship between particles and wafer 31
Shallow Trench Isolation (STI) CMP 32
Process of STI CMP 32
Mechanism of STI CMP 33
Mechanism of silicon dioxide using ceria particles 34
Mechanism of silicon nitride using ceria particles 35
High selectivity ceria-based slurry 37
Ceria Abrasive 38
Advantages of Ceria Abrasive 38
Disadvantages of Ceria Abrasive 39
Key Quality Issues 40
Removal Rate 41
Uniformity and Planarity 42
Global Planarization 42
Selectivity 44
Surface Defectivity 45

3 EXPERIMENTAL FACILITY AND PROCEDURES 58

Introduction 58
Sample Preparation 58
Wafers 58
Abrasive particles 59
Slurries 60
CMP Equipment 60
CMP Polishers 60
Slurry Delivery System 60
Characterization and Method 61
Abrasives 61
Microstructure and shape 61
Physical properties 62
Surface and chemical properties 62
Slurries 63
Electrical potential (Zeta Potential) 63
Particle size distribution 64
Polished Wafer 65
Film thickness measurement 65
Selectivity between silicon dioxide and nitride 66
Oxide CMP within-wafer nonuniformity (WIWNU) 67
Defectivity monitoring by wafer defect scattering analysis 68

4 NOVEL METHOD TO CONTROL THE SIZE OF SINGLE CRYSTALLINE CERIA PARTICLES BY HYDROTHERMAL METHOD AND ITS CMP PERFORMANCE 75

Introduction 75
Materials and Methods 77
Abrasives 77
Preparation of sol-type ceria precursor 77
Hydrothermal synthesis of ceria particles 78
CMP Evaluation 78
Preparation of ceria-based slurries 78
CMP tools and consumables 78
Characterization 79
Abrasives 79
Ceria-based slurry 79
CMP performance 79
Results and Discussion 80
Preparation of Ceria Particles 80
Influence of solvent type on ceria particle characteristics 80
Effect of the precipitation participating anions on nucleation and growth ... 83
Effect of hydrothermal conditions 84
CMP Performance 85
Ceria abrasives 85

Characteristics of ceria abrasive before and after CMP 87
Polishing performance 87
Conclusions 91
Synthesis of Ceria Particles by Hydrothermal Method 91
CMP Evaluation 91

5 POLISHING BEHAVIORS OF SPHERICAL CERIA ABRASIVES ON SILICON DIOXIDE AND SILICON NITRIDE CMP 109

Introduction 109
Materials and Methods 111
Abrasives 111
Preparation of as-prepared particles by hydrothermal method 111
Preparation of ceria abrasive particles by solid state reaction (flux method) 111
CMP Evaluation 112
Preparation of ceria-based slurries 112
CMP tools and consumables 112
Characterization 113
Abrasives 113
Ceria-based Slurry 113
Polishing of wafers 113
Results and Discussion 114
Ceria Abrasives 114
Morphological properties 114
Crystalline structure 114
Effects of molten salt and as-prepared particle 115
CMP Evaluation 116
Characteristics of ceria abrasives before and after CMP 116
Polishing Test 117
Conclusions 120
Ceria Abrasives 120
CMP Performance 121

6 PREPARATION AND CHARACTERISTICS OF THE CERIA COATED SILICA PARTICLES AND ITS CMP PERFORMANCE 134

Introduction 134
Materials and Methods 135
Abrasives 135
Preparation of monodispersed silica particles 135
Preparation of ceria precursors 136
Preparation of ceria coated silica particles 137
Preparation of Ceria-bases Slurry 138
CMP Evaluation 138
Characterization 139
Results and Discussion 140

Ceria Coated Silica Particles 140
Morphology 140
Crystalline phase 141
XPS spectra of the ceria coating on silica particles 142
Electrokinetic behavior 143
Control of thickness of the ceria coating on silica particles 145
Size control of the ceria coating on silica particles 145
CMP Evaluation 146
Effect of pH 146
Effect of down pressure 147
Wafer roughness (WIWNU) 147
Conclusions 148
Ceria Coated Silica Particles 148
CMP Evaluation 149

7 SYNTHESIS OF SPHERICAL CERIA PARTICLES BY THERMAL DECOMPOSITION METHOD AND ITS CMP PERFORMANCE 167

Introduction 167
Materials and Methods 168
Preparation of Spherical Ceria Abrasives 168
CMP Evaluation 169
Preparation of ceria-based slurries 169
CMP tools and consumables 169
Characterization 170
Abrasives 170
Ceria-based slurry 170
CMP performance 170
Results and Discussion 171
Properties of Spherical Cerium Carbonate Precursor 171
Influence of solvent type on particle morphology 171
Effect of dielectric constant on particle morphology 173
CMP Materials 174
Preparation of ceria abrasives 174
Characteristics of ceria-base slurry 175
CMP Evaluation 176
Effects of calcination temperature on physical properties of ceria abrasives 176
Effects of suspension pH on oxide and nitride CMP 178
Conclusions 180
Synthesis of Cerium Carbonates 180
Synthesis of Ceria Abrasives 180
Preparation of Ceria-based Slurry 181
CMP Evaluation 181

8 A COMPARISION OF CMP PERFORMANCE IN THE CERIA ABRASIVES SYNTHESIZED VIA VARIOUS METHODS 196

Introduction 196
Materials and Methods 196
Sample Preparation 196
Preparation of ceria abrasives 196
Preparation of ceria-based slurries 197
CMP tools and consumables 197
Characterization 197
Abrasives 197
Ceria-based slurry 198
CMP performance 198
Results and Discussion 198
Comparison in Polishing Removal Rate 198
Comparison in WIWNU 199
Abrasive Effects on Defectivity 200
Conclusion 201

9 CONCLUSIONS 207

Solution Growth Abrasives 208
Grain Control Abrasives 209
Core/shell Composite Abrasives 209
Solid State Abrasives 210
Comparison of Polishing Behavior 212

APPENDIX: DIELECTRIC CONSTANTS OF MIXED SOLUTION OF SOME ORGANIC SOLVENT AND WATER AT ROOM TEMPERATURE 213

LIST OF REFERENCES 214

BIOGRAPHICAL SKETCH 220

LIST OF TABLES

Table		page
2-1	Guiding principles for slurry design in chemical mechanical planarization	57
4-1	Comparison of slurries used in this study	107
4-2	The results of the CMP evaluation	108
5-1	Comparison of slurries used in this study.	132
5-2	The results of the CMP evaluation	133
6-1	The results of removal rate for the ceria coated silica particles	166
7-1	Dielectric constants of mixed solvent, zeta potentials and morphologies of cerium carbonate compounds with the ratio of ethanol to water	195
8-1	Comparison of ceria abrasives used in this study	205
8-2	The results of the CMP evaluation	206

LIST OF FIGURES

Figure		page
2-1	Schematic for CMP process.	48
2-2	Schematics of ideal oxide ILD CMP.	49
2-3	Oxide removal mechanism by CMP	50
2-4	Shallow trench isolation (STI) CMP process	51
2-5	Zeta potential of the oxide/nitride substrates and ceria abrasive as a function of pH.	52
2-6	Silicon nitride S_N2 hydrolysis reaction scheme.	53
2-7	(a) Zeta potential of the oxide/nitride substrates and ceria abrasive as a function of pH and (b) the formation of passivation layer on the surface of STI structure with anionic organic polymer.	54
2-8	The comparison on (a) removal rate for oxide substrate with different abrasives and (b) Mohs hardness of ceria and materials to be polished during CMP	55
2-9	The schematics of surface defectivity.	56
3-1	Layout of the SKW-1 pattern wafer: (a) pattern density and pitch size layout, (b) mask floor plan, and (c) cross-sectional view	70
3-2	Schematic diagram of rotational CMP tool	71
3-3	Schematic illustration of a slurry delivery system	72
3-4	Diagram of film thickness measurement system using NanoSpec.	73
3-5	Schematic illustration of light scattering analysis	74
4-1	XRD patterns of ceria particles synthesized from the mixture of water and different alcohols; (a) ethylene glycol, (b) methanol, (c) 1,4-buthylene glycol, (d) ethanol.	93
4-2	FETEM photomicrographs of ceria particles obtained by hydrothermal method using a new type of ceria precursor.	94
4-3	FESEM photographs of ceria particles prepared from the mixture of water and different alcohols; (a) ethanol, (b) 1,4-buthylene glycol, (c) methanol, (d) ethylene glycol.	95

4-4 (a) Average particle size and (b) crystallites sizes of ceria particles synthesized with different dielectric constants of alcohols 96

4-5 FESEM photographs of ceria particles prepared with different concentrations of potassium hydroxide; (a) 0.5 M, (b) 1.0 M, and (C) 1.5 M. 97

4-6 FESEM photographs of ceria particles prepared from different concentrations of nitric acid in hydrothermal conditions at 230 ^{o}C for 12 hr. ; (a) pH 4, (b) pH 2.5, (c) pH 0.5 and (d) pH 0.5. 98

4-7 Crystallites size for ceria particles prepared from different pH at (a) 150 ^{o}C, (b) 200 ^{o}C and 230 ^{o}C. 99

4-8 FESEM photographs of the ceria particles prepared with different hydrothermal conditions; (a) pH 3.0 at 220^{o}C, (b) pH 3.0, (c) pH 1.5 and (d) pH 0.5 at 230^{o}C, respectively. 100

4-9 XRD patterns and the (111) peaks analyzed to confirm grain size of the ceria abrasives dispersed in ceria-based slurry (a) A, (b) B, (c) C and (d) D. 101

4-10 FETEM micrographs and of ceria abrasive with average particle diameters of (a) 62 nm (slurry A) and (b) 232 nm (slurry D). 102

4-11 Particle size distribution of ceria-based slurry used in this study. 103

4-12 FESEM photographs of ceria abrasives (a) before and (b) after oxide CMP process. 104

4-13 Results of CMP field evaluation for removal rate and selectivity. 105

4-14 Results of CMP field evaluation for within-wafer nonuniformity (WIWNU) of silica film. 106

5-1 Schematic diagram of experimental procedure. 122

5-2 FESEM photographs of the ceria abrasives prepared with different calcination conditions; (a) slurry A, (b) B, (c) C and d(c) D 123

5-3 (a) XRD patterns and (b) the (111) peaks analyzed to confirm crystallite size of the ceria abrasives dispersed in slurry (a) A, (b) B, (c) C and (d) D 124

5-4 The variation of crystallite size as a function of the concentration of grain growth accelerator 125

5-5 FETEM micrographs of the ceria abrasives prepared with different cerium precursor; (a) cerium hydroxide, (b) cerium nitride, (c) cerium chloride and (d) cerium dioxide 126

5-6 Particle size distribution of ceria slurries as function of abrasive size..... 127

5-7 FESEM photographs of ceria abrasives (a) before and (b) after polishing 128

5-8 Results of CMP field evaluation for removal rate and selectivity 129

5-9 TGA curves of the ceria abrasives dried from (a) slurry A and (b) slurry D 130

5-10 Within-wafer non uniformity (WIWNU) of oxide film. 131

6-1 FESEM images of silica core particles obtained by modified Stöber method. .. 150

6-2 (a) FESEM and (b) HRTEM micrographs for the surface condition of coated particle and FESEM micrographs for ceria coated silica particles prepared by (c) precursor B and (d) precursor A, respectively. 151

6-3 XRD patterns of the synthesized particles; (a) bare silica particles, (b) ceria coated silica particles prepared by precursor B, and (c) precursor A 152

6-4 XPS survey spectrum of ceria coated silica particles 153

6-5 XPS spectra of O 1s peaks of ceria coated silica particles. 154

6-6 XPS Ce 3d multiplex of ceria coated silica particles 155

6-7 FESEM photographs for ceria coated silica particles prepared at different pH (a) 3.2, (b) 6.8 and (c) 9.7 156

6-8 Electrophoretic mobility for (a) silica particles (b) ceria coated silica particles and (c) ceria particles 157

6-9 Scheme of the formation mechanism of ceria coated silica particles at different pH. 158

6-10 FESEM micrographs of ceria coated silica particles prepared by different concentration of ceria precursors (a) 0.0 ml, (b) 1.0 ml, (c) 2.0 ml, (d) 4.0 ml and (e) 8.0 ml. 159

6-11 The variations of (a) coating thickness and (b) average particle size for samples obtained by changing the concentration of ceria precursors 160

6-12 FESEM micrographs of the silica particles with different size; (a) 105 nm, (b) 214 nm, (c) 332 nm, and (d) 442 nm 161

6-13 FESEM micrographs of the ceria coated silica particles obtained from different core silica particles with different size; (a) 146 nm, (b) 256 nm, (c) 334 nm, and (d) 384 nm. 162

6-14 Results of CMP field evaluation for removal rate as function of pH 163

6-15 Results of CMP field evaluation for removal rate as function of CMP pressure. 164

6-16 The result for within-wafer non uniformity (WIWNU) of oxide film..... 165

7-1 XRD patterns of cerium compositions produced under precipitation conditions with different solvent. 183

7-2 FESEM micrographs of cerium carbonate compounds obtained by using pure water as solvent..... 184

7-3 FESEM micrographs of spherical cerium carbonate particles prepared from the mixture of water and different alcohols; (a) methanol (CH_3OH), (b) ethanol (C_2H_5OH), (c) 2-propanol (C_3H_8O), and (d) 1, 4-butandiol ($C_4H_{10}O_2$). . 185

7-4 FESEM micrographs of cerium carbonate compounds prepared by various ratio of ethanol to water: (a) 0, (b) 1, (c) 3, and (d) 5 186

7-5 The XRD pattern of (a) cerium carbonate prepared by using mixed solvent of ethanol and water and (b) ceria abrasives obtained from thermal decomposition of the cerium carbonate at 700 ^{o}C. 187

7-6 FESEM micrographs of (a) as-prepared particles of ceria abrasives and (b) ceria abrasives obtained from thermal decomposition at 700 ^{o}C. 188

7-7 Relationship between surface area and crystalline size of ceria abrasives as a function of calcination temperature. 189

7-8 Electrokinetic behavior of silica, ceria and ceria with surface active agent added as a function of suspension pH..... 190

7-9 The changes in particle size distribution of ceria-based solvent as a function of suspension pH..... 191

7-10 The CMP evaluation for removal rate of oxide and nitride films as a function of calcination temperature 192

7-11 Results of CMP field evaluation for removal rate and selectivity 193

7-12 The CMP evaluation for removal rate of silicon oxide wafer as a function of suspension pH. 194

8-1 FESEM micrographs of various kinds of spherical ceria abrasives synthesized by variety methods; (a) hydrothermal method, (b) flux method, (c) surface-induced precipitation method, and (d) thermal decomposition. 202

8-2 Particle size distribution of ceria-based slurries. 203

8-3 Comparison of different ceria abrasives on surface defectivity. 204

A-1 The dependence of dielectric constant on the composition of different alcohols and water..... 213

LIST OF ABBREVIATIONS

μ	Viscosity
μm	Micrometer (1 $X10^{-6}$cm)
A	Specific surface area
Å	Angstrom (1 $X10^{-10}$ cm)
AW	Active trench
BET	Brunauer-Emmett-Teller
CMP	Chemical mechanical planarization
D	Crain size
d_{BET}	Average particle size determined by BET
DLVO	Derjaguin Landau Verwey Overbeek
d_{SEM}	Average particle size determined by FESEM
d_{XRD}	Crystalline size estimated from XRD patterns
FESEM	Field emission scanning electron microscopy
FTIR	Fourier transform infrared
h	Hour
IC	Integrated circuit
IEP	isoelectric point
ILD	Interlayer dielectric
K	Degrees Kelvin
kV	Kilo voltage
LOCOS	Local oxidation of silicon

LPCVD	Low-pressure chemical vapor deposition
M	Molarity
mA	Milliampere
mg	Milligram
min	Minute
mL/min	Milliliter per minute
MRR	Material removal rate
nm	Nanometer (1 X 10^{-9} cm)
^{o}C	Degrees Celsius
PAA	Poly acrylic acid
PECVD	Plasma enhanced chemical vapor deposition
psi	Pound per square inch
rpm	Rate per minute
SSA	Specific surface area
STI	Shallow trench isolation
TEM	Transmission electron microscopy
TG/DTA	Thermogravimetric and differential thermal gravimetry
TW	Trench width
ULSI	Ultra large scale integrate
WIWNU	Within-wafer nonuniformity
wt %	Weight percent
XPS	X-ray photoelectron spectroscopy

XRD	X-ray diffraction
β	Half-width of the diffraction peaks
ε	Dielectric constant
θ	Diffraction angle
λ	Wavelength
ξ	Zeta potential

Abstract of Dissertation Presented to the Graduate School
of the University of Florida in Partial Fulfillment of the
Requirements for the Degree of Doctor of Philosophy

NOVEL SYNTHESIS METHODS FOR PREPARATION OF CERIA ABRASIVES FOR CHEMICAL MECHANICAL PLANARIZATION APPLICATIONS IN SEMICONDUCTOR PROCESSING

By

Oh Myoung Hwan

December 2010

Chair: Rajiv. K. Singh
Major: Materials Science and Engineering

As the device design rule decreased, ceria-based slurries have been widely used instead of silica-based slurries in a variety of chemical mechanical planarization (CMP) applications for multilevel integrated circuit (IC) manufacture, since these slurries address many of the important issues resulting from the use of silica-based slurries. However, ceria (CeO_2) abrasives usually induce higher scratch level than silica particles due to its cubic crystalline structure, irregular shape, and poor dispersion stability in slurry. Therefore, this article is intended to establish novel synthetic methods of ceria abrasives leading to lower scratch level on wafer surface and ultimately present the direction of CMP abrasive for future technology nodes in order to meet the ever more challenging defectivity requirements.

To accomplish these aims, this article introduced the 4 types of novel synthetic methods for the formation of ceria abrasives. The ceria abrasives were synthesized by solution growth method, grain control method, core/shell composite method, and thermal decomposition method. In this investigation, the influences of solvent type and suspension pH on the formation of ceria particles were intensively investigated. The

size of ceria particles was controlled by adjusting the reaction parameters of each method without additional mechanical milling and filtration. The relationships between dielectric property of the solvent and morphological properties were also discussed in terms of the supersaturation of solution and electrostatic attraction mechanism. The resultant particles were characterized with field emission scanning electron microscopy (FESEM), transmission electron microscopy (TEM), X-ray photoelectron spectroscopy (XPS), X-ray diffraction (XRD), Thermogravimetric and differential thermal gravimetry (TGA/DTG), Fourier transform infrared (FTIR) spectroscopy, Brunauer-Emmett-Teller (BET), light scattering instruments and zeta potential measurements.

In order to investigate the effects of the synthesized ceria abrasives on CMP performance, CMP tests were carried out with the ceria-based slurry formulated by dispersing the synthesized ceria particles with anionic organic polymer. The effects of the synthesized ceria abrasives in CMP slurry were investigated for silicon dioxide and silicon nitride CMP process. The polishing behaviors of ceria abrasives were discussed in terms of morphological properties and mechanical abrasion of the ceria particle. In this CMP evaluation, material removal rate, selectivity, wafer uniformity, and defectivity of the polished wafer were measured by metrology tools, which are used in current integrated circuit (IC) fabrication plants in order to support polishing results obtained by this investigation.

CHAPTER 1
INTRODUCTION

Research Rationale

As the minimum feature size of microelectronic devices deceases, the newly developed planarization technique and new consumable materials have been utilized in modern semiconductor fabrication industry.[1] To continually satisfy more demanding devices, chemical mechanical planarization (CMP) has become one of the most critical semiconductor fabrication technologies because it offers a superior means for global and local planarization. Global planarization which is essential to produce a multilevel integrated circuit (IC) device is achieved by reducing topographic variation at the wafer scale.[2] Without CMP, it would be impossible to fabricate complex, dense, and miniaturizing multilevel IC devices. Over the past years, CMP has significantly advanced both in the development of more sophisticated processing tools and in the formulation of novel slurries to further enhance process performance.[3,4] Despite these advancements, the fundamental knowledge of the effects of the numerous CMP process variables on polishing performance is not clear, due to the lack of understanding of the substrate to be polished, the slurry that provides the chemistry and abrasives for mechanical removal and pad interactions involved. The lack of this understanding is a significant barrier to the development of next-generation CMP technologies. Therefore, many research has been investigate to understand the nature of substrate-slurry-pad interactions that occur during the CMP process.

The CMP has been used for interlayer dielectric (ILD) planarization, shallow trench isolation (STI) structure, and damascene technologies. For these various CMP processes, the characteristics of slurry particles are critical in determining the

planarization performance of CMP. During the past decade, silica (SiO_2) particles were traditionally used as CMP abrasives to remove deposited oxide topography at technology nodes of 90 nm and higher. Thus, previous studies for the planarization performance were focused on mechanical abrasion between silica particles and the substrate to be polished and chemical modification in silica-based slurry in order to increase the removal ratio of oxide to nitride layer in STI CMP. However, at the 65 nm technology node and at below nodes, ceria (CeO_2) particles are being introduced in a variety of CMP applications for IC manufacture, since ceria particles have the capability of achieving higher removal rates and global planarization than silica particles and ceria-based slurry can more easily be controlled by additives in the slurry formulation.[5] Recently, the demand of ceria particles as abrasives has been rapidly increased in semiconductor fabrication industry. Therefore, the fundamental knowledge for the characteristics of ceria particles as CMP abrasive is required in order to enhance the ability of current semiconductor devices.

Compared with other abrasives used in CMP slurry, ceria particles is commonly used in the ultra large scale integrated (ULSI) circuit structure due to the effective removal rate for oxide film and the softness of the particles. Recently, ceria-based slurry has been used in CMP of STI structures consisting of silicon dioxide and silicon nitride (Si_3N_4) deposition due to its high selectivity over nitride.[6] For the STI-CMP process, the use of high selectivity slurries is very important to halt the polishing at the nitride stop layer and reduce the amount of defects such as erosion and dishing. The structural properties, chemical aspects and morphological characteristics of the ceria abrasives have been identified as the important parameters that influence the CMP performance

such as oxide removal rate, removal selectivity, CMP-induced defects and wafer uniformity.[7] Therefore, many approaches to control these properties of ceria abrasives have been extensively investigated.

Even though the characteristics of ceria particles significantly affect the quality of CMP process, it is not easy to manufacture ceria particles as CMP abrasives. The commercial method for synthesis of ceria particles involves thermal decomposition of cerium salts such as cerium carbonate and cerium hydroxide. This method leads to very porous ceria particles with high surface area, inducing softness and high chemical reactivity to oxide films.[8] However, the size and the shape of ceria abrasives are very limited since particle growth is difficult to control during calcination process. To achieve the desired particle size and the uniform particle size distribution, mechanical milling and filteration is required. Other methods for preparing ceria abrasives are liquid phase processes. These methods can lead to ceria abrasives with desirable morphological characteristics by manipulating reaction parameters. However, the size of ceria abrasives is limited to less than 100 nm. Use of these small size particles results in low removal rates of target layers during CMP. Therefore, a new method to overcome these problems of ceria abrasives is required.

Scope of the Research

The research presented in this dissertation is intended to establish novel synthetic methods of preparing ceria abrasives for ILD and STI CMP with precise morphologies and chemical composition. The overall objective of this research is to investigate the effects of abrasive material properties on polishing removal rate and wafer defectivity by using different kinds of ceria particles obtained from a variety of synthesis methods. On the basis of results obtained from this study, this article will ultimately present the

direction of CMP abrasive for future technology nodes in order to meet the ever more challenging defectivity requirements. To achieve these aims, the research presented in this dissertation was devoted on a variety of preparation methods of ceria particles. For CMP performance evaluation, the effect of the resultant ceria abrasives on the removal rate, the oxide-nitride removal selectivity and within-wafer nonuniformity (WIWNU) was investigated. A synopsis of the efforts constituting this study is organized as follows.

Chapter 2 reviews the literature on the CMP process including main components in planarization performance. The procedure and mechanism for ILD and STI CMP was addressed in detail. From these backgrounds, the need of ceria abrasives was emphasized in CMP application and motivations for the implementation of the CMP process using ceria abrasives were discussed. Furthermore, the important issues for CMP evaluation were summarized and discussed in terms of abrasive characteristics. New approaches for developing more effective abrasives are introduced.

Chapter 3 was devoted to the studies conducted on the preparation and analysis techniques of consumables used in this study. For abrasive particles, the synthesized particles were analyzed by XRD, FESEM, TEM, XPS, FTIR, TG/DTA and BET. For slurry, slurry stability, mean particle size, and zeta potential measurements was reported using a variety of light scattering instruments. For CMP evaluation, film thickness, selectivity, nonuniformity, and defectivity of the polished wafer were measured by metrology tools using in current integrated circuit (IC) fabrication plants in order to support polishing results obtained by this investigation. Brief descriptions of measurement principles for each facility are also presented in this chapter.

Chapter 4 investigated the effects of single crystalline ceria abrasives on silicon dioxide and silicon nitride CMP process. The single crystalline ceria particles were synthesized by heating peptized ceria sol as precursor under hydrothermal conditions. In this chapter, the relationships between dielectric property of the solvent and particle size were investigated in terms of the supersaturation of solute. In addition, the influences of precipitation participating anions (OH^-) and acidic hydrothermal medium on crystallites size of ceria particles were studied. Furthermore, the polishing behavior of the single crystalline ceria abrasives was discussed in terms of morphological properties of the abrasive particle.

Chapter 5 discussed the effects of spherical ceria abrasives on planarization performance. The ceria abrasives were prepared by the flux method, using potassium hydroxide (KOH) as the grain growth accelerator. In this chapter, CMP test was carried out with four types of ceria-based slurry formulated by dispersing the ceria abrasives with different particle size in order to determine how the removal rate, removal selectivity, and wafer surface roughness of oxide and nitride films depend on the abrasive size and particle size distribution in slurry.

Chapter 6 presented studies conducted on the synthesis of monodispersed ceria coated silica particles and its CMP performance. The coated particles were prepared by the surface-induced precipitation method, in which a new type of ceria coating precursor was deposited on the surface of spherical silica particles via electrostatic attraction route. The ceria coating precursor was synthesized by the sol-gel technique, which employs ethanol as a solvent. In this chapter, the effects of solvent type and solution pH on the formation of ceria coating layer were investigated. CMP test

was performed with the different types of slurries with 146 nm of abrasive size controlled by using 135 nm of colloidal silica particles. The suspension pH effects were investigated as a function of the applied head load and explained in terms of absorption/repulsion behavior between abrasives and materials to be polished.

Chapter 7 introduced a novel method to synthesize the spherical ceria particles via two-step procedure. In first step, spherical cerium carbonate particles were prepared via simple precipitation method using alcohol/water mixed solvent. In second step, the ceria particles were obtained by subsequent thermal decomposition of the precursor. After calcination, the resultant particles were used as abrasives of ceria-based slurry without mechanical milling and filteration. In this chapter, the effects of physicochemical solvent properties on the crystalline phase, microstructures and morphological properties of particles were investigated. In addition, the effects of suspension pH in slurry on polishing performance were discussed in terms of electrostatic repulsive forces.

Chapter 8 investigated the effects of abrasive material properties on polishing removal rate and wafer defectivity by using different kinds of ceria particles obtained from previous chapters. In this chapter, the effects of the brittle behavior of ceria abrasives and particle size distribution of slurry on wafer surface were discussed.

Chapter 9 summarized the conclusions of this study and offered some suggests for future research.

CHAPTER 2
LITERATURE REVIEW

Chemical Mechanical Planarization (CMP)

Chemical mechanical planarization (CMP) is an abrasive process using chemical agents and a circular action to polish the surface of the wafer smooth. Planarization is the process of smoothing and planning surface. CMP can be also referred to chemical mechanical polishing that causes planarization of surface. However, the meaning of polishing is different from the meaning of planarization. Polishing generally refers to smoothing the surface not necessarily planar. Thus, the primary function of CMP is to planarize individual layers in complex integrated circuits. The slurry is the very important key player among the CMP consumables providing both chemical and mechanical effects.

CMP Process

A schematic of a typical CMP process is illustrated in Figure 2-1. The wafer is held on a rotating carrier force down and is pressed against a polishing pad attached to a rotating disk, while chemically and mechanically active slurries are applied. CMP slurry contains abrasive silica or ceria particles suspended in an aqueous medium. Both mechanical action of the abrasive particles and the chemical action of slurry constituents remove material from the wafer surface. Planarization results because material is removed faster from protruding regions on the surface than from recessed regions. The general requirements of CMP can be summarized as follows: First, there is a need for high removal rates of the material to be polished to achieve the needed throughput. Second, the selectivity of the slurry must be sufficiently high so that only the material of interest is polished. Third, the polished surface must exhibit excellent

topographical uniformity. Finally, local dishing and erosion effects must be minimized to satisfy the die-level flatness requirements of sub-0.3 micron devices. Therefore, in order to meet the requirements, it is necessary to understand in detail the nature of contact between chemical-mechanical consumable and individual films. Among these consumable, CMP slurry is one of the most crucial elements to improve the quality of multilevel interconnect networks. It is generally agreed that CMP slurries should be designed to optimize for specific applications.[1]

CMP Slurry

CMP slurry is typically contained with suspended abrasive particles, an oxidizing agent, corrosion inhibitor, and other additives including dispersants.[1] During the CMP process, the abrasives in the slurry and the rotating polishing pad provide the mechanical action that removes material on the surface layer. The chemical components of the slurry accelerate polishing and can be mixed to select specific substances on the surface of the wafer. The types of CMP slurry is categorized by the target materials polished in CMP process. Abrasives and chemical components are also changed by the properties of layers polished during CMP process. Abrasives in the slurry play the very important role of transferring mechanical energy to target material. Silica or ceria particles are commonly used as abrasive of oxide CMP process and alumina particles are used in metal CMP process.[1] During CMP process, it has been known that the abrasive particle size and size distribution have an enormous impact on the evolution of microscratches. Over the past 10 years, the chemical property of surface and the hardness of abrasive have been identified as the important parameters, which affect removal rate, selectivity, and the quality of surface polished during CMP process. Chemical components in the slurry can be designed for specific functions by

the addition of oxidizers or adjusting the pH of the chemical vehicle.[9] It is generally understood that additives modifies the surface to be polished and yields a softer and porous complex layer, which is then removed by mechanical force in the process. Moreover, dispersion agent is used to provide a stable dispersion of abrasive. Therefore, the quality of polishing, which is critical to yield, depends upon the quality and consistency of the CMP slurry. CMP slurry must continually improve to meet much higher performance specifications demanded by the trend of new types of CMP technique and the introduction of noble materials.

CMP of Dielectrics

CMP is commonly employed for both the front and back end processing of integrate circuit (IC) devices due to its unique global planarization capability. This process includes interlayer dielectric (ILD), shallow trench isolation (STI), pre-metal dielectric (PMD), and copper CMP. Slurry is specifically modified for each CMP process to improve the polishing performance such as removal rate, removal selectivity, global planarization, and minimized defectivity. Among these CMP processes, this paper will deal with oxide used as ILD and STI CMP to understand the fundamentals of slurry design for CMP. In this part, I discuss the procedure and mechanism for these CMP process.

Oxide CMP

Process of oxide CMP

Oxide planarization is probably the most common of all CMP processes. Inter-level dielectrics (ILD) are routinely planarized prior to the deposition of the next metal layer. Oxides layers vary thickness, but generally between 5000 Å and 10,000 Å of dielectric material is removed during CMP. Figure 2-2 shows the schematic for the ILD CMP.[10]

Mechanism of oxide CMP

Oxide removal does not occur as a result of physical abrasive action alone. Rather, it is the result of chemical reactions in which oxide bonds form between the slurry particles and the wafer surface.[11,12] The physical abrasive action then comes into play as the moving slurry particles break these bonds and move away. Although much research is still being conducted in this area, it is known that the process proceeds along these lines, as illustrated in Figure 2-3:

1. Hydroxylation - formation of hydrogen bonds between oxides on the wafer surface and the slurry particles
2. Formation of hydrogen bonds between slurry and wafer
3. Dehydration (expulsion of H_2O)
4. Breaking of bonds as the slurry particles are forced along

The most common slurries used for ILD CMP are silica-based and ceria-based. These slurries generally have particles which range in size from 30 ~ 150 nm.

Relationship between particles and wafer

An understanding of the nature of contact between particles and the wafer to be polished is essential to maintain the strict process requirements for manufacturing current and future generation integrated circuit (IC) chips. Especially in oxide CMP, particles play an important role in achieving desired CMP performance such as high material removal rate, low surface defects, and local global planarization via mechanical abrasion and chemical modification of the wafer surface.[10] In spite of its importance, the effect that the slurry particles have no polishing performance is not clear. For polishing of copper or ferrite, it was suggested that the polishing rate is proportional to particle size and solids loading.[13,14] Cook presented data suggesting that the polishing rate is

independent of particle size for glass polishing.[12] Izumitani suggested that the polishing rate decreases with increasing particle size.[15] Singh suggests two polishing mechanism in silica CMP.[16] One is a contact area based mechanism by which

$$A \propto C_0^{1/3} \phi^{-1/3} \tag{2-1}$$

where A is the contact area, C_0 is the particle concentration (the number of particles) and ϕ is the particle diameter (abrasive size). In this model, the polishing rate increases with an increase in particle concentration and a decrease in particle size, which was observed during tungsten CMP.[17] The other is an indentation volume based mechanism by which

$$V \propto C_0^{-1/3} \phi^{4/3} \tag{2-2}$$

where V is the indentation volume. According to this indentation volume based mechanism, the polishing rate increase with decreasing particle concentration and increasing particle size. This mechanism was observed via silica polishing experiments.

Shallow Trench Isolation (STI) CMP

Process of STI CMP

The shallow trench isolation (STI) process is one of the most important applications of CMP. This process has emerged as the primary technique for advanced ultra large scale integration (ULSI) technologies. This process was developed as an alternative to traditional local thermal oxidation processes (LOCOS). The LOCOS process has a major drawback known as the “bird’s beak” phenomenon. A bird’s beak defect occurs due to the diffusive nature of the oxide growth process.[1] As the oxide grows vertically downward into the underlying silicon, it also grows horizontally to the sides and underneath the silicon nitride mask, thus encroaching into the active device

regions. This becomes more of a problem at geometries below 0.25 μm. A secondary benefit of STI is that it can generally be done faster and at lower temperatures than LOCOS. Referring to Fig. 2-4, the STI processes begins with the growing of a very thin oxide layer (100 Å ~ 200 Å) sometimes called the “pad oxide”. Then, a thicker (500 Å ~ 1,500 Å) layer of CVD nitride is deposited on top of the pad oxide. These layers are then patterned with photoresist and trench is etched into the substrate. After the trench is etched, a thin oxide layer is grown on the trench sidewalls and bottom to smooth out the corners and to serve as a liner. Finally, 8,000 Å ~ 11,000 Å of CVD oxide is deposited to fill the trench. This oxide is then planarized using CMP. With the oxide serving as an etch stop, the nitride layer is then stripped away to expose the active device regions. One of the key issues of this process is the selectivity of the nitride vs. oxide. Results ranging from 5:1 to 175:1 have been reported.

Mechanism of STI CMP

STI is a specific CMP application which generally requires the selective removal of silicon dioxide to silicon nitride on a patterned wafer substrate. In this case etched trenches are overfilled with a dielectric (silicon dioxide) which is polished using the silicon nitride barrier film as a stop layer. The process ends with clearing the silicon dioxide from the barrier film while minimizing the removal of exposed silicon nitride and trench silicon dioxide. This requires slurry capable of achieving a high relative ratio of silicon dioxide material removal to silicon nitride removal (high selectivity slurry). Ceria-based suspensions have received considerable attention in STI applications because of their ability to achieve high selectivity.[18,19]

Mechanism of silicon dioxide using ceria particles

One mechanism of silica glass polishing using ceria particles previously proposed by Cook involves proton abstraction from silica followed by reaction with Ce-OH to form a Si-O-Ce bond.[13] Cook described the nature of chemical interaction leading to the accelerated removal rate with ceria abrasives, listed below:

1. Water penetrates into the glass surface
2. Water reacts with the surface, which leads to the dissolution under particle load
3. Abrasives adsorb some dissolution products and leave from the substrate
4. Some dissolution products redeposit onto the substrate
5. Surface dissolution happens between particle impacts

It is hypothesized that the formation of a strong Si-O-Ce bond leads to break of Si-O-Si bond on wafer surface because the free energy of the formation of cerium oxide (Hf = -260 kcal/mole) is much less than the free energy of the formation of silicon dioxide (Hf= -216 kcal/mole).[17,18] Maximum material removal happens when a neutrally charged ceria particle approaches a silica substrate with negative surface charges to form surface chemical bonds in aqueous environments.

$$-M-OH+H^{+} \rightarrow -M-OH_2^{+} \quad (\text{pH} < \text{pH}_{\text{IEP}}) \qquad (2\text{-}3)$$

$$-M-OH \rightarrow -M-O^{-}+H^{+} \quad (\text{pH} > \text{pH}_{\text{IEP}}) \qquad (2\text{-}4)$$

where –M-OH is the neutral hydroxyl group and pH_{IEP} is pH value at zero charge of ceria abrasives (isoelectric point), -M-O^- is the deprotonated surface groups and -M-OH_2^+ is the protonated surface groups, respectively. Figure 2-5 shows the variation of zeta potential with pH value for substrates (oxide and nitride) and ceria abrasives. At pH < pH_{IEP}, silica substrate has a negative surface charge and the ceria abrasives have a

positive surface charge, leading to absorption between two materials. On the other hand, with the increasing pH of the solution, the ceria surface becomes more negatively charged and the silica surface also has a negative surface charge, leading to repulsion between two materials. The removal of material from the surface of silica-glass during the polishing process is attributed to a temporary attachment (through surface chemical bonds) of ceria particles to the silica-glass surface.

$$-Si-O^{-}+-Ce--OH \rightarrow -Si-O-Ce-+OH^{-} \quad (2\text{-}5)$$

The material removal occur when a silica tetrahedron structure is broken from the silica substrate because the strength of Ce-O bonding is greater than Si-O bonding.[19]

$$-Si-O-Si-O-Ce- \rightarrow -Si-O-+Si-O-Ce- \quad (2\text{-}6)$$

Mechanism of silicon nitride using ceria particles

The proposed mechanisms for ceria-based slurry on silicon nitride substrate may be slightly more complex than proposed for silicon dioxide substrate.[22-24] As shown in Fig. 2-5, the surface charge of silicon nitride has a functionally difference in acidic pH region. Particularly, at pH 5 ~ 6, the surface of silicon nitride have a positive charge due to the presence of protonated amine groups which are not present on silicon oxide substrate.[25-27] However, hydrolysis reactions on the surface of silicon nitride occur readily in aqueous solutions which liberate ammonia and generate silica-like surface structures. Such a hydrolysis reaction depicted by Eq. 2-7 would favor formation of reactive surface silanol groups and surface charge at pH 5 ~ 6 would also become negative.

$$Si_3N_4 + 6H_2O \rightarrow 3SiO_2 + 4NH_3 \quad (2\text{-}7)$$

Therefore, the kinetics of the hydrolysis reaction on silicon nitride affects surface reactivity and functionality with ceria abrasives. Laarz et al.[28] proposed an acidic catalyzed pathway for hydrolysis of silicon nitride in aqueous environments. Fig. 2-6 depicts hydrolysis reaction scheme for a nucleophilic displacement reaction (S_N2) of silicon nitride, listed below:

1. Protonation of surface amine
2. Coordination of water
3. Concerted water insertion and Si-N cleavage
4. Proton transfer to amine leaving group
5. Continued hydrolysis at Si center

A water molecule can coordinate to the silicon via an S_N2 insertion known in organic chemistry as a nucleophilic displacement reaction (S_N2 = substitution, nucleophilic, bimolecular). In this pathway, an amine is liberated as a leaving group after the first water insertion. This reaction introduces a hydroxyl group into silicon and the resulting silicon is more electropositive and sterically less hindered. These electronic and steric considerations induce that subsequent hydrolysis should proceed more quickly than the initial water insertion. In this reaction, three proton transfer reactions occur[29]: (1) from the solution to a surface amine Si-NR2, (2) from the surface amine to the adjacent water, and (3) from the protonated silanol to the solution amine. R represents the subsurface neighboring atom covalently bonded to silicon (most likely nitrogen). R' represents the surface atom covalently bonded to nitrogen (either silicon or hydrogen). Based on this mechanism, molecules which can compete for surface

protons should have an impact on hydrolysis rates, affect Si_3N_4 surface functionality, and ultimately influence reactivity with ceria abrasives.

High selectivity ceria-based slurry

The surface potential for oxide and nitride are affected by the suspension pH, dispersants and organic additives during STI CMP process. In order to improve the selectivity and uniformity, an anionic acrylic polymer is commonly used to passivate the surface of the nitride film during STI-CMP, which prevents ceria abrasives from contacting the film surface. Hirai et al.[30] explained the selective absorption mechanism of acrylic polymers on silicon oxide and silicon nitride layers in water-based system. They showed that the characteristics of the passivation layer are determined by the acrylic polymers and suspension pH during CMP process. Moreover, many researchers reported that the selective adsorption is attributed to the difference in surface charge between silicon oxide and silicon nitride layers.[31-33]

Generally, the silicon oxide layer and the abrasives in ceria-based slurry with acrylic polymer have a negative surface charge at pH 3.0, while the silicon nitride layer has a positive surface charge at pH 3.0.[30-35] Figure 2-7(a) shows the variation of zeta potential as a function of pH value for substrates (oxide and nitride) and ceria abrasives including acrylic polymer. Philipossian et al.[32] also proposed a selective adsorption model based on the zeta potential of ceria-based slurry with anionic organic polymer in terms of high selectivity. Figure 2-7(b) represent the formation of passivation layer on the surface of silicon nitride layer and electrophoretic behavior of each material with anionic organic polymer during STI CMP process. The attraction/repulsion reaction between ceria abrasives and oxide/nitride layers results from the different electrophoretic mobility as a function of suspension pH. These behaviors affect CMP

performance such as material removal rate of substrate and removal selectivity between silicon oxide and silicon nitride layer. Anionic acrylic polymer is commonly used to improve the removal selectivity by formatting passivation layer on the surface of the silicon nitride.

Ceria Abrasive

Abrasives in the slurry play the very important role of transferring mechanical energy to the surface of substrates during CMP. Among these abrasives, ceria as abrasive has received considerable attention in CMP process due to its chemical functions leading to high removal rate, silicon oxide to silicon nitride selectivity, and lower solid content in slurry. However, there are some problems to be worked out.

Advantages of Ceria Abrasive

As mentioned earlier, ceria particles receiving intense attention as a main slurry component for CMP process in semiconductor manufacturing industry due to the effective removal rate for oxide film and the softness of the particles.[14] Fig. 2-8(a) compares the removal rate of oxide layers between fumed silica, colloidal silica, and ceria as a function of normalized polishing stress.[19] The removal rate with ceria-based slurry is greater than that with silica-based slurry. This is attributed to the fact that ceria abrasive exhibits a chemical reactivity for oxide layer leading to acceleration of the removal rate during oxide CMP. As a result, the chemical bonding between ceria and oxide layer can be rapidly removed by the mechanical force generated by pressed pad and abrasive, and this physicochemical reaction lead to the high removal rate of a silicon dioxide film by ceria abrasive. Moreover, the hardness of ceria is lower than that of substrates to be polished during CMP process as shown in Fig. 2-8(b). From this fact, it is expected that the scratches on the surface of wafer will be decreased by the lower

hardness of ceria abrasives. Additionally, ceria-based slurry has received considerable attention in STI CMP because of its ability to improve removal selectivity. The oxide-to-nitride removal selectivity is usually enhanced by adding of an acrylic polymer as additive to water-based slurry with ceria abrasives. Thus, removal selectivity is affected by the molecular weight, the concentration of acrylic polymer, and the morphological properties of ceria abrasive. Furthermore, although ceria is a relatively soft material, it has long been used to polish harder glass substrates effectively. Compared with as high as 30 wt % for conventional colloidal silica abrasives and 12.5 wt % for fumed silica abrasives, ceria-based slurries typically contain less than 1 wt % solid content.[36] This will induce a considerable reduction in manufacturing cost and solid waste discharge. Therefore, ceria particle can provide excellent CMP performance owing to high polishing efficiency for silicon dioxide film and lower hardness. Therefore, the ceria particle as abrasive for CMP slurry has been widely investigated to improve the quality of CMP process.

Disadvantages of Ceria Abrasive

In spite of many advantages of ceria abrasive, this contains critical disadvantages leading to serious defects on substrates during CMP process. Usually, commercial ceria abrasives for CMP slurry were synthesized by thermal decomposition of the cerium salt such as cerium carbonate and cerium hydroxide.[8] This method offers certain advantages, such as the higher chemical activity and the brittle property of ceria abrasive due to the high porosity of the surface.[35] However, the size and morphology of the ceria particles are very limited in that particle growth is difficult to control.[38-40] A large number of oversized particles in the distribution tend to give high scratch counts on the polished wafer.[41] Also, these particles need a complicated milling process to regulate

the size distribution. In order to overcome this problem, many approaches to control these properties of ceria particles have been extensively investigated by using liquid phase processes, such as precipitation method,[42] hydrothermal method,[43-45] sol-gel method,[46] and electrochemical method.[47] These is the attractive methods since particles with the desired size and morphology can be produced by carefully manipulating parameters such as solution pH, concentration, reaction temperature, time, and the type of solvent. Besides, these processes can directly synthesize well-crystallized particles without post-heat treatment. However, the size of ceria particles synthesized by using liquid phase process was limited to less than ~ 100 nm. These particles lead to the low removal rate in the CMP process. Moreover, the ceria abrasive in CMP slurry has easily sedimented because ceria is too dense to remain suspended in solution. The settling behavior is the different characteristics of ceria abrasive with respect to colloidal silica. The specific gravity of ceria and colloidal silica is about 7.13 g/cm^3 and 2.2 g/cm^3, respectively.[48] The particle settling is much more severe for ceria-based slurry than that for silica. The sedimentation of ceria abrasive induces an unstable polishing rate for changeable solid contain during CMP and hard aggregates resulting from poor dispersion stability creates surface scratches on the polished film. Therefore, the broader particle size distribution and the sedimentation aggregates have a bad influence on the quality of the polished films during CMP process. Many approaches have been extensively investigated to overcome these problems.

Key Quality Issues

The most important issues in slurry performance for CMP relate to removal rate, global planarity, surface topography (dishing and erosion), surface defectivity (including roughness, scratches, dents, and delaminating), and particle contamination.[10] To

develop a methodology for designing slurry formulations, one must be able to understand the mechanisms active during CMP processing. Table 2-1 lists some of the most important fundamental parameters that must be optimized in order to achieve acceptable characteristics in CMP slurry.

Removal Rate

A high removal rate is an essential aspect of a CMP performance. The removal rate is the amount of material removal by CMP in a given time frame. It is calculated according to the Preston equation, MRR = K_pP_0V, where MRR is the material removal rate, P_0 the down pressure, V the relative velocity of water, and K_p a constant representing the effect of other remaining parameters, and the amount is usually expressed in Å/min.[49] Removal rates depend on the film being removed, type of pad and slurry being used, amount of downforce and relative velocity of the wafer carrier and polishing platen.[50-52] Especially, the removal rate of dielectrics can be affected by:[51]

1. The size and distribution of the abrasives in slurry
2. The number of abrasives
3. The pH of the slurry
4. Pre-CMP film stress

Increasing any of these properties will usually result in an increased removal rate. However, it has been reported that in some instances raising the pH does not necessarily increase the removal rate. In fact, for some types of slurries reducing the pH can slightly increase the removal rate. The removal rate is affected by the size and concentration of slurry abrasives due to frictional force between the abrasives and the wafer as mentioned in CMP of dielectrics section. The type of oxide, thermal or CVD, also has an effect on the removal rate. Another factor which affects the removal rate is

the topography on the surface. Material is typically removed at a higher rate on small and isolated features. On larger or tightly spaced features the removal rate can be reduced drastically. This will also impact the uniformity of removal.

Uniformity and Planarity

Uniformity and planarity are two closely related but distinctly different topics. Uniformity is the measure of film thickness (or removal rate) variations across the wafer. Planarity is more a measure of overall die flatness. In other words, a given wafer may exhibit acceptable planarity but not be very uniform. All of the process variables mentioned can have direct effect on uniformity. Controlling the process is the key and much work and research still needs to be done. Uniformity is the standard deviation of thickness removal rate measurements and it is expressed as a percentage of the average thickness removed. Planarity, on the other hand, is simply a measurement of the degree of flatness and can be expressed as a percentage (planarity across the wafer) or as a specific number. Both of these issues are complicated by a variety of factors, such as topography spacing. The topography not only affects uniformity across the entire wafer, but it can cause problems within each specific IC device.

Global Planarization

Global planarization refers to the ability of the CMP abrasives to rapidly planarize pattern-dependent and large-scale surface morphologies. The lateral dimensions of surface topography can range from nanometers to several millimeters, due to large pattern size or gentle topographic variations. The CMP process is typically conducted on films deposited on patterned surfaces that as a result have significant surface topography. The pitch of the pattern (the sum of the width of the patterned lines and the spacing between them) as well as its density can vary significantly across the die, which

results in different local polishing pressures across the patterned surface. The variations in local polishing pressure lead to varying removal rates and thus to varying amounts of material removed before global planarization can be achieved. Compared with CMP, chemical etching decreases surface planarity and increases surface roughness, while mechanical polishing can enhance the planarity but only at a low removal rate and at the expense of a poor surface finish. A key condition for global planarization is the formation of a very thin passivating surface layer that is subsequently removed by mechanical component of the slurry. The thickness of this layer is commonly under 2 nm. The removal rate of thin passivated surface layer is greater at the highest regions of the wafer surface than at the lowest regions, due to differences in local pressure in these regions. If the passivated layer is thinner than the difference in height between the highest and the lowest regions significant planarization is expected to occur with CMP.

In the case of dielectric CMP, it is generally believed that by controlling the pH in the alkaline regions, a thin hydrated surface layer is achieved.[12] The role of the hydrated surface layer formed under alkaline pH conditions is to soften the surface so that higher removal rate can be obtained. It is speculated that the thickness and properties of the soft, gel-like layer depend on the pH as well as on the contact pressure. The removal rate of silica under purely mechanical conditions (at low to neutral pH) is less than a factor of two lower than those obtained under alkaline pH conditions. This indicates that oxide CMP is more mechanical in nature than metal CMP.

High-planarity polishing is typically observed for slurries that exhibit linear variation in removal rate with a change in applied pressure (P_{app}). The planarization capability of slurry is related to the sensitivity of the removal rate to high and low regions on the

wafer. Δz is the distance between highest and lowest regions, and then the planarity of the removal rate can be directly related to *dRR*/*dΔz*, or the rate of change in the removal rate with the variation in surface height. This parameter can be further expressed as[10]

$$\frac{dRR}{d\Delta z} = \left(\frac{dRR}{dP}\right) \times \left(\frac{dP}{d\Delta z}\right) \tag{2-8}$$

where *P* is the local pressure on the polishing surface, which is directly proportional to P_{app}. The first term in the product is strongly dependent on the characteristics of the slurry, while the second term is dependent on the mechanical properties of the pad. The values of *dRR*/*dP* are typically enhanced by having a thin layer that exhibits pressure-dependent material-removal characteristics and harder pad that transfer a significant portion of the applied pressure directly to the abrasives.

Selectivity

Another important criterion for STI CMP is selectivity, which represents the ratio of material removal rate (MRR) of silicon oxide to silicon nitride. Generally, a high selectivity value is desired because the CMP process needs to stop once the silica layer is removed. To enhance selectivity, the silica layer is typically polished by applying chemical/mechanical action and ensuring that chemicals do not extend their chemical assisted synergistic effects to the underlying layer, causing it to be mechanically removed. For STI CMP, conventional silica-base slurries achieve removal selectivity value of silica-to-silicon nitride layer in the range of 3 ~ 4.[10] These low values can lead to extensive loss of nitride thickness, especially for large pattern density variations across the die. Recently, the removal selectivity value has been significantly increased due to reduced mechanical and chemical effects on the silicon nitride layer with the use

of ceria-based slurries. A preferred STI process can be achieved by driving the removal rate of the protective nitride layer as low as practical while maintaining a reasonable rate for the fill oxide. Additionally, by suppressing the nitride removal rate, issues associated with pattern dependent nonuniformity with CMP can be reduced or minimized. Thus, selected additive and acidic polymer can be added to ceria-based slurry. Purely mechanical action on the underlying layer can result in high defectivity, especially in soft materials such as low-k dielectrics. Methods to reduce the mechanical component of the slurry, for example, by the use of even smaller particles or softer abrasives, may be required in the future.

Surface Defectivity

Another important aspect of CMP processing is surface defectivity. Defectivity issues include surface scratches, indentations, surface roughness, dishing, particle adhesion, and corrosion. Figure 2-9 shows the CMP defectivity for wafer surface. Among these defects, surface scratches are typical defects of the CMP process and are produced mainly due to the aggregates of slurry. One of the key ways to control microscratching is to control the size of the abrasive particles in the slurry and the size distribution of the particles (especially the proportion of lager particles in the slurry). The indentation depth and stresses are related to the mechanical properties of the interacting surfaces, the particle size, and the layer thickness. If one assumes elastic contact between the particles and the surface, the indentation depth δ as a function of particle size Φ is given by[10]

$$\delta = \frac{3}{4}\phi\left(\frac{P_{app}}{2KE}\right)^{2/3} \qquad (2\text{-}9)$$

where *K* is the particle fill factor at the surface and E is the Young's modulus of the surface layer. Thus, equation 2-9 clearly shows that indentation depth is directly proportional to particle size. Also, both the length and depth of microscratches are expected to increase as particle size increases. Besides the aggregates in the slurry lead to other complicating factors during CMP process. These include the time-dependent aggregation of particles, pH, drift, and issues related to the long-term stability of the slurry. Aggregation issues can lead to larger overall particle size. Depending on the shape of the aggregates and the aggregate strength, the wafer can be subjected to higher contact stresses, resulting in increased defectivity. If the slurry is unstable, the particles can settle on the wafer surface, resulting in a higher density of microscratches and increased particle adhesion that may be difficult to eliminate during post-CMP cleaning. To prevent large abrasives in slurry, filters can be used on the slurry line. The drawbacks of filters in the slurry line, however, are that the slurry flow rate may decrease as the filter is being clogged and the removal rate can decrease as the filter approaches its end of life. A choice of a filter with the correct membrane pore size can prevent the shift in removal rate. The pore size chosen must be significantly larger than the slurry particle size.

Additionally, in order to decrease in wafer scratches, the ideal particle is one that should be softer than the substrate material in choosing the abrasive for a particular CMP process. For ceria-based slurry, ceria abrasives induce defects on the wafer surface because of the large, abrasive agglomerated particles resulting from poor dispersion stability. During CMP, the agglomerated particles easily stick to the wafer surface, which results in residual particles and scratches on the wafer surface.[53-56] In

order to reduce the surface defects, particle agglomeration should be prevented by the stabilization of the ceria suspension. In general, the dispersion stability can be improved by adding an adequate polymeric dispersant. However, the stabilization of the ceria suspension using a polymeric dispersant has limitations in successfully eliminating the agglomerated particles which can induce scratches on the wafer surface. Therefore, a new method which can prevent the agglomeration of the ceria particle must be proposed in terms of intrinsic properties of ceria particles.

The primary problem which occurs during STI is known as dishing. Dishing occurs when the oxide in the trench is polished at a higher rate than the nitride. Dishing is a result of the fact that pressure and pad flexibility combine to polish the recessed areas. If the pad were completely stiff, then theoretically a completely planar surface would be the result. In the subsequent HF stripping of the nitride layer, some of the trench oxide will also be removed. The danger here is that the trench oxide could ultimately be reduced to a lower level than that of the active silicon. This causes a problem known as poly wraparound when the poly silicon gates are deposited. CMP processes for STI, including pad and slurry selection, must be optimized in order to avoid these problems.

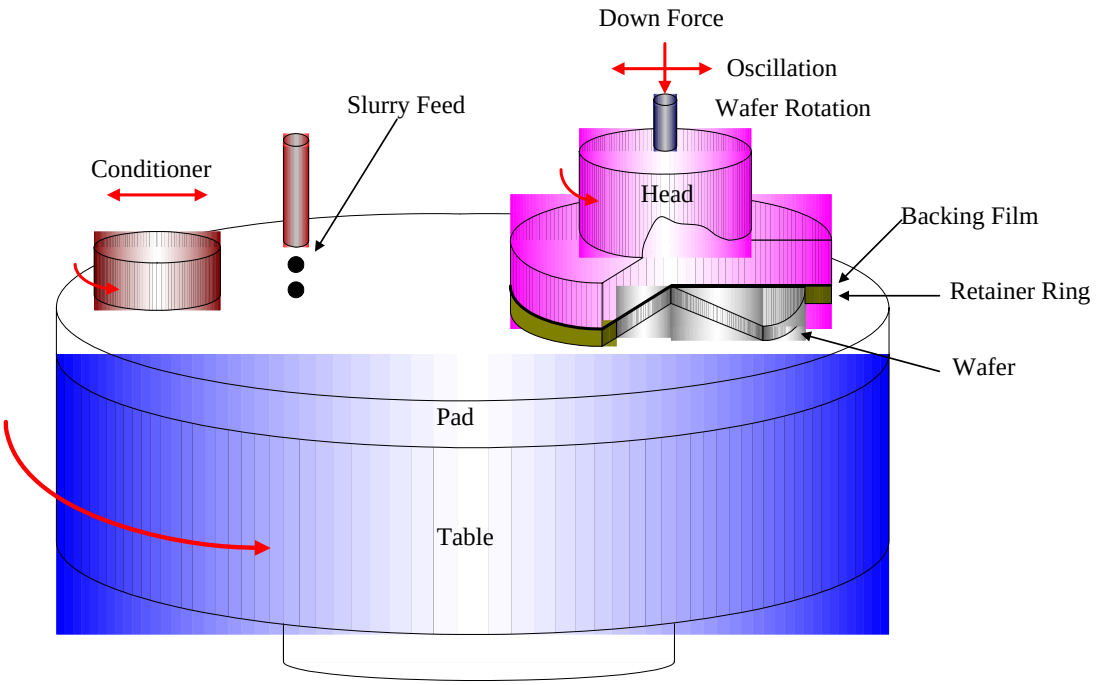

Figure 2-1. Schematic for CMP process

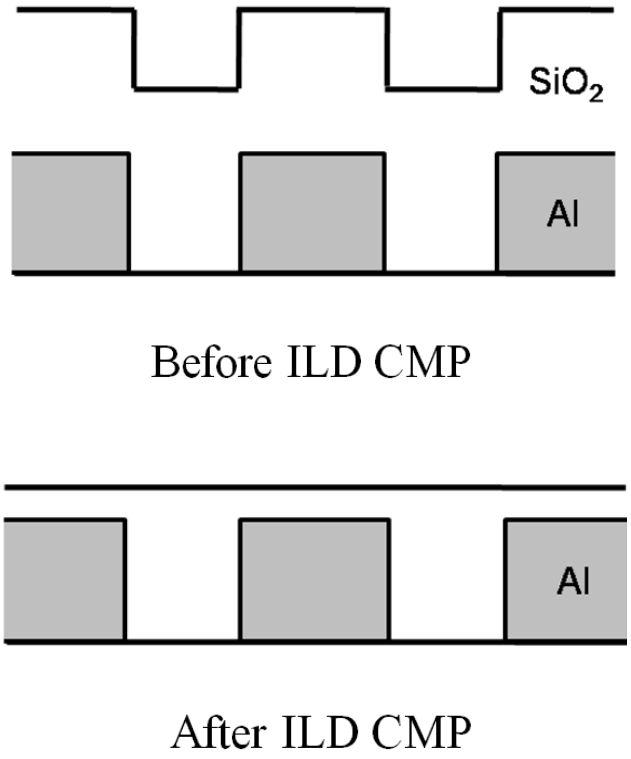

Figure 2-2. Schematics of ideal oxide ILD CMP

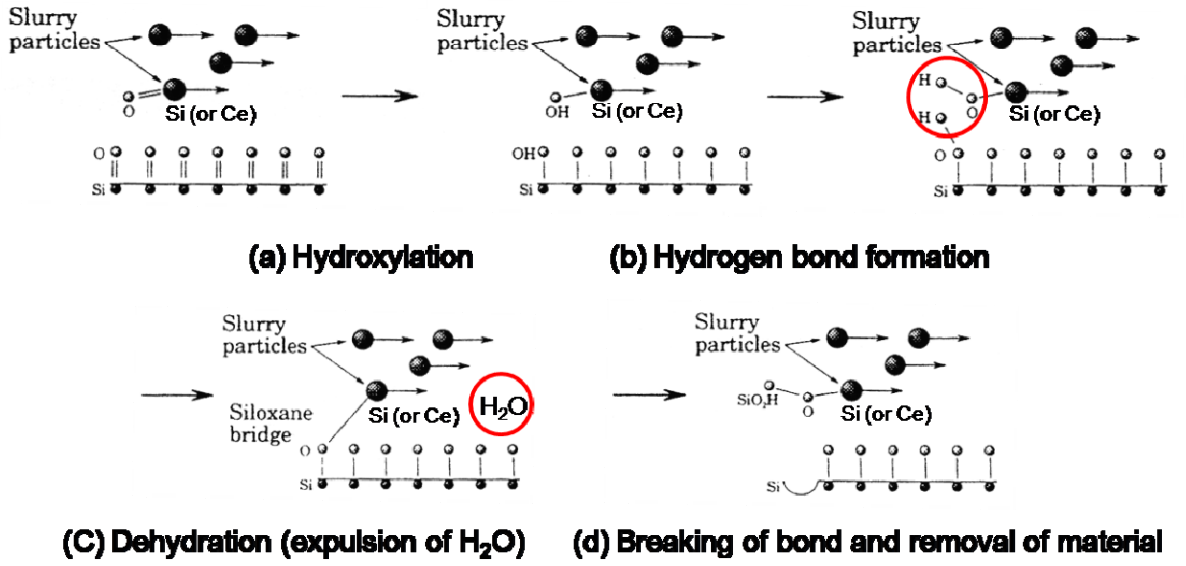

Figure 2-3. Oxide removal mechanism by CMP[1,12]

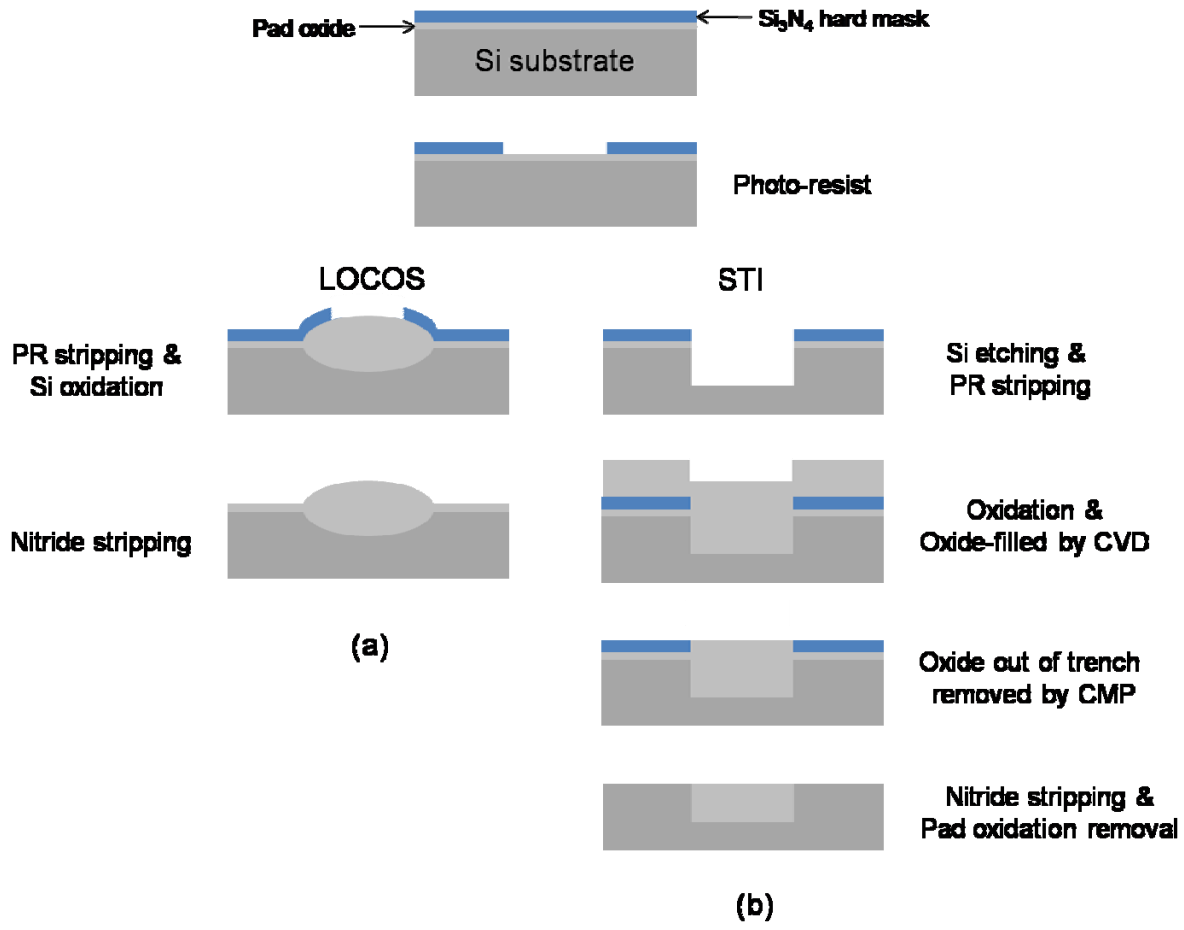

Figure 2-4. Shallow trench isolation (STI) CMP process

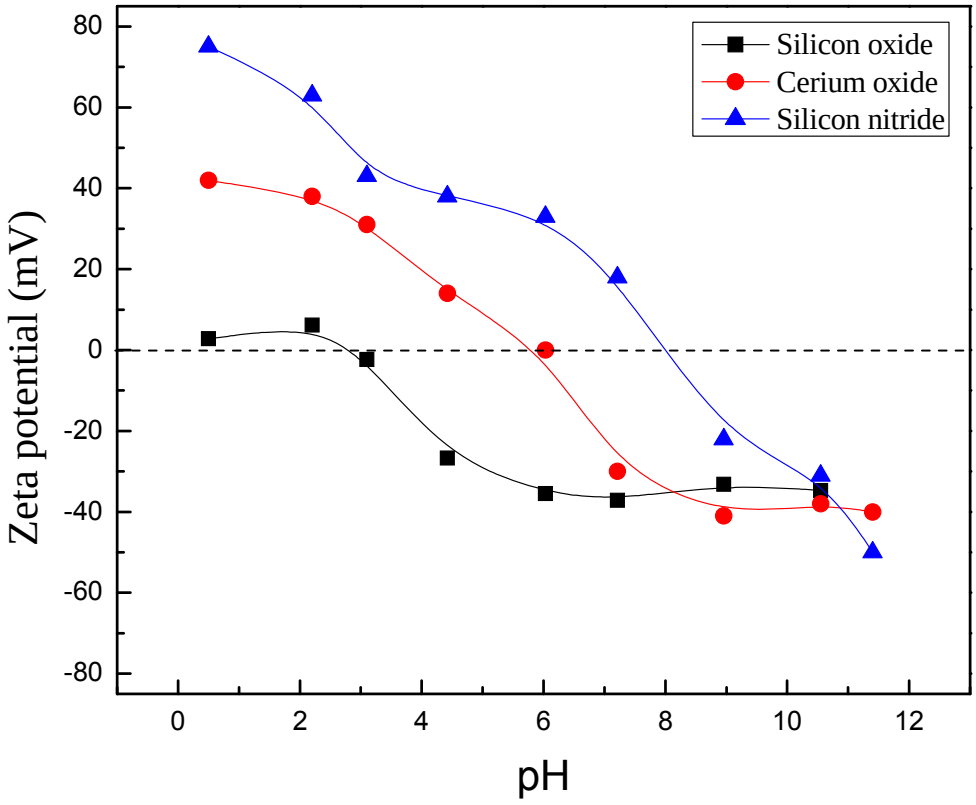

Figure 2-5. Zeta potential of the oxide/nitride substrates and ceria abrasive as a function of pH[29]

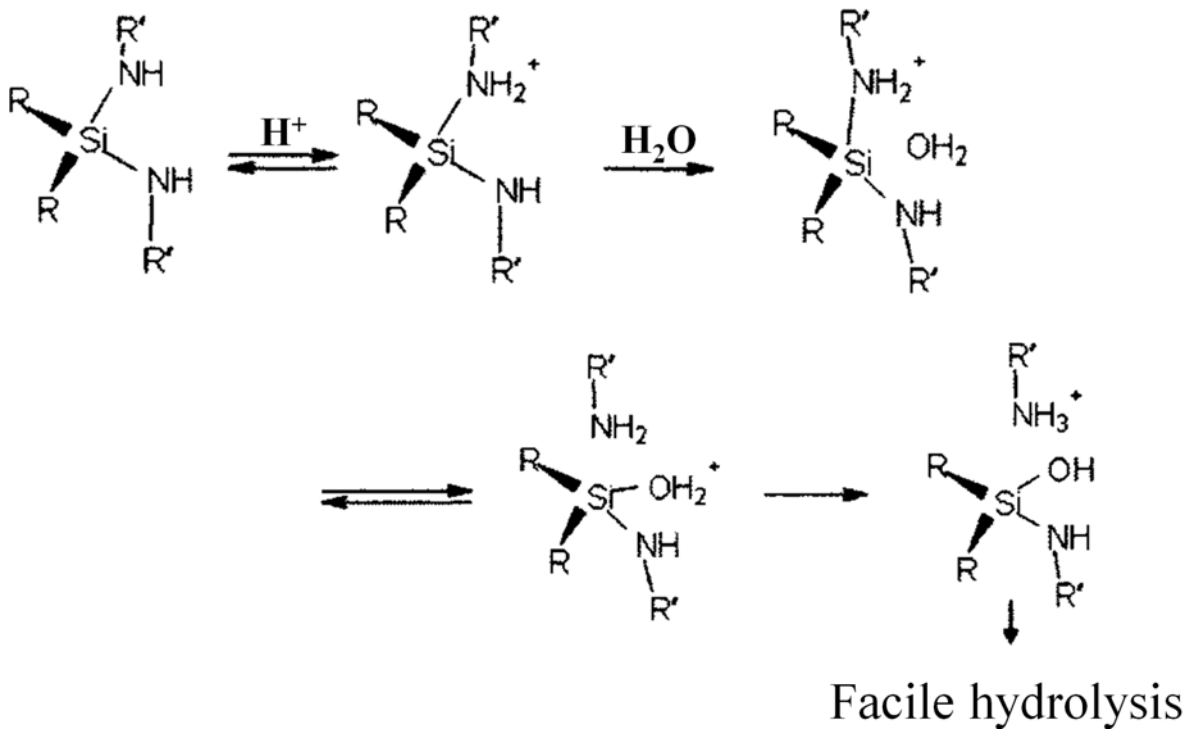

Figure 2-6. Silicon nitride S_N2 hydrolysis reaction scheme[28]

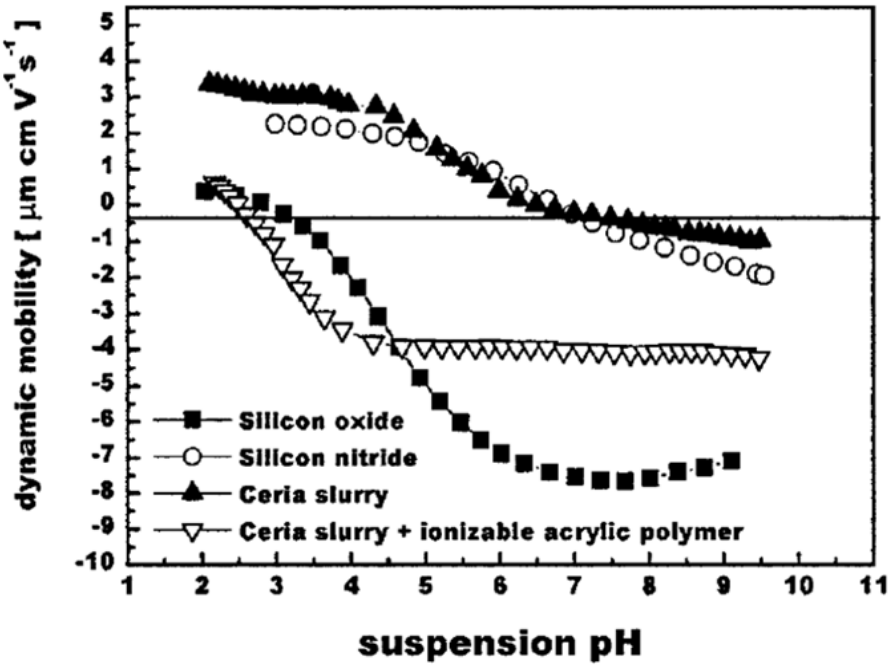

(a)

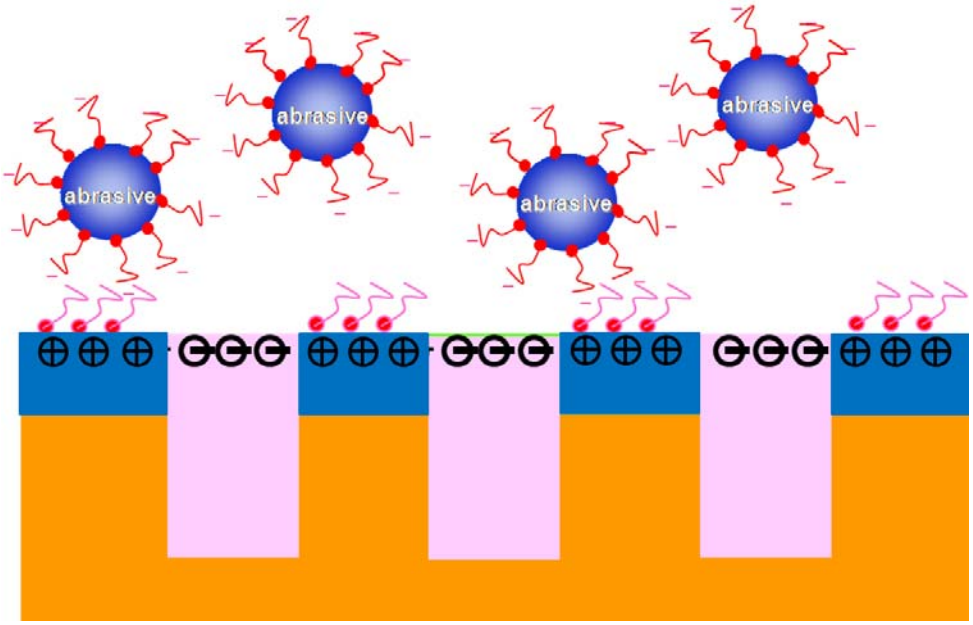

(b)

Figure 2-7. (a) Zeta potential of the oxide/nitride substrates and ceria abrasive as a function of pH[29] and (b) the formation of passivation layer on the surface of STI structure with anionic organic polymer

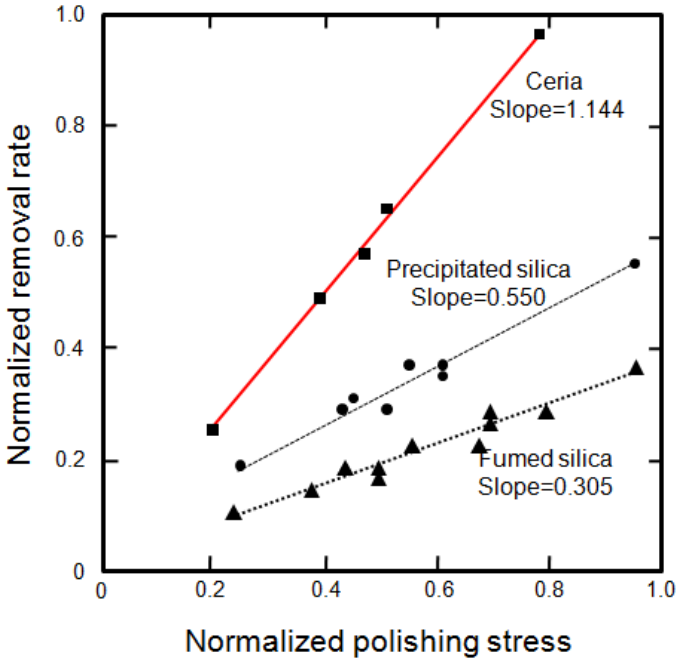

(a)

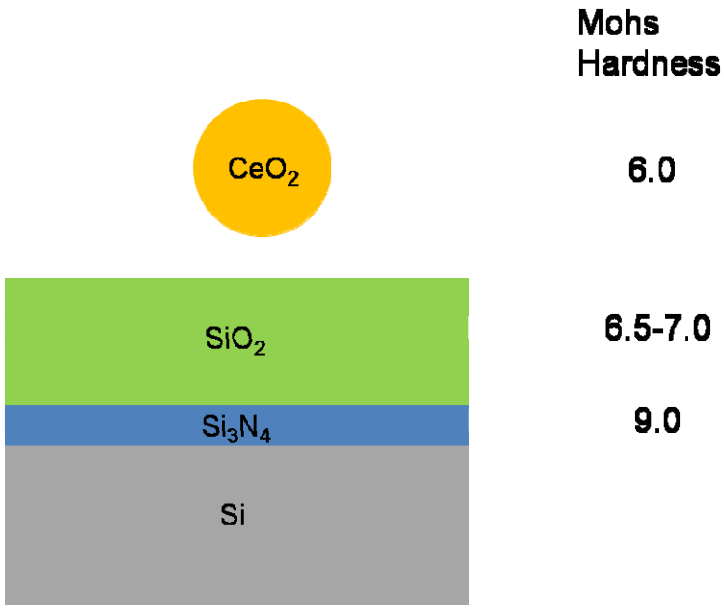

(b)

Figure 2-8. The comparison on (a) removal rate for oxide substrate with different abrasives[1] and (b) Mohs hardness of ceria and materials to be polished during CMP

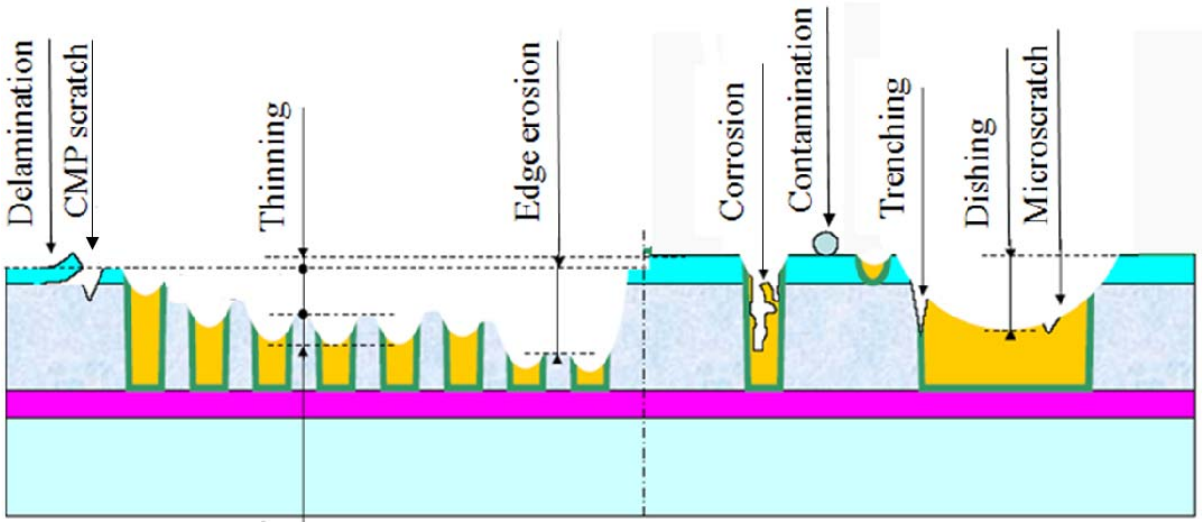

Figure 2-9. The schematics of surface defectivity

Table 2-1. Guiding principles for slurry design in chemical mechanical planarization[10]

CMP issues	CMP parameters
Removal rate	Rapid formation of the thin surface layer
	Control of the mechanical/interfacial properties of the surface layer
	Stress induction by abrasion to remove the surface layer
	Indentation-based wear
	Fracture/delamination-based removal
Global planarization	Formation of a thin passivated surface layer
	Minimization of chemical etching
	Minimization of mechanical polishing
Selectivity	Top-layer chemical/mechanical polishing
	Bottom-layer mechanical polishing
	Reduction of mechanical component in slurry
Surface defectivity	Rapid formation of a thin surface layer
	Minimization of mechanical polishing
	Control of particle size and hardness
	Control of particle size distribution

CHAPTER 3
EXPERIMENTAL FACILITY AND PROCEDURES

Introduction

This chapter is devoted to the studies conducted on the preparation and various analysis methods of consumables used in this investigation, the polishing experiment, and the measurement for CMP performance. Especially, accurate measurement for consumables and wafers after CMP experiment plays a significant role to an understanding the nature between abrasive particles and wafer to be polished. Therefore, various analysis tools were employed in this investigation. For abrasive particles, the synthesized particles were analyzed by XRD, FESEM, TEM, XPS, FTIR, TG/DTA and BET. For slurry, slurry stability, mean particle size, and zeta potential measurements are reported using a variety of light scattering instruments. For CMP evaluation, film thickness, selectivity, nonuniformity, and defectivity of the polished wafer were measured by metrology tools using in current integrated circuit (IC) fabrication plants in order to support polishing results obtained by this investigation. Brief descriptions of measurement principles for each facility are also presented in this chapter.

Sample Preparation

Wafers

For blanket wafer test, silicon dioxide films of 2 μm thick were formed on a 5-in. p-type silicon substrates with (001) orientation by plasma enhanced chemical vapor deposition (PECVD). Silicon nitride films were deposited with the thickness of 7000 Å by using low-pressure chemical vapor deposition (LPCVD). These wafers were obtained from Seyoung semi-tech. For the patterned case, the SKW-1 pattern wafer designed by

SKW Associates (Santa Clara, CA) was used for characterization with respect to the pattern density and pitch size.[57] The STI mask consisted of 4 mm × 4 mm density and pitch structures dividing the 20 mm × 20 mm die into 5 rows and 5 columns. Figure 3-1 illustrates the specially designed layout of the SKW-1 pattern wafer, including the pattern density and pitch size layout, the mask floor plan, and a cross-sectional view. In the density structure, density is defined as the trench area over the total area or expressed as

$$density = \frac{TW}{[TW + AW]} \tag{3-1}$$

where *TW* is trench width and *AW* is active trench. The pattern density is varied systematically from 0% to 100% in increments of 10%, with a fixed pitch of 100 μm. The density structures are fabricated in a random layout to place high-density regions next to low-density regions. In the pitch structure, the density is fixed with the same trench width and space (50%), and the pitch is varied from 1 to 1000 μm, with vertically oriented lines.

Abrasive particles

In this experiment, different types of particles were used as abrasives for CMP slurry. The particles were synthesized by induced-surface precipitation, hydrothermal, flux, and thermal decomposition method. The resultant particles have different characteristics in terms of morphology, crystalline structure, mechanical hardness, and thermal stress etc. The details for preparation methods of particles were explained in each chapter.

Slurries

Different slurries were formulated by dispersing abrasives each with different abrasives in deionized water containing an anionic organic polymer (Poly acrylic acid, PAA; Mw 4000, LG Chem.) as dispersant. The PAA was 2 wt% based on the total weight of the used abrasives. For each slurry, pH was adjusted to 6.5 ~ 6.7 by adding ammonium hydroxide (NH_4OH). The solid loading of the used abrasives was fixed to 2.0 wt%.

CMP Equipment

CMP Polishers

Polishing tests were performed on a rotary type CMP machine (GNP POLI 400, G&P technology) for one minute with each of the slurries. IC 1000/SUBA IV stacked pads (supplied by Rodel Inc.) were utilized as CMP pads. The polishing pressure, applied as a down force, was 280 g/cm^2. The relative velocity between the pad and the wafer was 90 rpm. During polishing, the slurry is continuously stirred by a magnetic bar, and pumped to the pad-wafer interface at a flow rate of 100 mL/min. The pad was conditioned before each polishing run with a grid-abrade diamond pad conditioner manufactured by TBW®. The diamond conditioner minimizes pad glazing. Figure 3-2 shows the schematic of the CMP tools used in this experiment. The average polishing data for removal rate were calculated by performing the same test more than three times in order to support the validity of the results from the statistical viewpoint.

Slurry Delivery System

Slurry performance on CMP process can be influenced by the complex delivery systems that are employed in the Lab. Pumps used for re-circulation and filters used to remove large particles and aggregates, defect causing particles can impart increased

shear to the slurry and provide enough energy to the particles that they surmount their repulsive force barriers and come into contact. Figure 3-3 shows a slurry delivery system, which consisted of filtering system, pumping devices and a slurry delivery loop. CMP profile® II filter capsule (Pall Microelectronics Inc.) was used as a filter to remove aggregates and larger particles. The filter size was 3.0 μm and the slurry on the tank was circulated three times by using diaphragm pump.

Characterization and Method

Abrasives

Microstructure and shape

Morphological characteristics of the abrasive particles have been identified as the important parameters that influence CMP performance. The morphology and size of particles were analyzed by a field emission scanning electric microscopy (FESEM, JEOL JSM-6335F) at an accelerating voltage of 15 kV. The samples for FESEM analysis were prepared by dropping the dispersed samples on the sample holder and then deposited with carbon coating under vacuum condition. The average primary particle size was determined by FESEM micrographs with counting more than 100 particles. The average particle size (d_{SEM}) can be calculated as

$$d_{SEM} = \frac{\sum d_i}{N_T} \tag{3-2}$$

where the d_i is identified with the individual particle size and the N_T is the total number of particles measured from SEM microscopy. The large magnified microscopy and linear structures of the precipitates were observed by a transmission electron microscopy (TEM, JEOL TEM-2010F) at an accelerating voltage of 120 kV. The samples for TEM analysis were prepared by dispersing the final particles into distilled

water under ultrasonic treatment and then the dispersion was dropped on carbon-coated copper grids.

Physical properties

X-ray diffraction is an extremely important technique in the field of materials characterization to obtain information on an atomic scale from both crystalline and noncrystalline (amorphous) materials. Especially, the crystalline size of abrasive particles has influence on CMP performance such as removal rate and the defects of film polished. The crystal structure was identified through x-ray diffraction (XRD, Philips APD 3720) using CuKα radiation (λ=0.154 nm in this study). The accelerating voltage and the applied current were 40 kV and 20 mA, respectively. The crystalline size (d_{XRD}) of samples can be estimated from XRD patterns by applying full-width half-maximum (FWHM) of characteristic peak to Scherrer equation as[5]

$$d_{XRD} = \frac{0.9\lambda}{\beta \cos\theta} \tag{3-3}$$

where d_{XRD} is grain size, λ is the wavelength of x-rays, β is the half-width of the diffraction peaks, and θ is the diffraction angle. For ceria particles, the broadening of the (111) peak in XRD was analyzed to confirm the primary grain size of particles. Thermogravimetric and differential thermal gravimetry (TGA/DTG, Mettler Toledo 851) analysis was performed in an air flow of 100 ml/min at a heating rate of 10 ^{o}C min^{-1} from room temperature to 800 ^{o}C. The typical sample quantity was between 80 – 100 mg.

Surface and chemical properties

The chemical composition of the samples was determined by X-ray photoelectron spectroscopy (XPS, Physical Electronics Perkin-Elmer PHI 5100). The XPS measurements were performed with a non-monochromatic MgKα or AlKα source at a

base pressure of 5 X 10^{-1} mbar. The analysis chamber included an aluminum anode. As the sample were insulating, the energy calibration was achieved by setting the binding energy of carbon at 284.6 eV. Fourier transform infrared (FTIR) spectroscopy (Thermo Nicolet Magna 760) was used to determine the chemical interaction between the core particles and coating materials. The FT-IR spectra for the samples of investigation were carried out in the range 4000 - 500 cm^{-1}. Infrared absorption spectra were recorded for KBr disk containing the synthesized particles and the FT-IR cell was purged for 20 min prior to spectral collection. FTIR spectroscopy was used with a dry air purge. The specific surface area of ceria abrasives was determined by Brunauer-Emmett-Teller (BET, Micrometric ASAP 2010) method using nitrogen adsorption/desorption at 77 K. All samples degassed at 200 ^{o}C prior to measurement. The BET surface area was determined by the multipoint BET method with the adsorption data in the relative pressure (P/P_0) range of 0.05–0.25. Assuming that the samples are spherically and no-porous, the corresponding particle size (d_{BET}) can be estimated as

$$d_{BET} = \frac{6}{\rho A} \tag{3-4}$$

where *A* is specific surface area and ρ is the true density of sample. For ceria abrasives, ρ is 7.28g/cm^3.

Slurries

Electrical potential (Zeta Potential)

Electrophoresis measurements were used to obtain the electrophoretic mobility and isoelectric point (IEP) of the prepared particles. These electrostatic behaviors of particles play an important role in the preparation of the coated particles and dispersion stability of abrasive particles in CMP slurry. The zeta potential (type Brookhaven

ZetaPlus) of particles was measured by utilizing an electrophoresis method to measure the electrophoretic velocity (v_E) of colloidal particles.[58] When the electrical double layer (*1/k*) is much smaller than particle size, the Smoluchowski equation can be applied to measure the zeta potential (ξ).

$$\xi = \frac{\eta v_E}{\varepsilon E_0} \tag{3-5}$$

where μ and ε are the values of viscosity and dielectric constant in the solution and E_0 is the electric field. If the electrical double layer (*1/k*) is much larger than the particle size, the Huckel equation can be applied, and expressed as

$$\xi = \frac{3\eta v_E}{2\varepsilon E_0} \tag{3-6}$$

An electrolyte solution (1 mM) was used to keep the ionic strength constant while the pH value was varied by adding 0.01 N KOH or HCl into solution. The pH of the suspension was taken as the isoelectric point (IEP) at which the zeta potential was zero.

Particle size distribution

Average particle size of abrasive particles in CMP slurry was measured by dynamic light scattering method (type Honeywell Microtrac UPA 150). The light scattering technique has been commonly employed for measuring particle size below 1 μm. This technique can be divided into two groups, dynamic light scattering (or quasielastic light scattering or photon correlation spectroscopy) and low angle laser light scattering (or laser diffraction). Dynamic light scattering can quickly and accurately measure the particle size range from 0.8 nm to 6.5 μm. When the particle size is smaller than a submicron, colloidal particles have a behavior of Brownian motion due to thermal

vibration. Thus, for a monodisperse distribution of spherical particles, an intensity of autocorrelation function is employed for analyzing the intensity fluctuations.

$$g(t) = \exp(-Dq^2 t) \tag{3-7}$$

where *g(t)* is the normalized autocorrelation function, and *D*, *q*, and *t* are the Brownian diffusion coefficient (Stokes-Einstein relation), scattering vector, and delay time of the autocorrelation function.

$$D = \frac{K_B T}{3\pi\eta d} \tag{3-8}$$

where K_B is Boltzmann constant, T is the absolute temperature, μ is the liquid viscosity, and d is the particle diameter. Thus, smaller particles move more rapidly and have more intensity fluctuations than bigger particles. The laser diffraction has been commonly employed for detecting large particles. When a particle size is larger than incident wavelength, the diffraction phenomenon occurs while light beam interacts with particles. The smaller particles have a higher angle of diffraction than bigger particles.[59]

Polished Wafer

Film thickness measurement

Thickness measurements of films before and after CMP were measured by using a Nanometrics NanoSpec® 6100. The NanoSpec is an instrument for measuring the thickness of optically transparent thin films (photoresist or oxide etc) on silicon wafers. It uses reflectometry or measurement of reflected light to determine film thicknesses based on interference effects. The basic operating principle is that the intensity of monochromatic reflected light depends strongly on film thickness because of interference (the film thicknesses are comparable to the wavelength of the incident light). The machine uses a computer-controlled grating monochromator and a photomultiplier

tube detector to measure the reflected optical spectrum (over the 350 to 800 nm wavelength band) from a bare silicon reference wafer and from the wafer under test. Given an index of refraction for a thin film and the two measured spectrums, the computer will analyze the interference pattern to determine film thickness. The equation for describing the interference is

$$\chi_0 = \frac{\lambda}{2n_i}\left[g - (\phi_s - \phi_f)\right] \tag{3-9}$$

where X_0 is film thickness, λ is the wavelength (in vacuum) of the incident radiation, ϕ_s is the relative phase shift at the SiO_2/Si interface, ϕ_f is the relative phase shift at the air/SiO_2 interface, n_i is the index of refraction of the thin film, and g is the order of the interference. The intensity is a maximum when the bracketed term is an integer and a minimum when it is an integer plus 1/2. In this experiment, the thickness of each silicon dioxide film was measured with the NanoSpec using a refractive index of 1.46. To determine a film thickness, the instrument scans the film measuring the change in intensity as a function of wavelength. The spectral fluctuation in intensity results from constructive and destructive interference of the electromagnetic waves as they travel through the film and reflect off the underlying substrate. From the spectral intensity distribution, the thickness of the deposited film can be computed. Figure 3-4 shows schematically the principles of film thickness measurement using NanoSpec® 6100.

Selectivity between silicon dioxide and nitride

Chemical mechanical planarization (CMP) has enabled replacement of previously used device isolation method, local oxidation of silicon (LOCOS), by STI. The major requirements of the STI CMP step are: complete removal of silicon dioxide over silicon nitride layer (nitride layer acts as a CMP stop and protects the active device area);

minimal nitride erosion to prevent damage to the underlying silicon material in active areas; and minimal dishing of the trench oxide. Among these requirements, the relationship between removal rate of oxide and nitride as stop layer is one of the most important issue in STI-CMP process. Usually, this has been designated as selectivity, which represents the ratio of material removal rate (MRR) of silicon oxide to silicon nitride:

$$Selectivity = \frac{Material \quad removal \quad rate \quad of \quad silica}{Material \quad removal \quad rate \quad of \quad silicon \quad nitride} \tag{3-10}$$

In this experiment, the effects of various abrasive particles on removal selectivity were investigated.

Oxide CMP within-wafer nonuniformity (WIWNU)

The primary purpose of using CMP is to planarize the surface of film. WIWNU is of critical important in evaluating equipment, developing and comparing process, monitoring process performance. For instance, the edge effects, namely, the rapid variation of the material removal rate at the edge, require an exclusion of the wafer edge after CMP. This reduces the yields of the process. The uneven material removal rates across the wafer will bring the over-polishing in the faster removal regions in the shallow trench isolation (STI) and copper damascene processes. This causes a degeneration of the circuit performance in that area. In addition, WIWNU will bring a systematic variation of the circuit performance across the wafer. A better understanding of the formation mechanism of the WIWNU will be able to increase the yields and help to optimize the circuit performances. The WIWNU can be expressed as follows:[50-52]

$$WIWNU = (\frac{MRR_{\max} - MRR_{\min}}{MRR_{avg}}) \times 100\% \tag{3-11}$$

where, MRR_{max} is maximum material removal rate, MRR_{min} minimum material removal rate, and MRR_{avg} is average material removal rate. The non-uniform removal rate across the wafer in CMP can be attributed to the uneven distribution of a number of parameters such as the temperature and slurry distributions. However, if the distributions of the pressure *P* and velocity V are the two major contributors, equation 3-10 can be revised by Preston's Equation of material removal rate $MRR = K_e PV + MRR_0$:[50-52]

$$WIWNU = \left(\frac{K_e(PV)_{\max} + MPR_0 - K_e(PV)_{\min} - MPR_0}{K_e(PV)_{avg} + MPR_0}\right) \times 100\% = \frac{K_e[(PV)_{\max} - (PV)_{\min}]}{MRR_{avg}} \times 100\% \quad (3\text{-}12)$$

where K_e and MRR_0 are two experimental fitting parameters. In this experiment, the pressure and velocity was fixed in order to investigate the effects of abrasive particles on WIWNU during CMP process. Therefore, the WIWNU of material removal rate was measured by equation 3-10.

Defectivity monitoring by wafer defect scattering analysis

A common technique for measuring defects on unpatterned wafers employs a laser to scan across the entire wafer. This is designated as wafer defect scattering analysis. If a defect is present, light is scattered away at the point of incidence. A photomultiplier tube collects the scatted light, whose magnitude is proportional to the size of the particle. Laser scanning can also be used to detect defects on patterned wafers using dark field light scattering. Scattered laser light is detected using charge-coupled diode (CCD) camera. Through an image processor and the intensity calculations, defects can be detected and quantified on the wafer. Another method of

defect detection is digital image comparison. The tool works by comparing a pixel of one die to that of the preceding and succeeding die. If there difference in contrast value, that coordinate is flagged as a defect. In this experiment, defects of pattern wafer after CMP were measured by using a KLA-Tencor® puma 91XX. This system uses a UV/visible light source to illuminate defect types. Figure 3-5 shows schematically the principle of wafer defect scattering analysis.[60] This system is as follows: a UV laser beam is illuminated onto the wafer surface from above, scattered light from a defect is collected by a receiving lens, and the scattered light is converted to an electrical signal by a detector. The wafer is set on the rotating stage, and by moving the stage in the radial direction while it rotates, the whole wafer surface can be inspected at high speed. And by fixing an encoder to the stage, positional data of the wafer defect can be obtained.

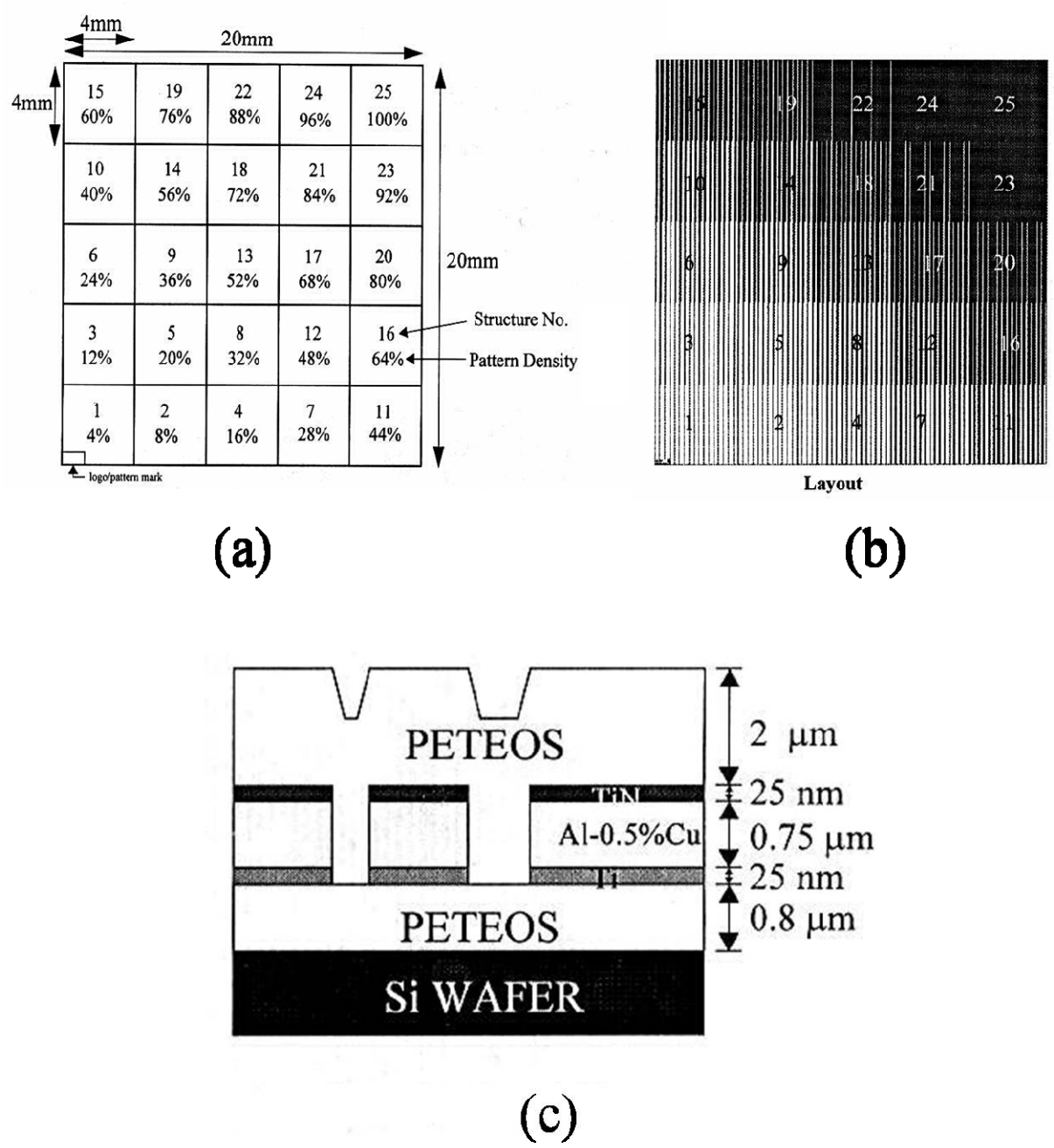

Figure 3-1. Layout of the SKW-1 pattern wafer: (a) pattern density and pitch size layout, (b) mask floor plan, and (c) cross-sectional view[61]

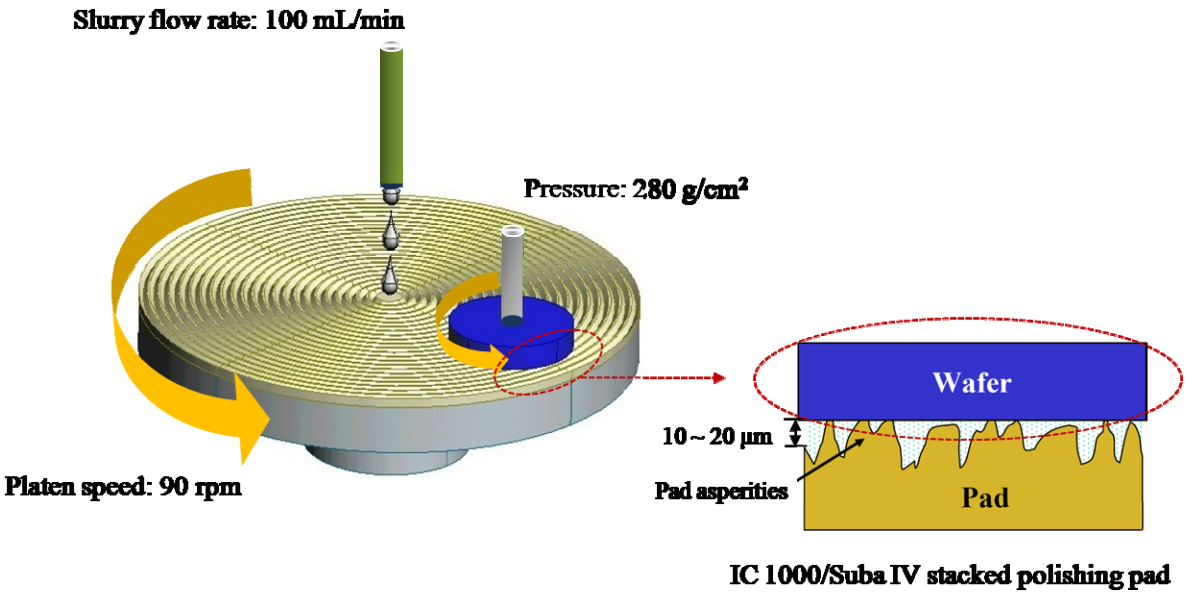

Figure 3-2. Schematic diagram of rotational CMP tool

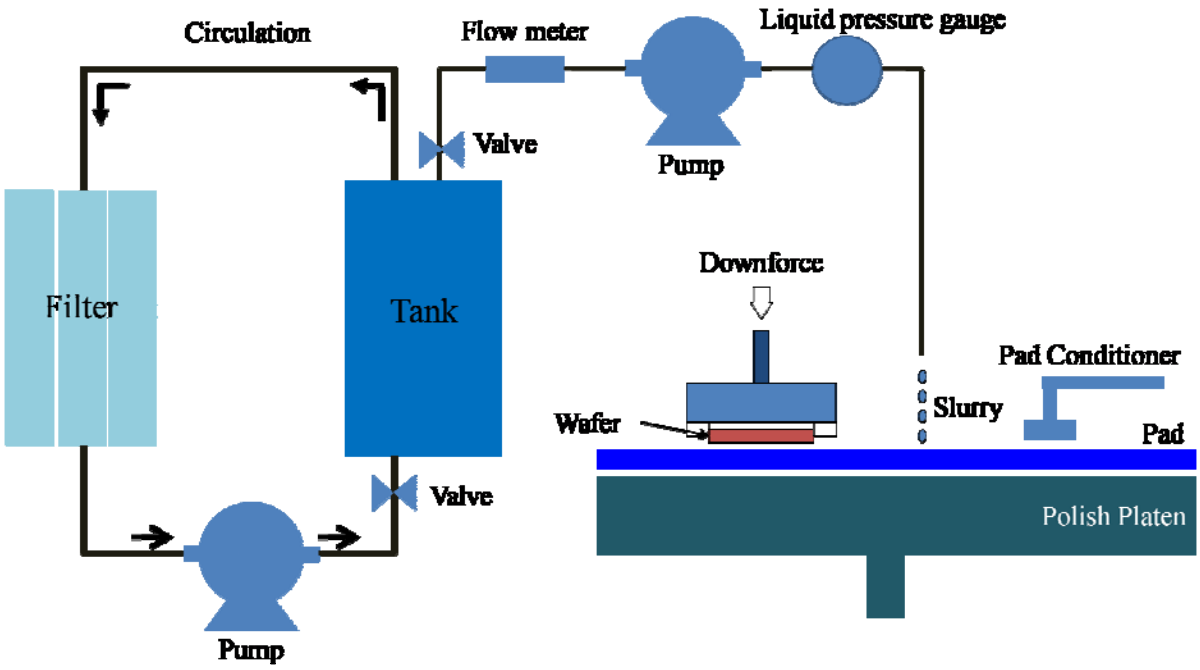

Figure 3-3. Schematic illustration of a slurry delivery system

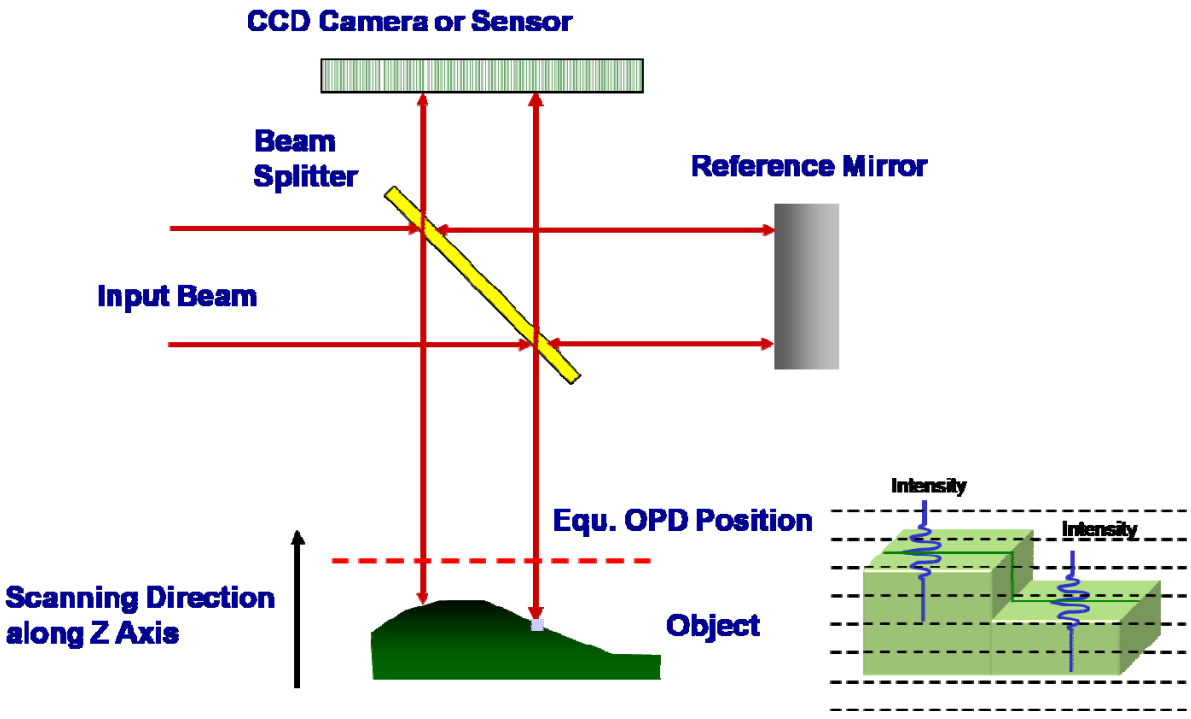

Figure 3-4. Diagram of film thickness measurement system using NanoSpec

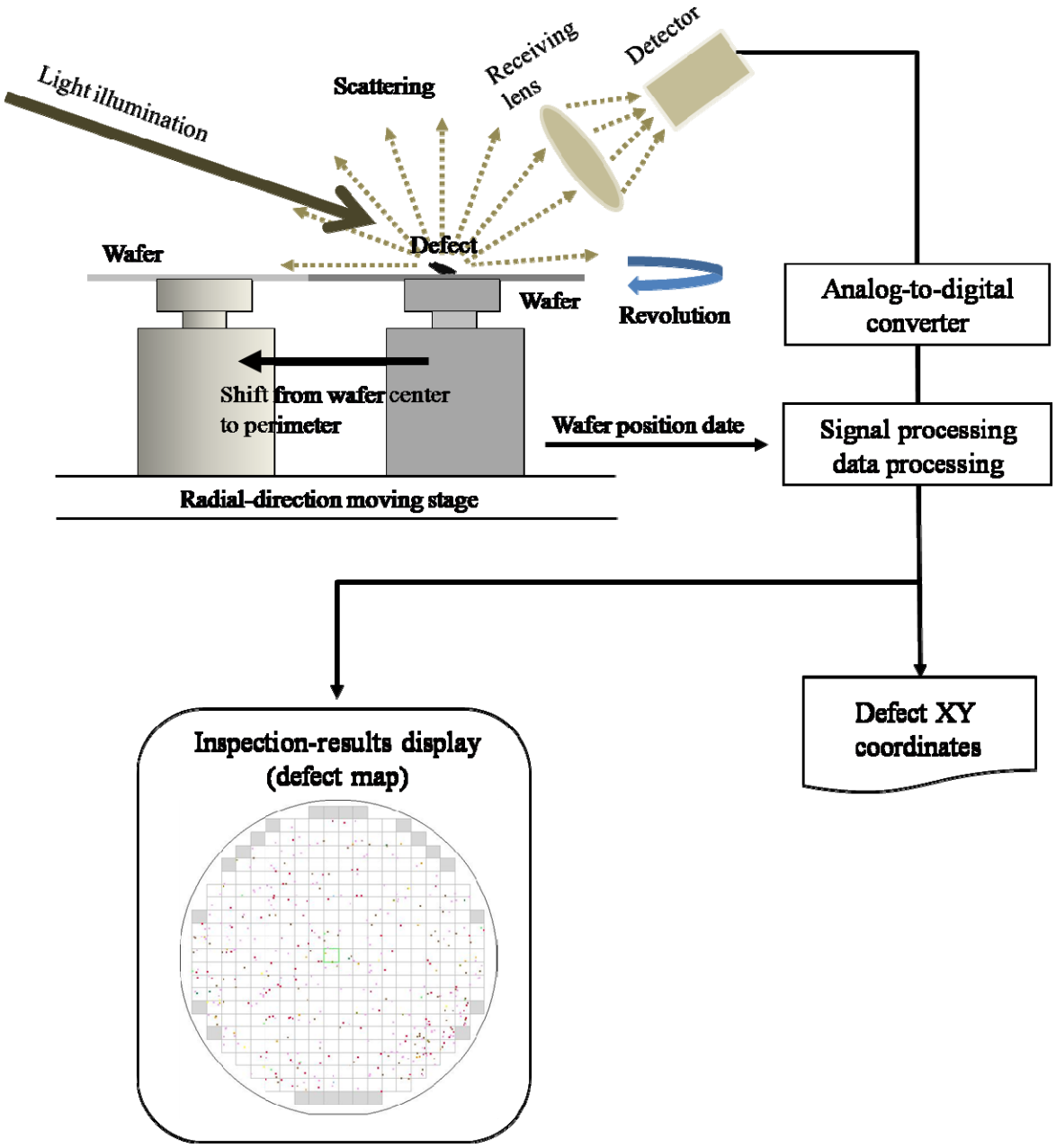

Figure 3-5. Schematic illustration of light scattering analysis[60]

CHAPTER 4
NOVEL METHOD TO CONTROL THE SIZE OF SINGLE CRYSTALLINE CERIA PARTICLES BY HYDROTHERMAL METHOD AND ITS CMP PERFORMANCE

Introduction

This chapter is devoted to the studies on synthesis of single crystalline ceria particles by using hydrothermal method and its CMP performance. During the past decade, the usual method for synthesizing ceria abrasives is thermal decomposition of the cerium salt such as cerium carbonate and cerium hydroxide.[8] These ceria abrasives have polycrystalline structure with an easily brittle system, which affects a high removal rate of oxide films during polishing.[35] However, the size and the shape of ceria abrasives are very limited since particle growth is difficult to control during calcination process. The irregular shape and aggregates lead to defects on the surface of film during CMP process. To achieve the desired particle size and the uniform particle size distribution, thermal technique requires a complicated combination of mechanical milling process and filtration system.[41] Other methods for preparing ceria abrasives are liquid phase processes.[62,63] Other methods for preparing ceria abrasives are liquid phase processes, such as precipitation method, [42] hydrothermal method, [43-45] sol-gel method[46] and electrochemical method. [47] Among these approaches, hydrothermal synthesis is an attractive method for the preparation of crystalline ceramic oxide particles and has been employed for the synthesis of fine particles at relatively low temperature. The hydrothermally synthesized particles have excellent homogeneity and particle uniformity without post-heat treatment. However, the size of ceria particles obtained from conventional hydrothermal synthesis is limited to less than 100 nm leading to a low removal rate during CMP process.

To overcome this problem, this research introduced a new type of ceria precursor in hydrothermal synthesis. This precursor was synthesized by alkoxide method, which employs alcohols with different dielectric properties as solvent. Over the past years, several researches using the mixed solvent system showed the possibility to increase the controllability of ceramic morphology. Park et al.[64] introduced the alcohol/water mixed solvent to thermally hydrolyze titanium tetrachloride ($TiCl_4$) in the preparation of spherical titania (TiO_2) particles. The DLVO (Derjaguin Landau Verwey Overbeek) theory was proposed to explain the effect of the alcohol/water mixed solvent on the morphology of the particles. Fang et al.[65] found that the morphology of titania particles was controlled by the dielectric constant of the solvents, which can be regulated by changing the volume ratio of n-propanol to water. Hu et al.[66] employed the alcohol/water mixed solutions for synthesizing zirconia particles. They found that the dielectric property of the mixture affects the nucleation and growth of the zirconia particles. However, these reports about the mixed solvent system were focused on formation of metal oxide through precipitation reaction. In addition, synthesis of single crystalline ceria particles of more than 100 nm under solution phase has not been reported yet. Furthermore, previous studies for the polishing performance of ceria abrasives have limited to polishing behaviors of polycrystalline ceria particles for silica layer and have mainly focused on the chemical interactions between ceria abrasives and silica layer during CMP process.

Therefore, the first purpose of the present work is to control the morphology of the ceria crystallites under hydrothermal conditions using a new type of ceria precursor obtained by precipitation method and investigate the effects of the dielectric property of

organic solvent on formation of ceria particles. In addition, the influences of the hydrothermal temperature and an acidic hydrothermal medium on particle characteristics have been studied. This study will provide the new approach to modulate the particle size of ceria crystallites using hydrothermal method. The second purpose of the present work is to investigate the effects of single crystalline ceria abrasives on silicon oxide and silicon nitride CMP. The single crystalline ceria particles as abrasives for ceria-based slurry have seldom been applied to CMP processing. In this chapter we synthesized the single crystalline ceria particles of different mean sizes using hydrothermal method. For CMP performance evaluation, the effect of single crystalline ceria abrasives on the removal rate, the oxide-nitride removal selectivity and within-wafer nonuniformity (WIWNU) was investigated.

Materials and Methods

Abrasives

Preparation of sol-type ceria precursor

Cerium (III) nitrate hexahydrate ($Ce(NO_3)_3 \cdot 6H_2O$) and potassium hydroxide (KOH) were used as the starting materials for the ceria precursor. Cerium (III) nitrate hexahydrate and potassium hydroxide were separately dissolved in distilled water with a desired concentration and then mixed with the various kinds of alcohols. The volume ratio of alcohol to water was kept at 2:3. Alcohols, including methanol (CH_3OH), ethanol (C_2H_5OH), ethylene glycol ($C_2H_6O_2$) and 1, 4-butylene glycol ($C_4H_{10}O_2$) were used to investigate the influence of the dielectric constant of the mixed solvents. The reaction was carried out at a temperature of 50 ^oC with stirring rate of 100 rpm for 12 h. Air was bubbled into the precipitation reactor with passage through a gas distributor as an oxidizer. The precipitated ceria precursor was separated via centrifugation and then

redispersed in distilled water under continuous stirring. The weight ratio of distilled water to a precipitated ceria precursor was kept 5:1. The pH of the suspension solution was adjusted at pH 0.5 to 4.0 by adding concentrated nitric acid (HNO_3). After reaction, light yellow solution was obtained.

Hydrothermal synthesis of ceria particles

The sol-type ceria precursor was put into an autoclave with a reaction chamber of 100 cm^3. Three quarters of the volume of the chamber was filled with the light yellow solution. The hydrothermal reactions were carried out at 150 to 230 ^oC for 6 h, corresponding to a pressure range from 200 to 800 psi. After the hydrothermal reaction, the synthesized particles were washed with distilled water three times and were subsequently dried at 90 ^oC.

CMP Evaluation

Preparation of ceria-based slurries

Different ceria-based slurries were formulated by dispersing abrasives each with different primary particle size in DI water containing an anionic organic polymer (Poly acrylic acid, PAA; Mw 4000, LG Chem.) as dispersant. 2 wt% of PAA based on the total weight of the ceria abrasives was added. For each slurry, pH was adjusted to 6.5 ~ 6.7 by adding ammonium hydroxide (NH_4OH). The solid loading of ceria abrasives was fixed to 2.0 wt%.

CMP tools and consumables

Silicon dioxide film of 2 μm thick was grown on a 5-in. p-type silicon substrates with (001) orientation by plasma enhanced chemical vapor deposition (PECVD). The silicon nitride films were deposited by using low-pressure chemical vapor deposition (LPCVD). Polishing tests were performed on a rotary type CMP machine (GNP POLI

400, G&P technology) for one minute with each of the ceria-based slurries. IC 1000/SUBA IV stacked pads (supplied by Rodel Inc.) were utilized as CMP pads. The downforce was 4 psi and the rotation speed between the pad and the wafer was 100 rpm. The slurry flow rate was 100 mL/min.

Characterization

Abrasives

The crystal structure and grain size was identified by x-ray diffraction (XRD) using CuKα radiation. The grain size was estimated by the Scherrer equation according to the formula $D = 0.9 \lambda / (\beta \cos \theta)$, where D is the grain size, λ is the wavelength of x-rays, β is the half-width of the diffraction peaks, and θ is the diffraction angle. The broadening of the reflection from the (111) plane was used to calculate the grain size. The morphology and size of the precipitate particles were examined by high resolution transmission electron microscope (HRTEM) and field emission scanning electron microscope (FESEM). The average primary particle size was calculated by measuring ca. 100 particles from FESEM micrographs. The specific surface area (SSA) of the ceria abrasives was determined by Brunauer-Emmett-Teller (BET) method using nitrogen adsorption/desorption at 77 K.

Ceria-based slurry

The abrasive size distribution of slurry was measured using light scattering method (UPA 150, Microtrac Inc.).

CMP performance

The film thickness on the wafers before and after CMP was measured using spectroscopic reflectometry (Nanospec 6100, Nanometrics) to calculate the removal rate. In this experiment, the WIWNU was defined as the standard deviation of remaining

thickness divided by the average of the remaining thickness after the CMP process. The average polishing data for removal rate was carried by performing the same tests more than three times in order to support the validity of the results from the statistical viewpoint.

Results and Discussion

Preparation of Ceria Particles

Influence of solvent type on ceria particle characteristics

The XRD patterns of the synthesized particles are shown in Fig. 4-1. The 0.5 M of cerium (III) nitrate hexahydrate solution and the 0.5 M of potassium hydroxide solution were mixed with the various kinds of alcohols in precipitation reaction. The synthesized ceria precursors were hydrothermally treated at 230 ^{o}C after adjusting to pH 3.0. The dielectric constant of alcohols decreases in the following order: ethylene glycol (41.4) > methanol (33.0) > 1, 4-butylene glycol (31.9) > ethanol (25.3).[67,68] As shown in Fig. 4-1, the major reflections associated with fluorite structure of ceria can be observed on all specimens regardless of the kinds of alcohols used to prepare the ceria precursors.

Fig. 4-2 shows the HRTEM image of the ceria particles which were synthesized from the mixed solvent of water and ethylene glycol. They appear to be single crystalline structure based on the fact that the lattice fringes corresponding to reflections are clearly observed. Fig. 4-3 shows the FESEM micrographs of ceria particles prepared in different mixed solvents. The synthesized particles were prepared without hard aggregates. It is interesting to note that the ceria particles prepared using higher dielectric constants show bigger morphology in spite of using same processing parameters and steps. The average particle size of the ceria particles increased in proportion to dielectric constant of alcohol used in the precipitation reaction as shown in

Fig. 4-3. These results indicate that the alcohol affects the physical properties of the reaction medium without changing the reaction paths and arrangements of the crystal structure.

This can be quantitatively seen from Fig. 4-4. The curve (a) depicts the average particle size whereas curve (b) shows the crystallites size with respect to the dielectric constant of alcohols used in the mixed solvent. It is found that the size and the crystallites size of ceria particle increased with increase in the dielectric constant. These results indicate that the solvent type may affect properties of the synthesized particles because different alcohols show different dielectric constant and different affinity forwards water.

The dielectric constant of a solvent is the quantitative measure of its ability to decrease attraction between two oppositely charged ions. The dielectric constant is defined by the free energy for the coulomb interaction between two charges. The relationship between the concentration of a saturated solution in equilibrium and dielectric constant can be expressed as following.[69]

$$X_l = \exp(\frac{-\Delta\mu^i}{kT}) \approx \exp\left[-\frac{z_+ z_- e^2}{4\pi\varepsilon_0 \varepsilon kT(a_+ + a_-)}\right] \quad (4\text{-}1)$$

where the X_l is identified with the solubility of solute in any solvent. $\Delta\mu^i$ is the difference in energy when going from the associated state to the dissociated state of two systems. a_+ and a_- are ionic radii of ions charged z_+ and z_- and ε is the dielectric constant of the medium and e represents the elementary charge (e = 1.602 X 10^{-19} C). As can be seen from the equation (1), the solubility of the solute is larger when the dielectric constant of the solution is higher. This infers that the solubility is larger as

increasing the dielectric constant and can be adjusted by changing the dielectric constant of solution.

According to the classical nucleation theory,[70] the particle size is dependent on the supersaturation of solute, which affects strongly the nucleation rate. This can be expressed in the form of the Arrhenius velocity equation.[70]

$$J = A\exp\left[-\frac{16\pi\gamma^3\upsilon^2}{3k^3T^3(\ln S)^2}\right] \quad (4\text{-}2)$$

where J is the nucleation rate, A is the rate constant, γ is interfacial tension between the solute and the solution, υ is the number of ion formula units, k is the Boltzmann constant and S is the supersaturation of solute. This equation indicates that the increase in supersaturation induces a great number of nuclei due to the rapid increase of the nucleation rate.

Additionally, the relationship between solubility and the radius of nuclei can be expressed by the basic Gibbs-Thomson equation.[70]

$$\ln\left[\frac{X}{X_l}\right] = \ln S = \left[\frac{2V_m\gamma}{\upsilon RT\rho r}\right] \quad (4\text{-}3)$$

where X is the concentration of solution, S is the supersaturation of solute, ρ is the density of the solid, V_m is the molar mass of the solid in the solution and R is the gas constant. With increasing solubility of the solute, the supersaturation of the solute is decreased. Moreover, the nuclei radius is proportional to the solubility of the solute. From (1) to (3) equations, it can be found that the dielectric constant of solution affects nucleation rate and the radius of nuclei. Moreover, the size of crystallites can be modulated by varying the solvent type.

In this work, the nucleation rate has been modulated by changing of the dielectric constant of mixed solvent. A number of nuclei are decreased with increasing the dielectric constant of alcohols used in precipitation reaction. Therefore, the crystallites size and the morphology of the ceria particles increased with the increase of dielectric constant of the solvent.

Effect of the precipitation participating anions on nucleation and growth

Fig. 4-5 shows FESEM micrographs of the ceria particles synthesized from different ceria precursors which were precipitated in the mixed solvent of ethylene glycol and water using different concentrations of potassium hydroxide. The hydrothermal reactions were carried out at 230 ^{o}C for 6 h. As shown in Fig. 4-5, it is found that the size of ceria particles was strongly dependant on the potassium hydroxide concentration. Particle size was decreased with the increase in potassium hydroxide concentration.

The formation of ceria particles involves a series of chemical reaction[71] and the whole process can be classified into four stages.[72] During these stages, hydrated cerium hydroxide complexes were generated and dehydrated. Precipitation participating anions (OH^-) were generated via the hydrolysis of potassium hydroxide with the molecular water of cerium salt. Precipitation participating anions were exhausted by hydration of tetravalent cerium ions (Ce^{4+}) and subsequently caused the decrease in the pH. Moreover, the formation of crystalline particles includes usually two steps: nucleation and growth. In order to prepare the particles with designed size, both steps should be controlled. In nucleation step, the increase of nuclei induces the smaller particle size. In growth step, secondary nucleation occurs in high supersaturation because crystal growth has a lower energy barrier than that of the nucleation.

In order to investigate the effect of precipitation participating anions on the formation of ceria particles, 0.5 M and 1.5 M of potassium hydroxide solution added in cerium salt solution and the pH of these solutions was kept 7.8 and 11.6, respectively. The pH of the solution was changed to 4.4 and 9.1 after precipitation for 12 h, respectively. It is attributed to the fact that precipitation participating anions under basic solution are more slowly consumed during growth of nuclei. This result indicates that increasing precipitation participating anions induces continuously the large number of nuclei and the decrease of solubility which help to decrease the growth rate. Under basic condition, the solubility product is much higher than the solubility constant, meaning the supersaturation (S) is very large.[73]

$$S = \frac{[Ce^{3+}][OH^{-}]}{K_{sp}} \quad (4\text{-}4)$$

where K_{sp} is the solubility constant of $Ce(OH)_3$. A high supersaturation induces a great number of nuclei due to secondary nucleation. Therefore, the crystallites size and the particle size of ceria decrease with increasing precipitation participating anions.

Effect of hydrothermal conditions

The effect of an acidic hydrothermal medium on the formation of ceria particles is shown in Fig. 4-6. Ceria precursor was synthesized using the mixed solvent of ethylene glycol and water with 0.5 M of potassium hydroxide solution. With decreasing the pH of the solution, the size of the ceria particles increased under hydrothermal condition. This result is related to Ostwald ripening phenomena in the liquid phase system .[74] Wu et al. found that the acidity of hydrothermal medium played a key role in dissolution of smaller particles, which directly influences the structure. In this work, the increase in hydrogen ions led to a sizable increase in the solubility of the ceria precursor. This implies that the

solute diffuses quickly and the crystal growth is more rapid with dissolution of the cerium precursor in an acidic medium.

The effect of the hydrothermal treatment temperature on the crystalline size is summarized in Fig. 4-7. The crystallites size was increased with an increase in hydrothermal treatment temperature. Under hydrothermal conditions, the concentration of the hydrogen ion (H^+) is increased with increasing temperature.[43,74] It appeared that higher temperature in hydrothermal reaction promotes the crystal growth in the ceria particles from the hydrated cerium hydroxide complexes according to the dissolution-precipitation mechanism.

CMP Performance

Ceria abrasives

Fig. 4-8 shows the four types of abrasive particles prepared in different hydrothermal conditions as described in Table 4-1. The primary particle sizes determined in the FESEM examination were 62, 116, 163, and 232 nm for slurry A, B, C and D, respectively. The well-dispersed particles of spherical shape as shown in Fig. 4-8(a) were transformed into square shape as a result of grain growth which is clearly seen from FESEM image (Fig. 4-8(d)). These images indicate that the primary particle size increases with hydrothermal temperature and strength of acidic medium and the morphology of abrasives can be controlled by changing the hydrothermal conditions, which affect the grain growth of ceria crystallites.

The major reflections associated with cubic fluorite structure of ceria can be observed from the XRD pattern as shown in Fig. 4-9. Sharp intensity peaks are observed for ceria abrasives with increased primary particle size. The average grain size of various abrasives were calculated from the Scherrer equation by using the line-

broadening of the (111) peak in XRD pattern. The grain size gradually increased from 29 nm to 66 nm as the hydrothermal temperature and the acidity of hydrothermal medium were increased. This result coincides with the trend of increasing primary particle size in the FESEM images shown in Fig. 4-8.

Fig. 4-10 shows the high resolution TEM images of two samples with average particle diameters of 62 nm and 232 nm, respectively. As shown in the Fig. 4-10(a), the sample with diameter of 62 nm appears to be well-defined crystallites based on the fact that the lattice fringes corresponding to the (111) reflections are clearly observed from the crystal orientation. For 232 nm ceria particle, the TEM image (Fig. 4-10(b)) shows homogenous single phase of the lattice fringes without disorder and defects in the lattice. These results indicate that ceria abrasives used in this study have a single crystalline structure regardless of grain growth and particle size.

Well-crystalline ceria (CeO_2) particles were synthesized by using sol-type ceria precursor under hydrothermal conditions at pH 0.5 to 4.0. The ceria precursor was prepared by chemical precipitation in mixed solution of water and alcohols, including methanol, ethanol, 1,4-butylene glycol and ethylene glycol (EG), separately. The resultant particles exhibit cubic fluorite structure with size ranged from 20 to 400 nm. The particle sizes were determined by XRD and SEM analyses. The results showed that the crystallites size and the morphology of the hydrothermal ceria particles increased with an increase in the dielectric constant of alcohols used in precipitation reaction and hydrothermal treatment temperature and a decrease in the pH of hydrothermal medium, which affect nucleation rate and crystal growth. Consequently,

the size of ceria particles was easily controlled in the range from 20 nm to 400 nm without post-heat treatment.

Characteristics of ceria abrasive before and after CMP

To evaluate the effects of single crystalline ceria abrasives, Polishing tests for four types of slurries with different abrasive particle size were preformed. Fig. 4-11 shows the particle size distribution of different slurries without PAA dispersant. The size distribution of secondary particle size determined by light scattering method were 178, 273, 326, and 484 nm for slurry A, B, C and D, respectively. The dispersed particle size is much larger than the crystallite size estimated by X-rays and the primary particle size calculated by FESEM. This mismatch in size is due to extensive overlapping of the ceria particles in water-based solution.[75] As shown in Fig. 4-11, the increase in size of the primary particles led to broader particle size distribution in water-based solution. Fig.4-12 shows the FESEM images of ceria abrasives before and after silicon dioxide polishing for slurry D. The ceria abrasives after polishing were washed with distilled water three times via centrifugation. According to Fig. 4-12, no definitive difference between both abrasives before and after polishing can be seen except that square edges of some abrasives were changed to round edges after polishing. This indicates that the single crystalline ceria abrasives synthesized in this study are less brittle and don't fracture upon applied pressure during polishing.

Polishing performance

Fig. 4-13 shows the results of CMP field evaluation and quantitative results of the slurry are presented in the Table 4-2. For oxide CMP process, it is clear that the removal rate increases with increasing size of ceria abrasives. The polishing of oxide film is mainly affected by the chemical contribution of ceria particles and mechanical

factors, such as the CMP conditions, morphological characteristics of abrasives and particles size distribution. During the polishing of the oxide film, ceria abrasives exhibit a chemical tooth property.[12] As a consequence, chemical interaction between the silica film and the ceria abrasives occur during CMP process and Si-O-Ce bonding is formed on the surface of silica film. The Si-O-Ce bonds can be rapidly removed by the mechanical force generated by pressed pad. This physicochemical reaction leads to the high removal rates of oxide film. Furthermore, polishing behavior is closely associated with shape and size of the ceria abrasives. As shown in Fig. 4-8, the shape of the small abrasives (Fig. 4-8(a) and (b)) is spherical, whereas the large abrasives (Fig. 4-8(a) and (b)) have a square shape with sharp edges. The sharp edge and large size of abrasive particles can induce higher local pressure to generate more frictional force during polishing.

The removal rate of nitride film increases with the increase in the abrasive size. According to previous report,[76] the removal rate of nitride film is affected by the physical properties of ceria-based slurry systems and the amount of surfactant adsorbed on the film surface. In order to improve the selectivity and uniformity, an anionic acrylic polymer is generally used to passivate the surface of the nitride film during STI-CMP, which prevents ceria abrasives from contacting the film surface.[30] In this study, the amount of polymer added was same for all the slurries. Therefore, it seems that the increase in removal rate of the nitride film is related to the mechanical factors rather to the effect of adsorbed polymer passivation layer. These mechanical factors are influenced by several physical parameters of the CMP process, such as morphological aspects of the abrasives, crystallite size of the abrasives and the CMP conditions.

The removal selectivity can be calculated by comparing the removal rate between oxide and nitride film. As shown in Fig. 4-13, the removal selectivity showed a transition behavior at the slurry C. The removal rate of oxide film rapidly increased from 1174 Å/min at 62 nm to 2369 Å/min at 163 nm, whereas it slowly increased to 2674 Å/min for 232 nm. This phenomenon is explained by two related factors: the contact area reduction[17] and the particle surface activity.[76] In the case of oxide CMP process, the polishing behavior should be also considered from the viewpoint of the contact area between the abrasives and the film surface. According to contact area mechanism,[16,54] the removal rate increases with decreasing abrasive size and increasing solid loading, due to the increase in contact area between the abrasives and the film surface. At a fixed solid loading, the number of ceria abrasives in slurry decrease as the abrasive size increases which leads to relatively low removal rate for the target material during CMP process even though the abrasive size increases. For nitride film, the removal rate increased slightly and did not vary much with increasing abrasive size, which can be explained by the relationship between additive polymer and abrasive size. The additive polymer can be more easily attached on the surface of the small abrasives than on the surface of large ones, due to high surface activity and specific surface area of the small abrasives. The slurry with small abrasives can induce a relatively high removal rate for nitride film in comparison with its abrasive size, since the passivation layer is insufficiently formed on the nitride film surface as polymer is largely adsorbed on the particle surface. As described in Table 1, the specific surface area decreased with increasing abrasive size. This means that removal rate for nitride film can be relatively increased in spite of decrease in the abrasive size. As a result, the removal rate of

nitride film showed relatively low increase in rates with increase in the abrasive size. Such behavior is suggestive of existence of an optimum size of ceria abrasives for high removal selectivity.

Additionally, the results for surface uniformity of the oxide films are shown in Fig. 4-14. The slurry shows a higher WIWNU for the oxide film with increase in the size of ceria abrasives. This polishing behavior is attributed to a broader particle size distribution of the slurry and the shape of the large abrasives. The distribution data in Fig. 4-11 shows that the particle size distribution broadens with the increase in abrasive size. The broader particle size distribution of large abrasives can cause different removal rates between the center and the edge of the wafer due to their limited mobility on the wafer surface. This result is also consistent with the observations of Moudgil et al.[54] They investigated the polishing mechanism of slurry with non-uniform particle size distribution, which not only created surface deformation but also changed the polishing removal rate. In this report, the sharp edge of the abrasives can be regarded as another factor for roughness of wafer. The film abraded by the sharp edge has a higher local pressure to generate more friction force during polishing. This can induce a significant increase in the local surface roughness caused by pit formation on the wafer surface.[15] As a result, the surface uniformity shows deterioration with increase in abrasive size. Therefore, it seems that surface uniformity of oxide film is related to the mechanical factors and morphological properties of ceria abrasives and particle uniformity of the ceria-based slurry. Interestingly, there exists an optimum abrasive size distribution at which enhanced removal rates and selectivity are observed.

Conclusions

Synthesis of Ceria Particles by Hydrothermal Method

Well-crystalline ceria (CeO_2) particles were synthesized by using sol-type ceria precursor under hydrothermal conditions at pH 0.5 to 4.0. The ceria precursor was prepared by chemical precipitation in mixed solution of water and alcohols, including methanol, ethanol, 1,4-butylene glycol and ethylene glycol (EG), separately. The resultant particles exhibit cubic fluorite structure with size ranged from 20 to 400 nm. The particle sizes were determined by XRD and SEM analyses. The results showed that the crystallites size and the morphology of the hydrothermal ceria particles increased with an increase in the dielectric constant of alcohols used in precipitation reaction and hydrothermal treatment temperature and a decrease in the pH of hydrothermal medium, which affect nucleation rate and crystal growth. Consequently, the size of ceria particles was easily controlled in the range from 20 nm to 400 nm without post-heat treatment.

CMP Evaluation

In this study, we investigated the effects of single crystalline ceria abrasives on polishing performance during silicon dioxide and silicon nitride CMP. The abrasive size was directly controlled by varying hydrothermal conditions without post-heat treatment and mechanical milling process. The resultant abrasives have a single crystalline phase regardless of the size of particles. The results showed that the single crystalline ceria abrasives were not easily broken-down by mechanical force between abrasives and film surface during polishing. With increasing abrasive size, the removal rate of silicon dioxide and silicon nitride films increased. On the other hand, the surface uniformity deteriorated with increasing abrasive size, due to a broader particle size distribution of

the abrasives in slurry and the morphology of the large abrasives. In addition, the removal selectivity showed a transition at the slurry C (with particle size of 163 nm). Considering these polishing behaviors of single crystalline ceria abrasives, it was found that there exists an optimum abrasive size for optimum removal rate and selectivity in silicon dioxide and silicon nitride CMP.

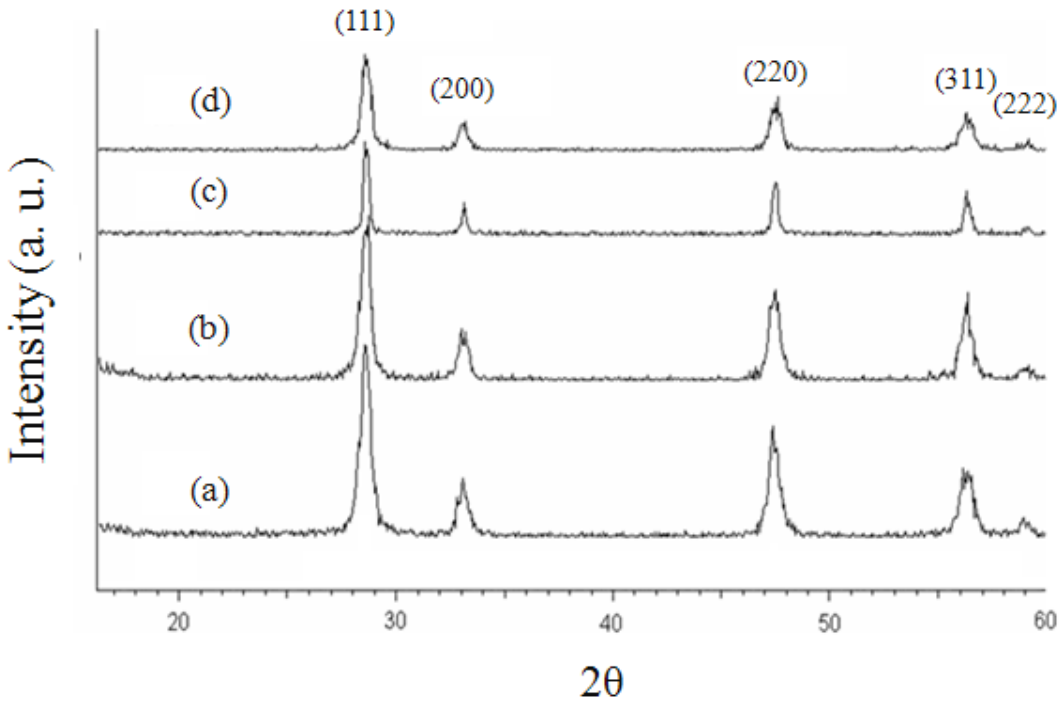

Figure 4-1. XRD patterns of ceria particles synthesized from the mixture of water and different alcohols; (a) ethylene glycol, (b) methanol, (c) 1,4-buthylene glycol, (d) ethanol

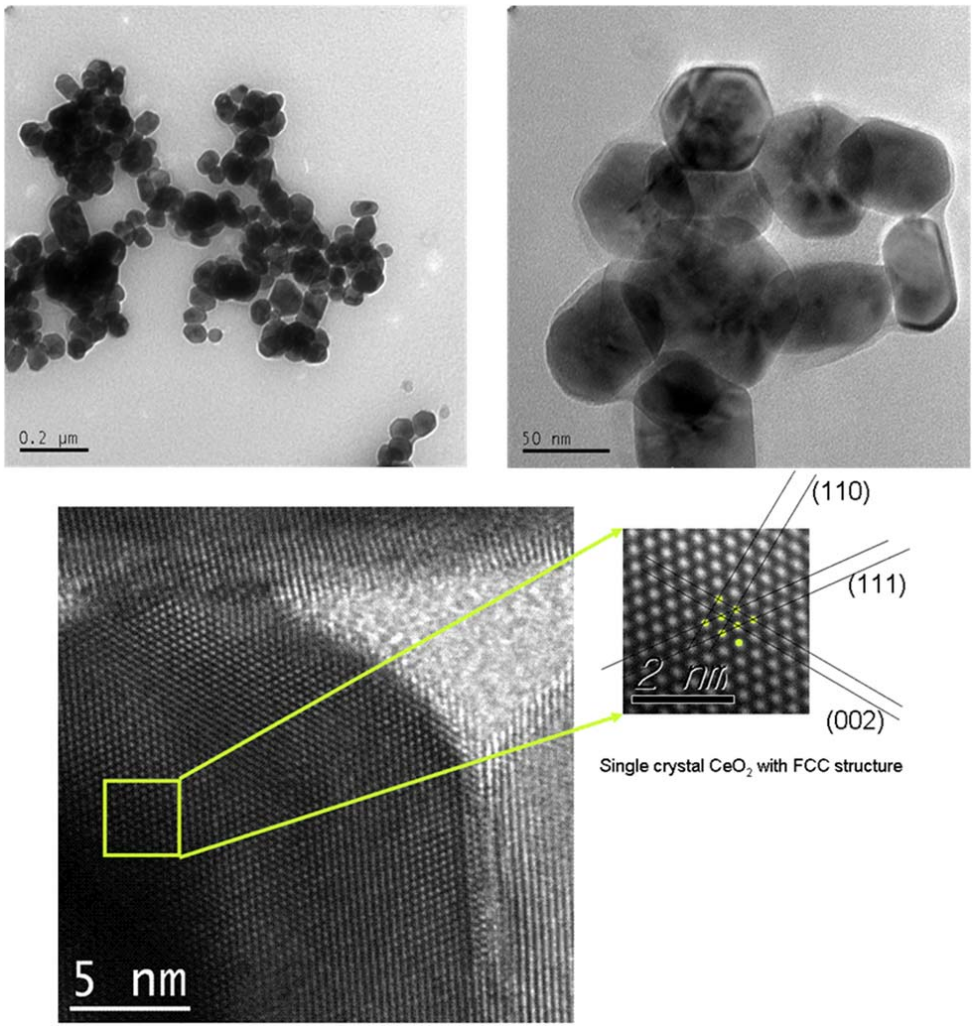

Figure 4-2. FETEM photomicrographs of ceria particles obtained by hydrothermal method using a new type of ceria precursor

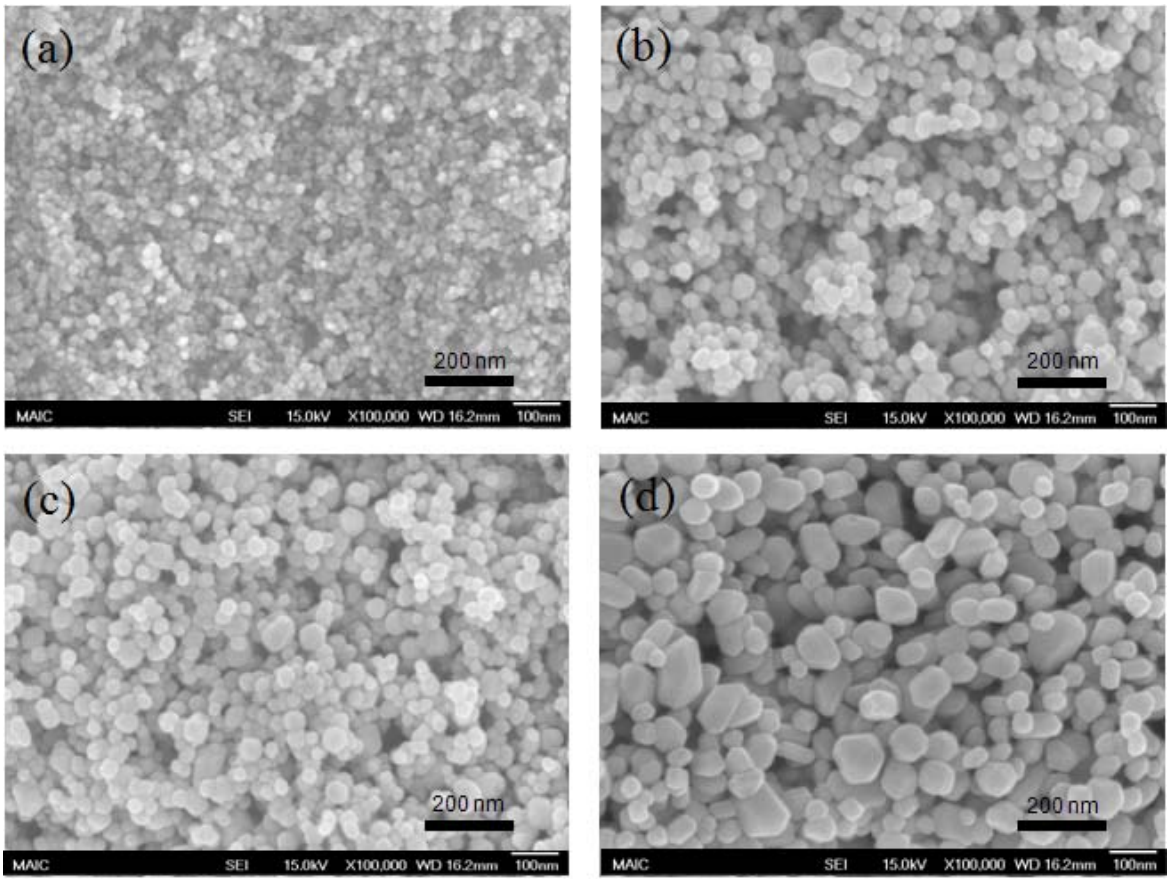

Figure 4-3. FESEM photographs of ceria particles prepared from the mixture of water and different alcohols; (a) ethanol, (b) 1,4-buthylene glycol, (c) methanol, (d) ethylene glycol

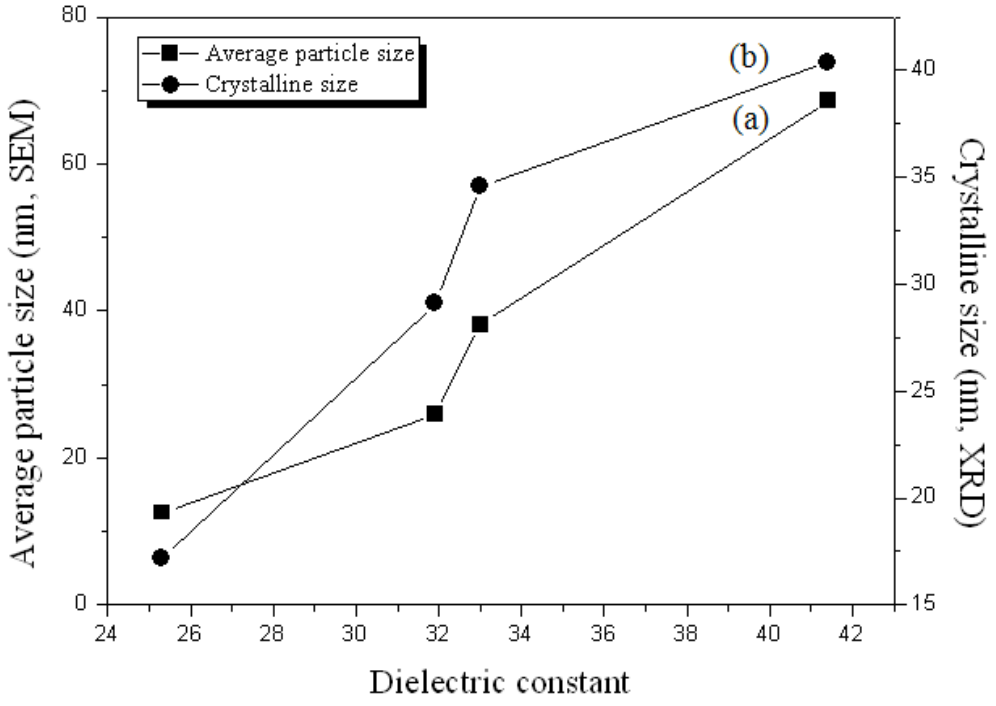

Figure 4-4. (a) Average particle size and (b) crystallites sizes of ceria particles synthesized with different dielectric constants of alcohols

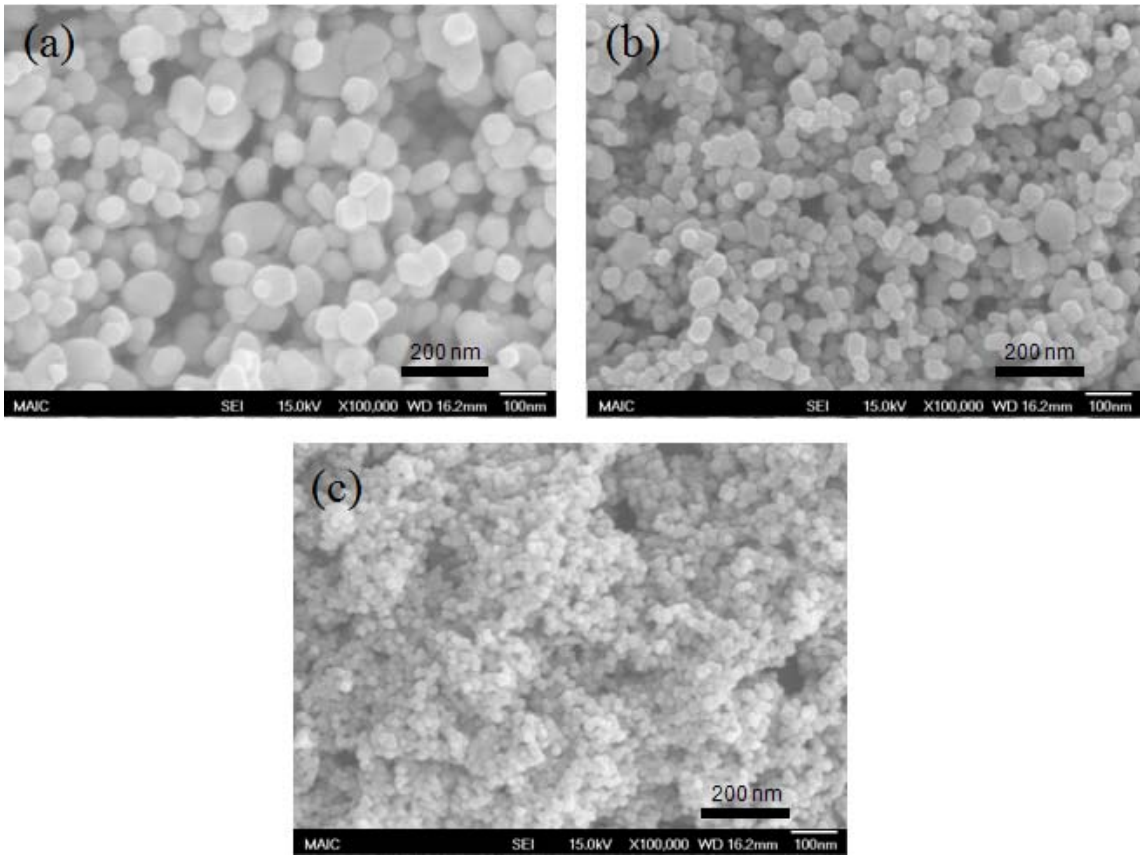

Figure 4-5. FESEM photographs of ceria particles prepared with different concentrations of potassium hydroxide; (a) 0.5 M, (b) 1.0 M, and (C) 1.5 M

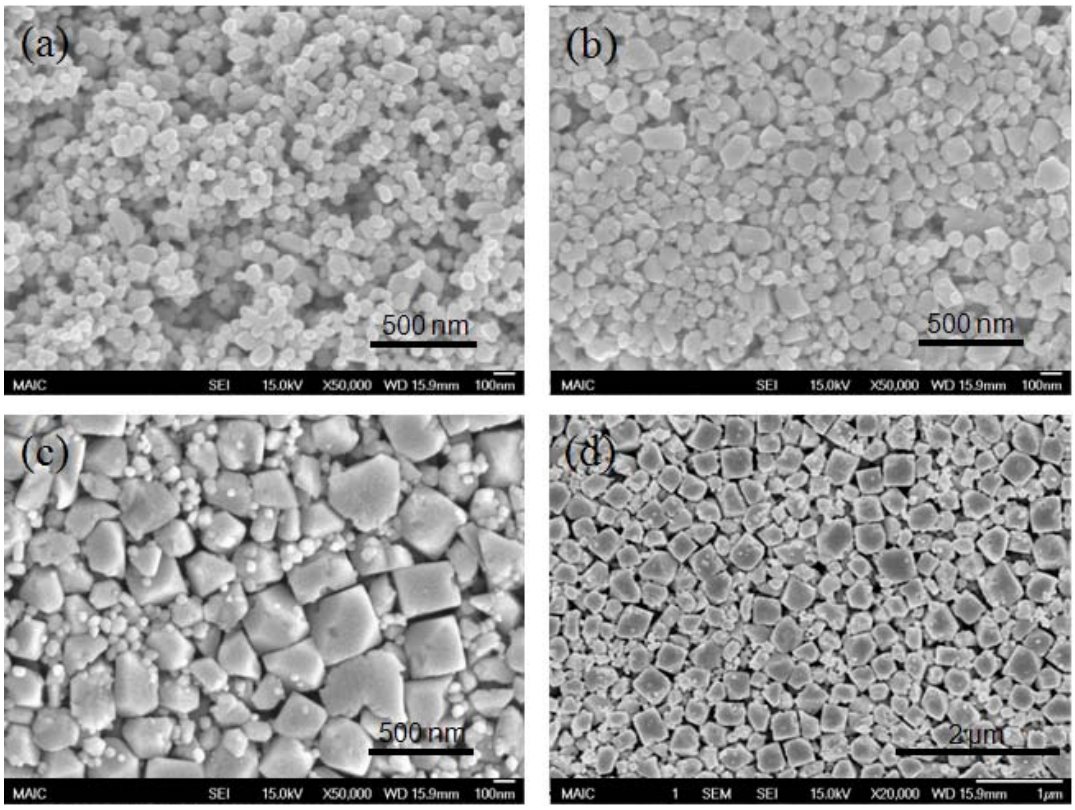

Figure 4-6. FESEM photographs of ceria particles prepared from different concentrations of nitric acid in hydrothermal conditions at 230 ^{o}C for 12 hr. ; (a) pH 4, (b) pH 2.5, (c) pH 0.5 and (d) pH 0.5

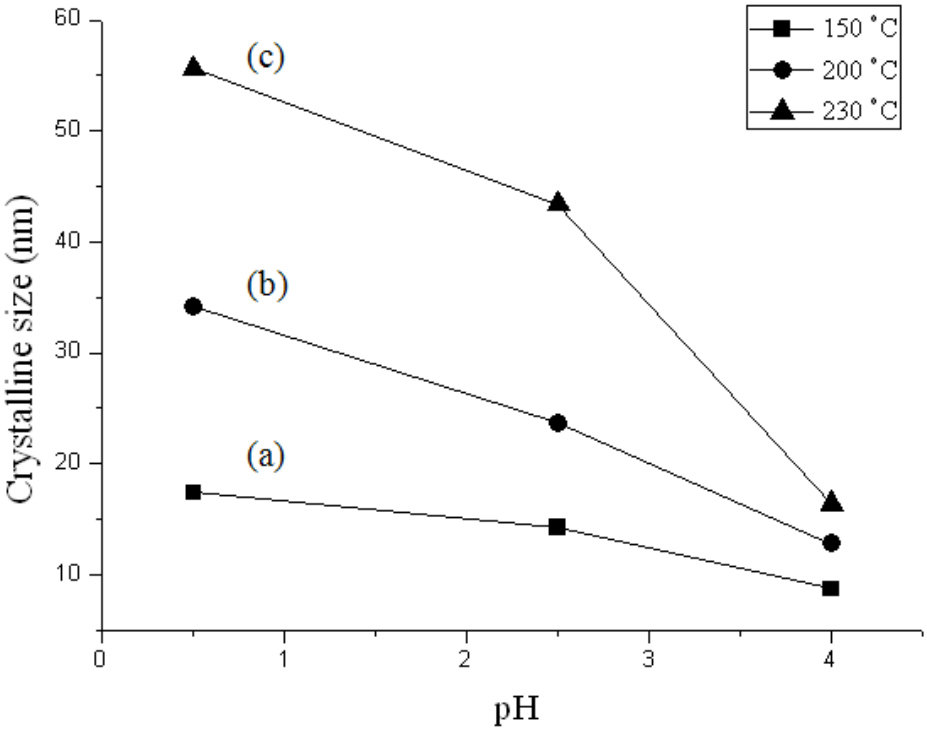

Figure 4-7. Crystallites size for ceria particles prepared from different pH at (a) 150 ^{o}C, (b) 200 ^{o}C and 230 ^{o}C

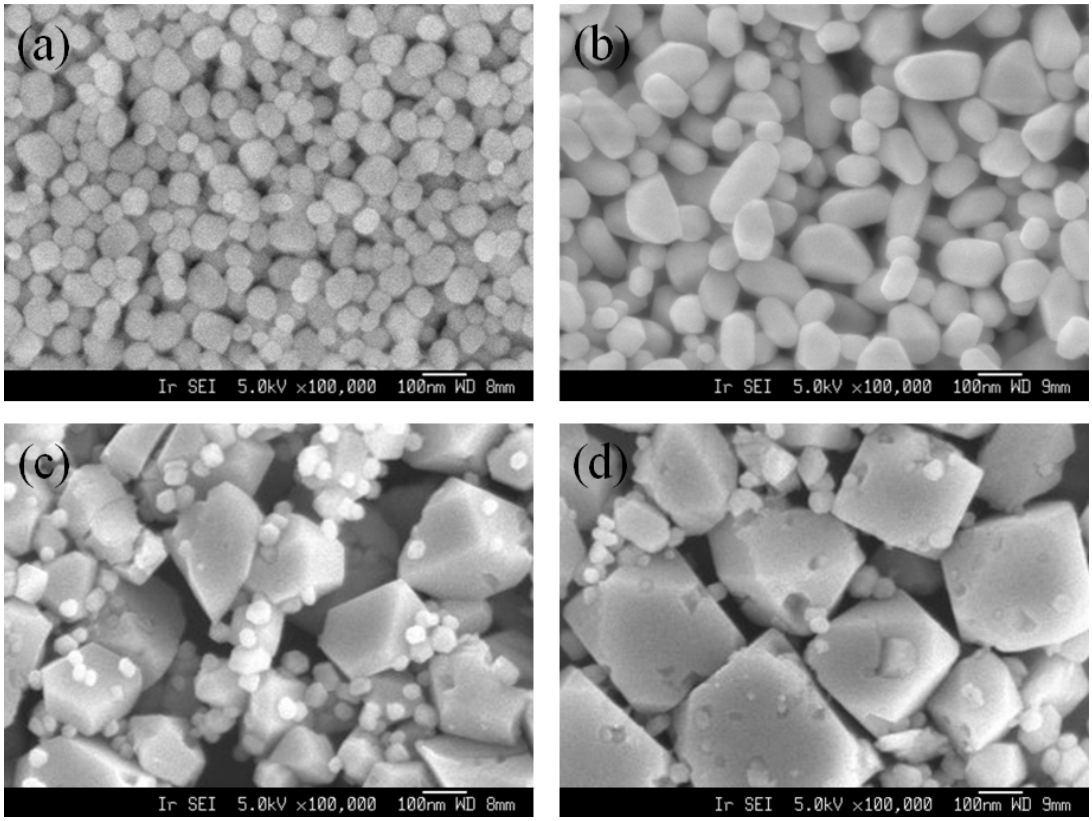

Figure 4-8. FESEM photographs of the ceria particles prepared with different hydrothermal conditions; (a) pH 3.0 at 220^{o}C, (b) pH 3.0, (c) pH 1.5 and (d) pH 0.5 at 230^{o}C, respectively

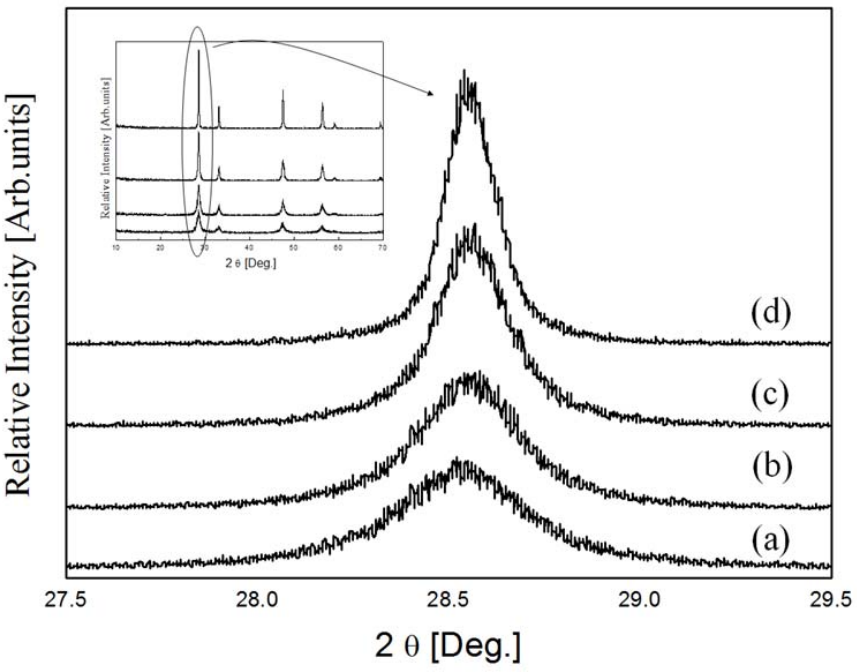

Figure 4-9. XRD patterns and the (111) peaks analyzed to confirm grain size of the ceria abrasives dispersed in ceria-based slurry (a) A, (b) B, (c) C and (d) D

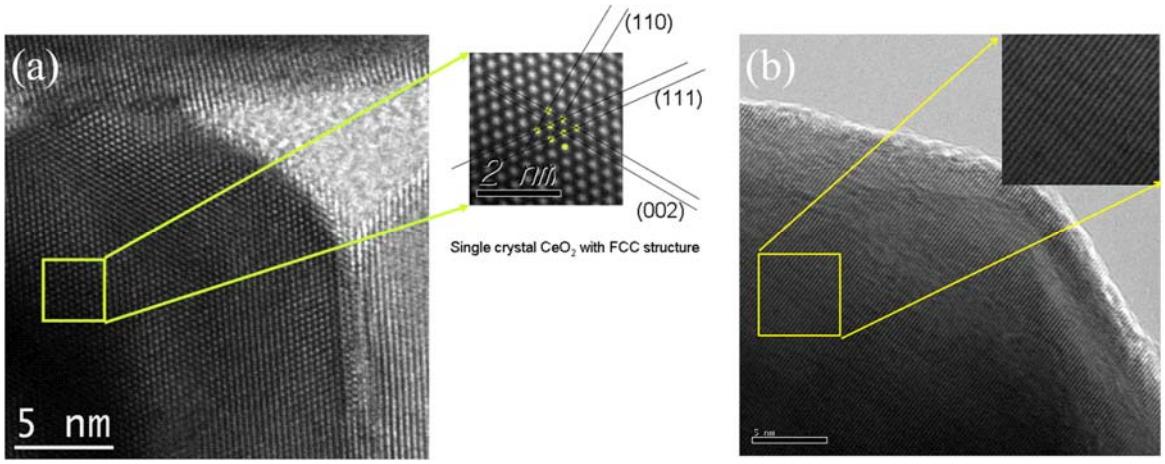

Figure 4-10. FETEM micrographs and of ceria abrasive with average particle diameters of (a) 62 nm (slurry A) and (b) 232 nm (slurry D)

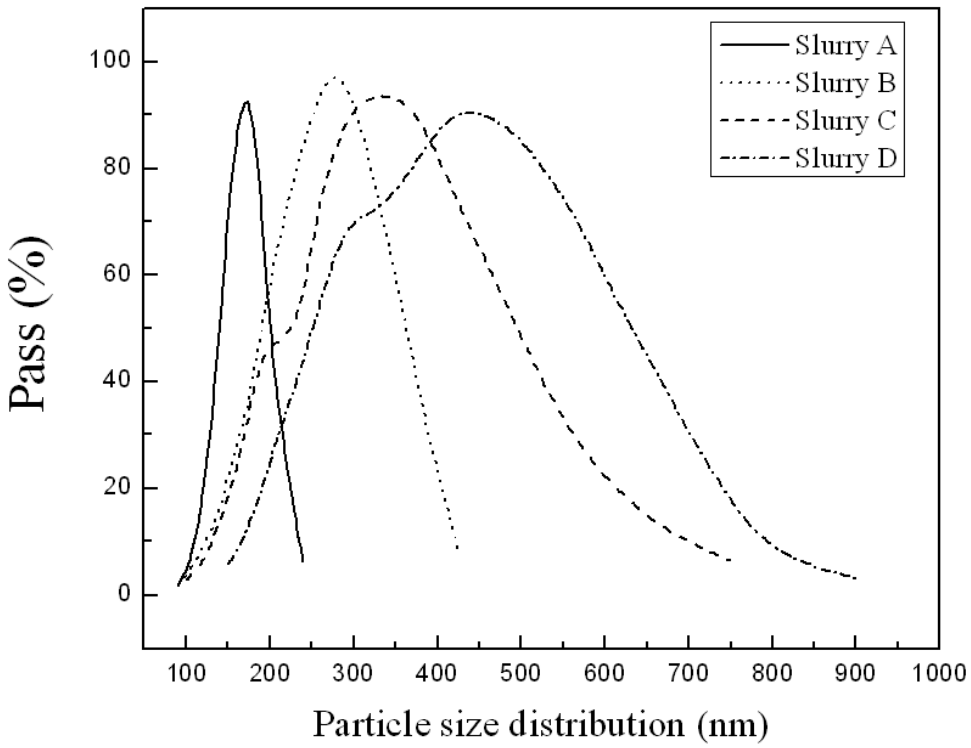

Figure 4-11. Particle size distribution of ceria-based slurry used in this study

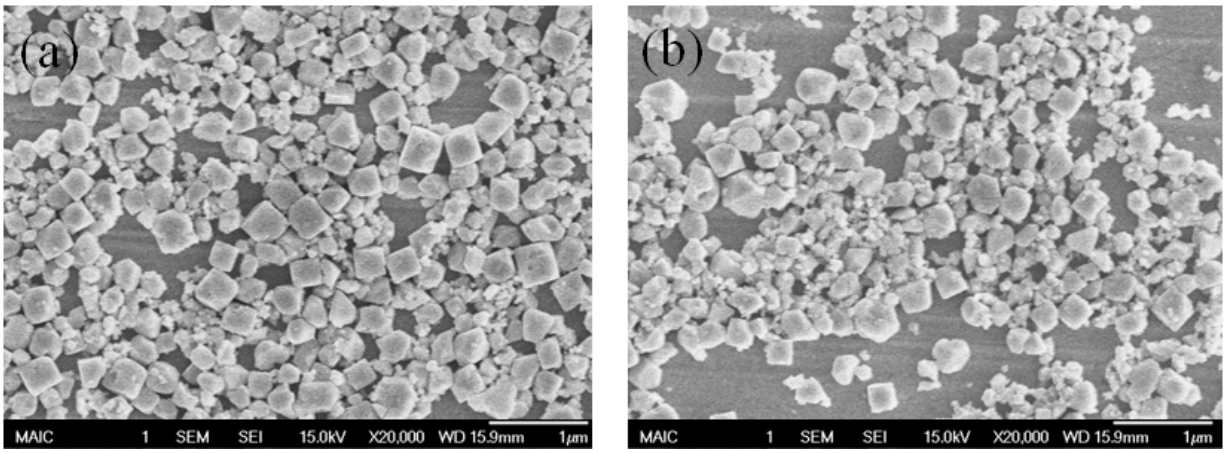

Figure 4-12. FESEM photographs of ceria abrasives (a) before and (b) after oxide CMP process

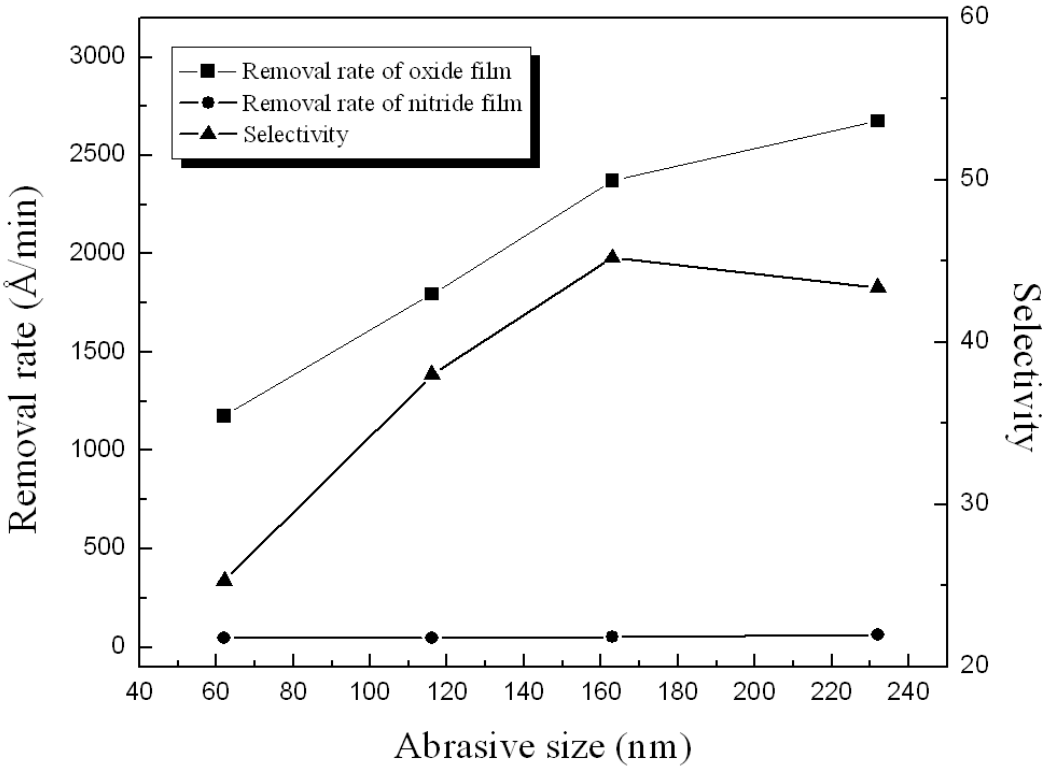

Figure 4-13. Results of CMP field evaluation for removal rate and selectivity

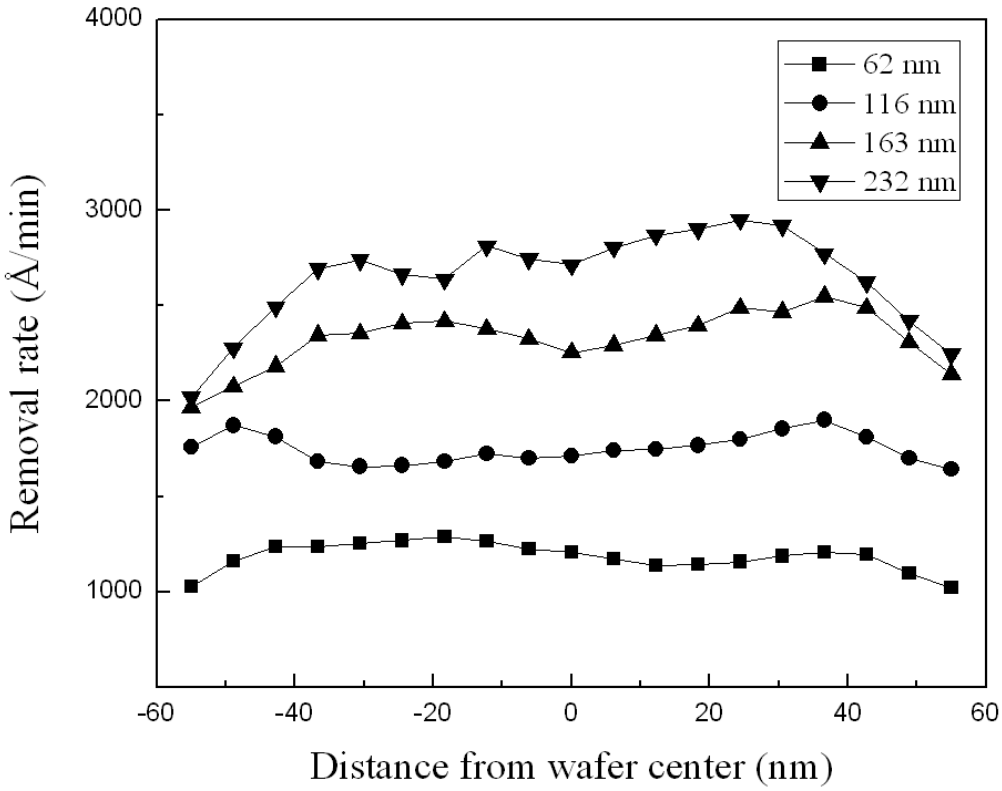

Figure 4-14. Results of CMP field evaluation for within-wafer nonuniformity (WIWNU) of silica film

Table 4-1. Comparison of slurries used in this study

Samples	Hydrothermal conditions		Primary particle Size (SEM, nm)	Grain size (XRD, nm)	Slurry mean size (UPA, nm)	Surface area (m^2/g)
	pH	Temp.(^oC)				
Slurry A	3.0	220	62	29	178	22.12
Slurry B	3,0	230	116	40	273	16.37
Slurry C	1.5	230	163	45	326	11.44
Slurry D	0.5	230	232	66	484	7.48

Table 4-2. The results of the CMP evaluation

Samples	Oxide removal rate (Å/min)	Nitride removal rate (Å/min)	Selectivity	WIWNU of oxide film (%)
Slurry A	1174 ± 105	46 ± 3	25.3 ± 0.5	3.0
Slurry B	1794 ± 125	47 ± 4	38.0 ± 0.6	5.5
Slurry C	2369 ± 194	52 ± 4	45.2 ± 0.1	8.1
Slurry D	2674 ± 201	62 ± 5	43.4 ± 0.5	11.89

CHAPTER 5
POLISHING BEHAVIORS OF SPHERICAL CERIA ABRASIVES ON SILICON DIOXIDE AND SILICON NITRIDE CMP

Introduction

In Chapter 4, the structure and size of ceria abrasives were controlled by liquid phase method. However, the shape of ceria particles was transformed into square shape with increasing in the size of particles because of it cubic fluorite structure. The square shape may lead to serious defects on the wafer during CMP process. Thus, other methods will investigate on how to control the shape and size of ceria abrasives.

As mentioned in Chapter 4, the commercial method for synthesis of ceria abrasives involves thermal decomposition of cerium salts such as cerium carbonate and cerium hydroxide. This method leads to very porous ceria particles with high surface area, inducing softness and high chemical reactivity to oxide films. However, the size and the shape of ceria abrasives are very limited since particle growth is difficult to control during calcination process. To achieve the desired particle size and the uniform particle size distribution, mechanical milling and filtration is required. This leads to expensive installation cost. To overcome this problem, flux method is proposed to synthesize the ceria abrasives with a well-defined morphology in this chapter.

This method consists of adding precursor in the required ratio to a molten salt mixture often close to an eutectic stoichiometry, which accelerates the kinetics of the formation of ceria particles.[77] Reactions in molten salts provide an original method for the preparation of solid. This method has been used in the past to synthesize a number of compounds (binary and ternary oxide, sulfides) at relatively low temperature, which would otherwise require in excess of 1100 ^{o}C for conventional solid state synthesis. Molten salt mixtures either serve the role of a solvent with no direct participation in the

reaction or may actually enter into reaction with the oxide additives. In cases where the molten salt serves merely as a solvent medium, its sole purpose is to accelerate the kinetics by enhancing diffusion, since coefficients in the liquid state are lower than those in the solid state. Reactions are presumed to occur by the dissolution of constituents, reaction of the constituents in solution, and precipitation of the required compounds upon exceeding the solubility limit.

The ceria particles obtained by this method have the several advantages over other methods such as narrow size distribution, desirable characteristics including very fine size, high chemical purity and good chemical homogeneity.[78] However, this method has seldom been applied to the synthesis of ceria abrasives for CMP slurry. Furthermore, the polishing performance of spherical ceria abrasives synthesized using flux method has not been reported so far for the silica and silicon nitride films.

In this chapter, ceria particles with spherical shape were synthesized using the flux method. Potassium hydroxide was employed as molten salt to accelerate the growth of ceria crystallites. The effects of the molten salts and reaction conditions on the formation of ceria particles were investigated. Field emission scanning electron microscopy (FESEM), transmission electron microscopy (TEM), X-ray techniques, and surface area analysis (BET) were used to study the morphology and particle size distribution of the solid products. To evaluate the size effects of ceria abrasives on CMP performance, the size of abrasives was controlled by adjusting reaction parameters. For CMP performance evaluation, the effect of spherical ceria abrasives on the removal rate, the oxide-nitride removal selectivity and the within-wafer non uniformity (WIWNU) was investigated.

Materials and Methods

Abrasives

Preparation of as-prepared particles by hydrothermal method

Cerium (III) nitrate hexahydrate ($Ce(NO_3)_3 \cdot 6H_2O$) and potassium hydroxide (KOH) were used as the starting materials for synthesis of ceria abrasive particles. 0.5 M of cerium (III) nitrate hexahydrate and 1.0 M of potassium hydroxide were separately dissolved in mixed solvent of ethylene glycol ($C_2H_6O_2$) and deionized (DI) water. The volume ratio of ethylene glycol to water was kept at 2:3. The reaction was carried out at a temperature of 50 ^oC with stirring rate of 100 rpm for 12 h. Air was bubbled into the precipitation reactor with passage through a gas distributor as an oxidizer. The precipitated substance was separated via centrifugation and then redispersed in distilled water under continuous stirring. The weight ratio of distilled water to a precipitated substance was kept 5:1. The suspension solution was put into an autoclave. The hydrothermal reaction was carried out at 230 ^oC for 6 h.

Preparation of ceria abrasive particles by solid state reaction (flux method)

After the hydrothermal reaction, the precipitated particles were washed with distilled water three times via centrifugation and then uniformly wetted in a potassium hydroxide/water mixed solution. The concentration of potassium hydroxide was 0.1 ~ 2.0 wt% depending on the total weight of the precipitated particles. The wetted particles were sintered for 2 hr at 800 - 900^oC temperature. The synthesized particles were washed with distilled water until the ion conductivity of the washed solution was less than 0.5 μS. The schematic diagram of experimental procedure was shown in Fig. 5-1.

CMP Evaluation

Preparation of ceria-based slurries

Different ceria-based slurries were formulated by dispersing abrasives each with different primary particle size in DI water containing an anionic organic polymer (Poly acrylic acid, PAA; Mw 4000, LG Chem.) as dispersant. 2 wt% of PAA based on the total weight of the ceria abrasives was added. For each slurry, pH was adjusted to 6.5 ~ 6.7 by adding ammonium hydroxide (NH_4OH). The solid loading of ceria abrasives was fixed to 2.0 wt%. In other to investigate the adsorption characteristics of ceria abrasives for the additive polymer, slurry A and D were dried at 80 ^oC for 24 hours. The weight loss of the abrasives dried from slurries was measured by thermogravimetric analysis (TGA). TGA was performed in an air flow of 100 ml/min at a heating rate of 10 ^oC/min from 30 ^oC to 600 ^oC.

CMP tools and consumables

Silicon dioxide film of 2 μm thick was grown on a 5-in. p-type silicon substrates with (001) orientation by plasma enhanced chemical vapor deposition (PECVD). The silicon nitride films were deposited by using low-pressure chemical vapor deposition (LPCVD). Polishing tests were performed on a rotary type CMP machine (GNP POLI 400, G&P technology) for one minute with each of the ceria-based slurries. IC 1000/SUBA IV stacked pads (supplied by Rodel Inc.) were utilized as CMP pads. The downforce was 4 psi and the rotation speed between the pad and the wafer was 100 rpm. The slurry flow rate was 100 mL/min.

Characterization

Abrasives

The crystal structure and grain size were identified through x-ray diffraction (XRD) using CuKα radiation. The crystallite size was estimated by the Scherrer equation according to the formula $D = 0.9 \lambda / (\beta \cos \theta)$, where D is crystallite size, λ is the wavelength of x-rays, β is the half-width of the diffraction peaks, and θ is the diffraction angle. The broadening of the reflection from the (111) plane was used to calculate the crystallite size. The morphology and sizes of the abrasive particles were also examined by field emission scanning electron microscope (FESEM). The average primary particle size was calculated by measuring ca. 100 particles from FESEM micrographs. The specific surface area (SSA) of ceria abrasives was determined by Brunauer-Emmett-Teller (BET) method using nitrogen adsorption/desorption at 77 K.

Ceria-based Slurry

The abrasive size distribution of slurry was measured using light scattering method (UPA 150, Microtrac. Inc.). For the light scattering measurements, ceria particles were dispersed in deionized water without dispersant, using an ultrasonic probe for 15 min.

Polishing of wafers

The film thickness on the wafers before and after CMP was measured using spectroscopic reflectometry (Nanospec 6100, Nanometrics) to calculate the removal rate. In this experiment, the WIWNU was defined as the standard deviation of remaining thickness divided by the average of the remaining thickness after the CMP process. The average polishing data for removal rate was carried by performing the same tests more than three times in order to support the validity of the results from the statistical viewpoint.

Results and Discussion

Ceria Abrasives

Morphological properties

Fig. 5-2 shows the FESEM images of abrasive particles prepared in different calcination conditions as described in Table 5-1. The primary particle sizes determined using the FESEM micrographs were 84, 166, 295, and 417 nm for slurry A, B, C and D, respectively. As shown in Fig. 5-2, the ceria particles consisted of crystalline grains with a well-defined morphology. The size of spherical ceria particles increased with the increase in concentration of potassium hydroxide and the calcination temperature. These images indicate that the primary particle size can be controlled by changing the calcination conditions, which influence the crystal growth of ceria particles.

Crystalline structure

Fig. 5-3 shows the X-ray diffraction patterns of the prepared particles. As shown in Fig. 5-3(a), the characteristic peaks corresponding to (111), (200), (220), (311), and (222) planes are located at 2θ = 28.51, 33.06, 47.48, 56.20, and 59.05^{o}, respectively. They show very close to the ones with cubic fluorite structure of ceria crystal in JCPDS database. The sharp intensity peaks were observed for ceria abrasives with larger primary particle size as shown in Fig. 5-3(b). The crystallite size of ceria abrasives was calculated from the Scherrer equation using the line-broadening of the (111) peak in the XRD pattern. The crystallite size gradually increased from 38 nm to 88 nm as the calcination temperature and the concentration of additive were increased. This result coincides with the trend of increasing primary particle size in the FESEM images shown in the Fig. 5-2.

Effects of molten salt and as-prepared particle

The synthesis method employed in this study is characterized by a low sintering temperature process, using grain growth accelerator. The eutectic mixed solvents as an accelerator is used to promote the kinetics by enhancing diffusion, due to their low melting temperature. In this study, potassium hydroxide/water mixed solvent was used as the accelerator to reduce sintering temperature. Considering that the conventional sintering of ceria requires high temperatures leading to partial reduction above 1200 ^{o}C,[79] potassium hydroxide/water mixed solvent might offer a liquid phase to promote interdiffusion on contact surface between the smaller particle and the larger ones during the sintering process.

Fig. 5-4 shows this dependence of the crystallite size on the concentration of potassium hydroxide at a fixed temperature (850^{o}C). It can be observed that an increase in the crystallite size was seen with addition of KOH at same calcination temperature. These results indicate that potassium hydroxide strongly affects the growth rate of ceria particles at relatively low temperature. Therefore, the physical properties and the morphology of ceria abrasives could be controlled by manipulating the concentration of potassium hydroxide in this system.

Additionally, cerium dioxide particles obtained by hydrothermal method were used as the precursor in this study, instead of cerium salts such as hydroxide, nitride, and chloride. Fig. 5-5 shows the FESEM images of the particles prepared with different cerium precursors. Compared with other particles as shown in Fig. 5-5(a), (b), and (c), it can be observed that the uniformity of ceria particles (Fig. 5-5(d)) prepared using oxide is superior. This result is attributed to the fact that in case of cerium dioxide as a precursor, direct grain growth of crystallite is involved during heat treatment. However,

in case of other precursors (hydroxide, nitride and chloride), the formation of cerium dioxide crystallites involves two steps via thermal decomposition followed by grain growth. Thermal decomposition of such precursors involve series of chemical reactions[80] leading to retarded growth of ceria particles. Furthermore, it is difficult to achieve uniform ceria particle morphology because of the high surface energy and chemical reactivity of the volatile cerium compounds. Therefore, it seems that the direct formation to ceria induces the absence of hard aggregates and surface necking in the ceria crystallites.

CMP Evaluation

Characteristics of ceria abrasives before and after CMP

To investigate the CMP performance using spherical ceria abrasives, we performed polishing test for the four types of slurries with different abrasive size. Fig. 5-6 shows the particle size distribution of these slurries without surfactant addition. The average particle sizes determined by light scattering method were 165, 278, 483, and 742 nm for slurry A, B, C and D, respectively. The dispersed particle size is much larger than the crystallite size estimated by X-rays and the primary particle size calculated by FESEM. This observation is due to the extensive overlapping of the ceria particles in water-based solution.[75] The general tendency when using light scattering (LS) size distributions of particles is to oversize the coarse end of the distribution because LS uses the longer axis of an elongated particle to determine the mean particle diameter. Another reason for obtaining a larger LS size is that the fundamental size distribution, as derived via LS, is based on volume; in other words, if a sample consists of an equal number of two sizes of particle, e.g., 50 nm and 100 nm, the volume of the 100 nm particles is 8 times larger than that of the 50 nm particles. Hence, as a volume

distribution, the larger particles represent most of the total volume, which yields a mean particle size by volume that is larger than that obtained by population. As shown in Fig. 5-6, the increase in the size of the primary particle led to broader particle size distribution in water-based solution.

Fig.5-7 shows the FESEM images of ceria abrasives before and after silicon dioxide polishing for slurry C. The ceria abrasives after polishing were washed with distilled water three times via centrifugation. According to Fig. 5-6, we can confirm that the ceria abrasives are brittle and break during polishing process. This indicates that the ceria abrasives used in this study are easily broken-down by applied pressure and shear force during polishing.

Polishing Test

Removal rate. Table 5-2 summarizes the quantitative results of the polishing test. It is clear that the removal rate of the oxide films increased with increasing size of ceria abrasives. The removal rate of oxide film is mainly influenced by chemical contribution of ceria abrasives and mechanical factors, such as the CMP conditions, morphological characteristics of abrasives and particles size distribution. During the polishing of the oxide film, ceria abrasives exhibit a chemical tooth property which accelerates the polishing removal rate of oxide film.[12] As a consequence, the Si-O-Ce bonds can be rapidly removed by the mechanical force generated by pressed pad and abrasives, and this physicochemical reaction lead to the high removal rate of oxide film. In this work, it was found that the removal rate of oxide film was essentially dependent on the size of ceria abrasives. As with the removal rate of oxide film, the removal rate of nitride film increased with increasing in the crystallite size of ceria abrasives. However, the removal rate of nitride film is affected by the physical properties of ceria-based slurry systems

and the amount of surfactant adsorbed on the film surface.[5] In order to improve the selectivity and uniformity, an anionic acrylic polymer is commonly used to passivate the surface of the nitride film during STI-CMP, which prevents ceria abrasives from contacting the film surface.[76] In this study, the amount of the polymer was maintained constant for all slurry. Therefore, it seems that the increase in the removal rate of nitride film is relate to the mechanical factors rather that to the effect of passivation layer of the polymer absorbed on the film surface. These mechanical factors are influenced by several physical parameters of the CMP process, such as morphological aspects of the abrasives, crystallite size of the abrasives and the CMP conditions.

Selectivity. It is well known that the removal rate increases with increasing particle size due to mechanical indentation. However, the increase in removal rate shows lower slope between slurry C and D as compared to that from slurry A to C as shown in Fig. 5-8. This led to a transition in removal selectivity between oxide and nitride film at slurry C. This result is attributed to two related factors: the contact-area reduction and the particle surface activity. In the case of oxide CMP process, the removal rate is mainly affected by contact area between the abrasives and the film surface. According to contact-area mechanism,[16] the removal rate increases with decreasing abrasive size and increasing solid loading, due to the increase in contact-area between the abrasives and the film surface. At a fixed solid loading, the number of ceria abrasives in slurry decrease as the abrasive size increases. This implies the decrease in contact area between ceria abrasives in slurry D and oxide film during CMP processing. Additionally, large abrasives with spherical shape lead to the decrease in interfacial contact with film surface, due to their rolling motion.[4] Furthermore, relatively

lower removal rate are attributed to the inhomogeneous distribution of slurry on the wafer. For the slurry D, the broader size distribution induces a loss in the frictional occasion of smaller abrasives by bigger abrasives and a local friction interaction of bigger abrasives on the wafer. The frictional force between the abrasives and the wafer is decreased by using slurry D because the frictional force is directly proportional to the contact area.[81] These polishing behaviors would lead to a relatively lower increase in removal rate for the oxide wafer during CMP. In this study, such behavior can be clearly seen from the change in oxide removal rate from slurry A to C and slurry C to D. As shown in Fig. 5-8, the removal rate rapidly increased from 1662 Å/min for 84 nm to 3990 Å/min for 295 nm, whereas it slightly increased to 4343 nm for 417 nm in spite of size effect of bigger abrasives during CMP process. In case of the nitride film CMP, the polishing behavior can be explained by the relationship between additive polymer and abrasive size. The additive polymer can be more easily attached on the surface of the small abrasives than on the surface of large ones, due to high surface activity and specific surface area of the small abrasives. The slurry with small abrasives can induce a relatively high removal rate for nitride film, since the passivation layer is insufficiently formed on the nitride film surface as polymer is largely adsorbed on the particle surface. As described in Table 5-1, the specific surface area decreased with increasing abrasive size. Moreover, the compositional changes associated with the additive polymer adsorbed on the surface of ceria abrasives were investigated with thermal analysis. Fig. 5-9 presents the TGA curves of the ceria abrasives dried from slurry A and D. The TGA curves of the ceria abrasives show two weight losses (curve (a) and (b)). The initial weight loss below the temperature of 100 ^{o}C can be attributed to the evaporation of

physically absorbed water in the air. The second weight loss observed at 200 ~ 260 ^{o}C is related to the decomposition of the additive polymer adsorbed on the abrasive surface. As shown in Fig. 5-9, final weight loss for two abrasives was different because the additive polymer content adsorbed on abrasive surface was different. This means that removal rate for nitride films can be relatively increased in spite of decrease in the abrasive size. As a result, the removal rate of nitride film showed relatively low increase in rate with increase in the abrasive size. Therefore, these polishing behaviors for oxide and nitride films result in the transition of removal selectivity, suggestive of existence of an optimum size of spherical ceria abrasives for high removal selectivity.

WIWNU. The results for surface uniformity of the oxide films are shown in Fig. 5-10. As the size of ceria abrasives increased, the slurry had a higher WIWNU for the oxide film. This polishing behavior is attributed to a broader particle size distribution of the slurry with large abrasives. The distribution data in Fig. 5-6 showed that the slurry has a rather-wide particle size distribution as abrasive particles increases. The broader particle size distribution of large abrasives can cause a different removal rate between the center and the edges of the film surface due to their limited mobility on the wafer surface. Consequently, the surface uniformity deteriorated with increasing abrasive size during CMP process. It seems that surface uniformity of oxide film is related to the mechanical factors and the morphological factors of ceria abrasives on the film surface.

Conclusions

Ceria Abrasives

The ceria abrasives were prepared by the flux method, using potassium hydroxide (KOH) as the grain growth accelerator. The synthesized particles consisted of crystalline grains with a well-defined morphology. The size of spherical ceria particles

increased with the increase in concentration of potassium hydroxide and the calcination temperature. Considering the sintering temperature of ceria, potassium hydroxide strongly affected the growth rate of ceria particles at relatively low temperature. The physical properties and the morphology of ceria abrasives could be controlled by manipulating the concentration of potassium hydroxide in this system. The FESEM analysis showed that ceria particles obtained from oxide phase is superior to other particles in terms of uniformity and shape. This method proposed in this study is very simple and can lead to well-crystalline particles with desirable characteristics, including very fine size, narrow size distribution, high purity, and good chemical homogeneity.

CMP Performance

In this study, we investigated the effects of spherical ceria abrasives on polishing performance during silicon dioxide and silicon nitride CMP. The size of the ceria abrasives was controlled by changing the calcination conditions without mechanical milling process. With increasing abrasive size, the removal rate of silicon dioxide and silicon nitride films increased. On the other hand, the surface uniformity deteriorated after CMP process, due to a wide particle size distribution of the slurry with large abrasives. In addition, the removal selectivity showed a transition behavior at the slurry C (with particle size of 295 nm). This result indicates that there exists an optimum for removal selectivity as a function of abrasive size in the used slurry system. Therefore, we concluded that the control of abrasive size and particle size distribution of spherical ceria abrasives is an important parameter for high removal selectivity and surface uniformity in the CMP process.

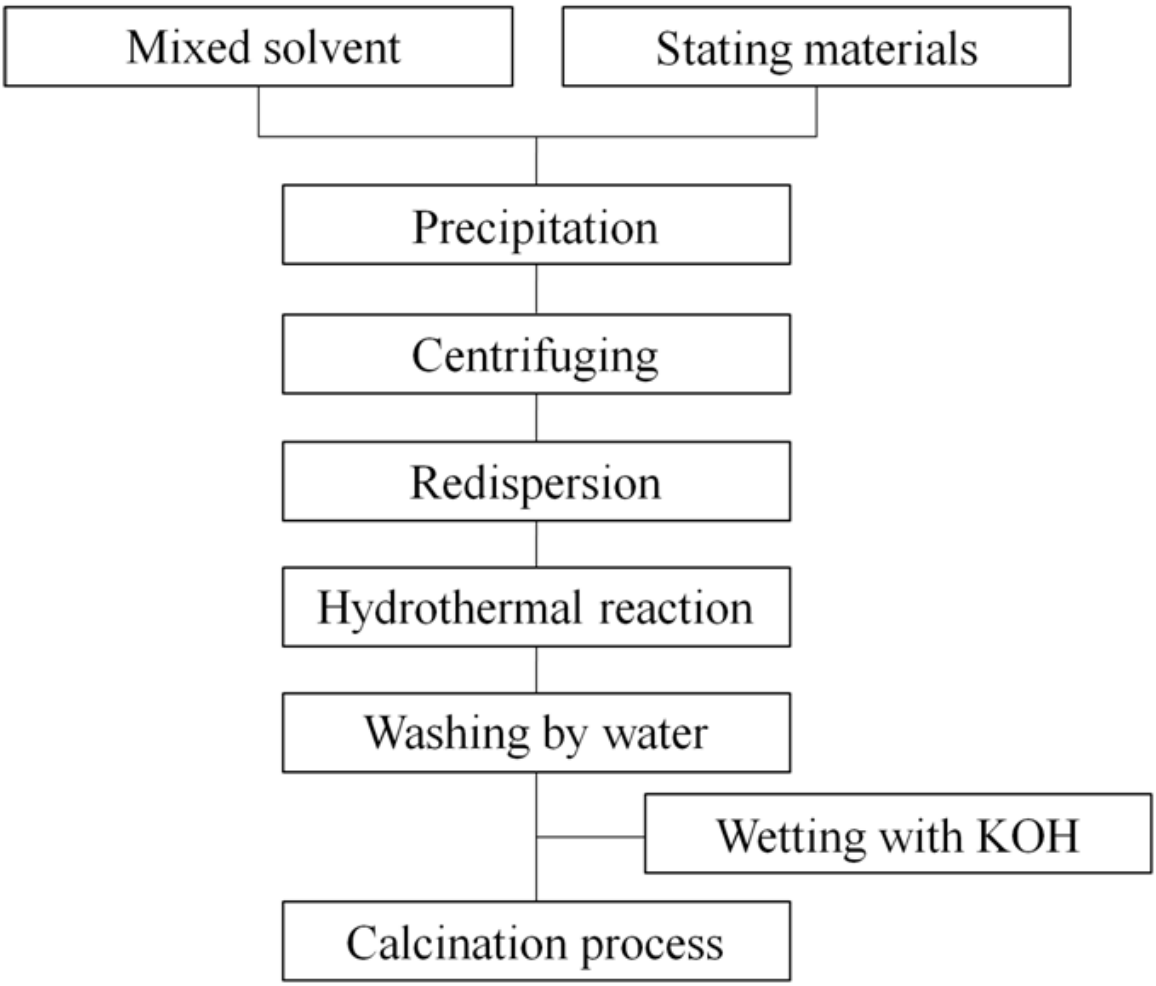

Figure 5-1. Schematic diagram of experimental procedure

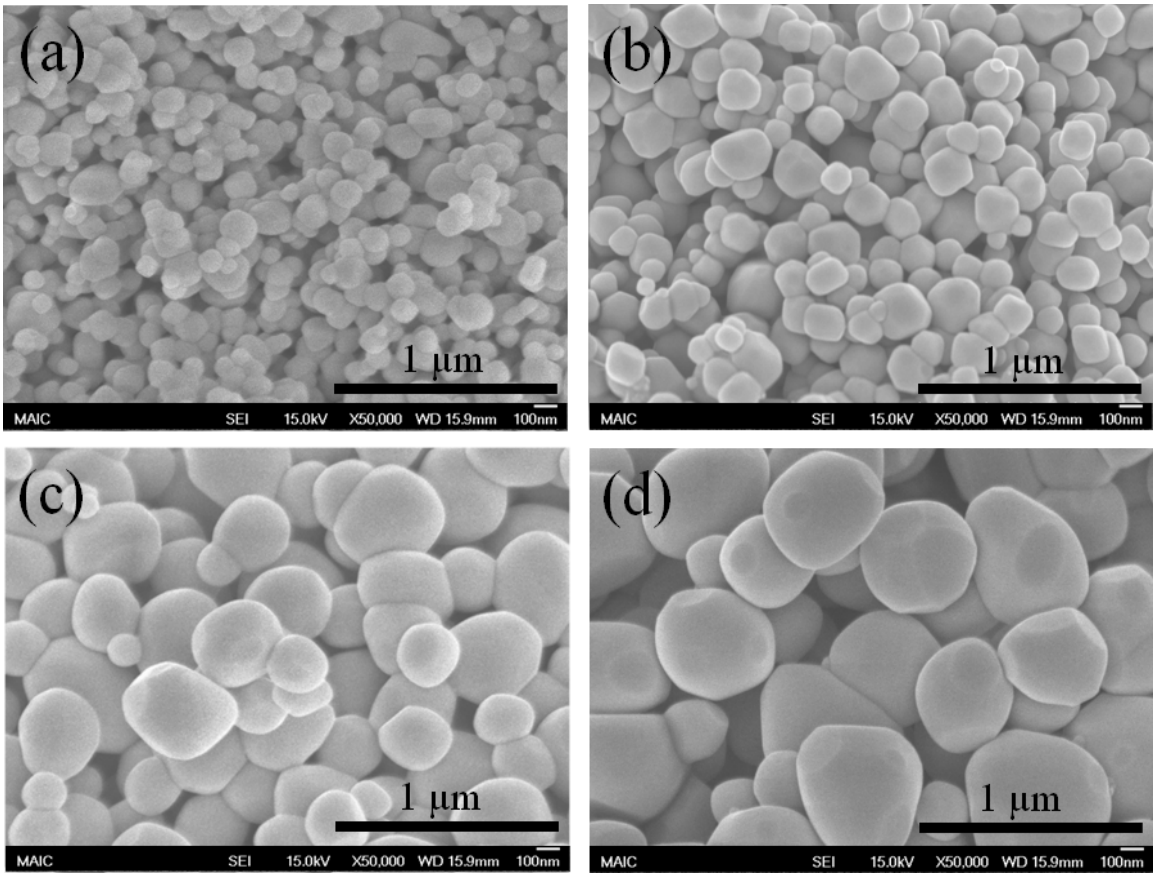

Figure 5-2. FESEM photographs of the ceria abrasives prepared with different calcination conditions; (a) slurry A, (b) B, (c) C and d(c) D

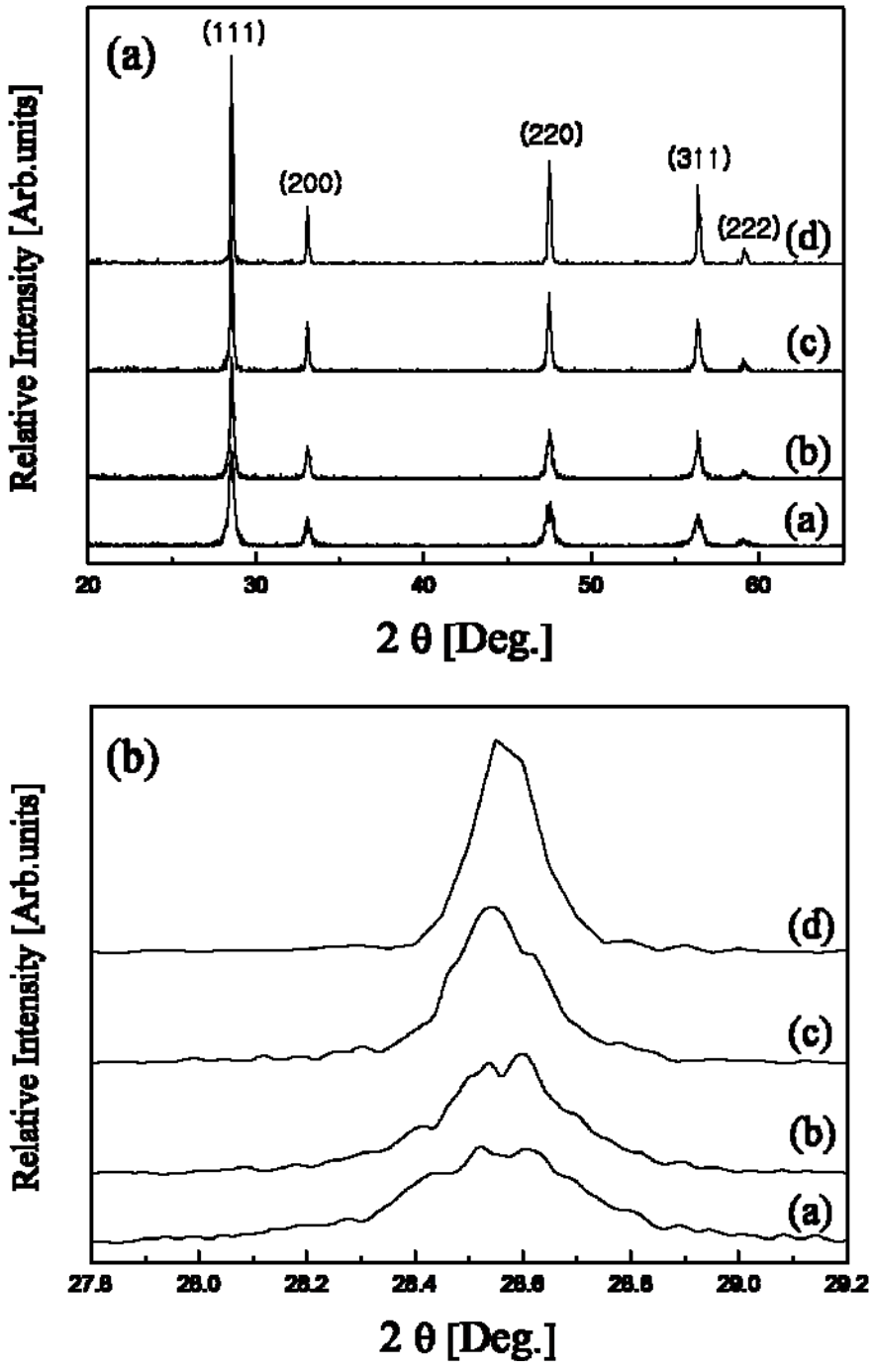

Figure 5-3. (a) XRD patterns and (b) the (111) peaks analyzed to confirm crystallite size of the ceria abrasives dispersed in slurry (a) A, (b) B, (c) C and (d) D

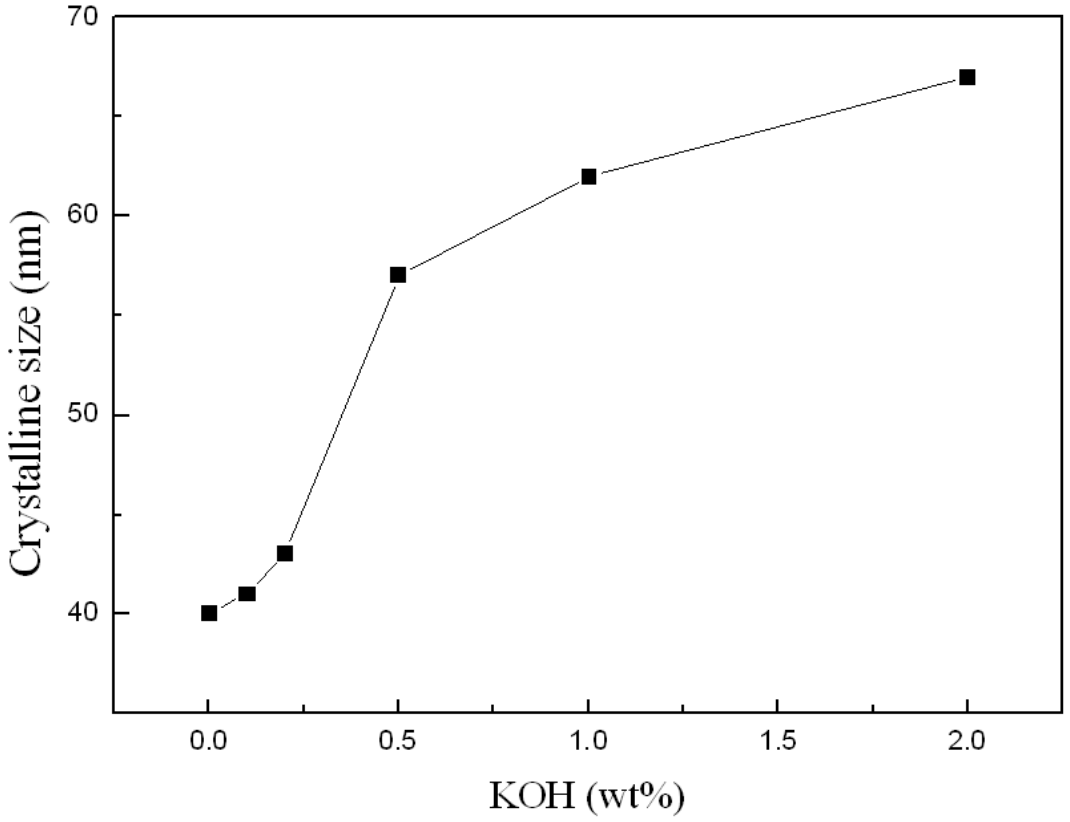

Figure 5-4. The variation of crystallite size as a function of the concentration of grain growth accelerator

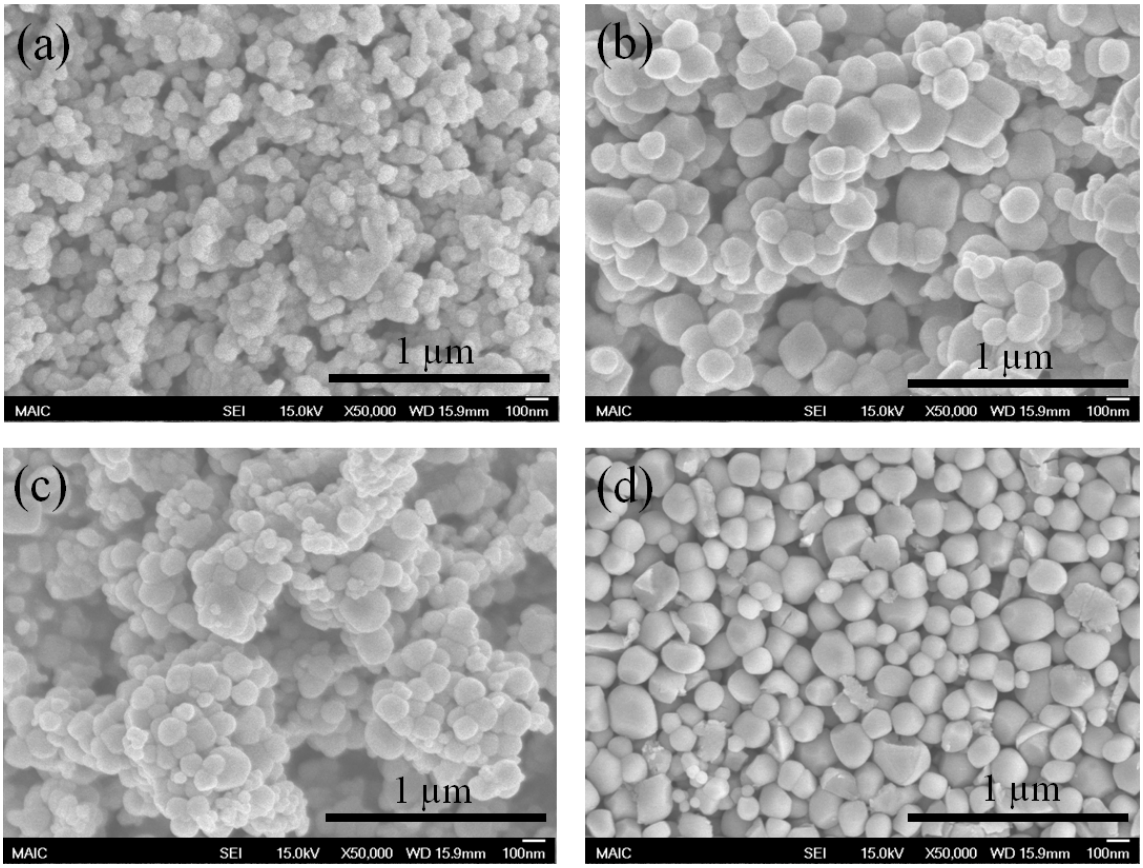

Figure 5-5. FETEM micrographs of the ceria abrasives prepared with different cerium precursor; (a) cerium hydroxide, (b) cerium nitride, (c) cerium chloride and (d) cerium dioxide

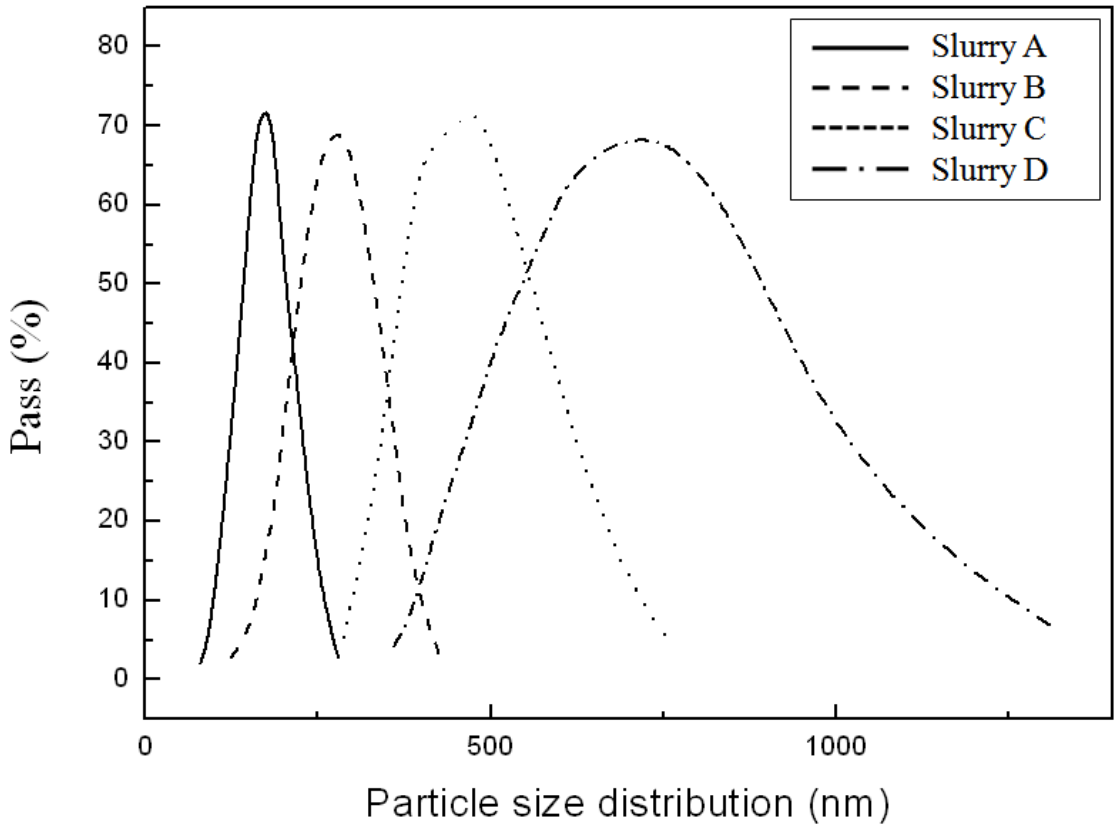

Figure 5-6. Particle size distribution of ceria slurries as function of abrasive size

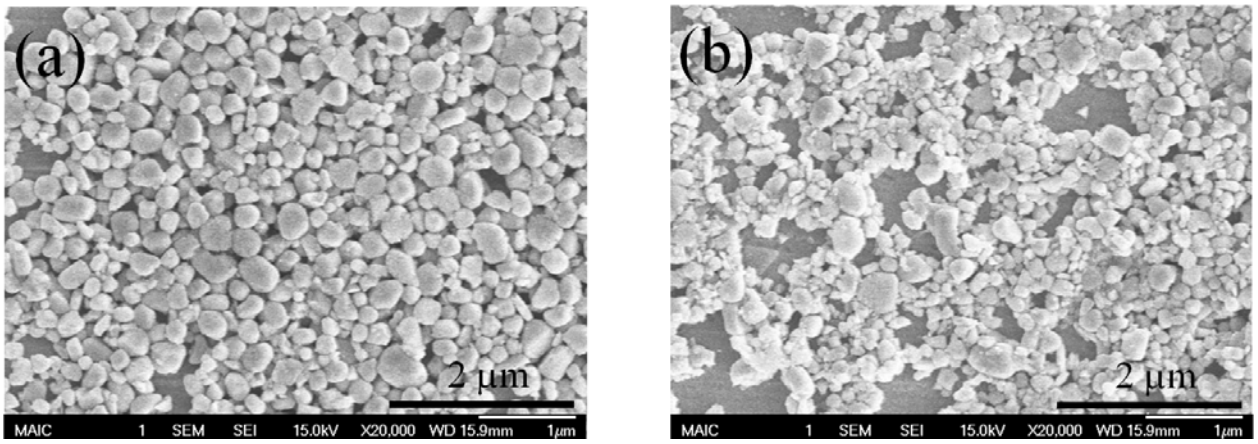

Figure 5-7. FESEM photographs of ceria abrasives (a) before and (b) after polishing

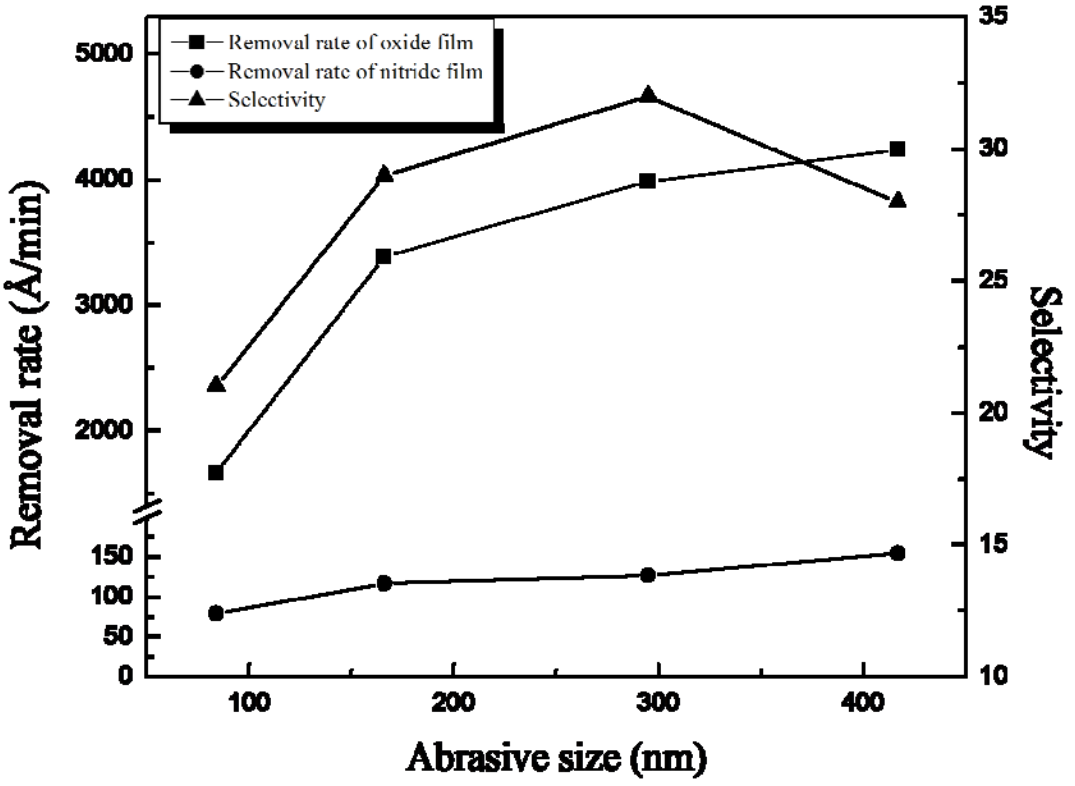

Figure 5-8. Results of CMP field evaluation for removal rate and selectivity

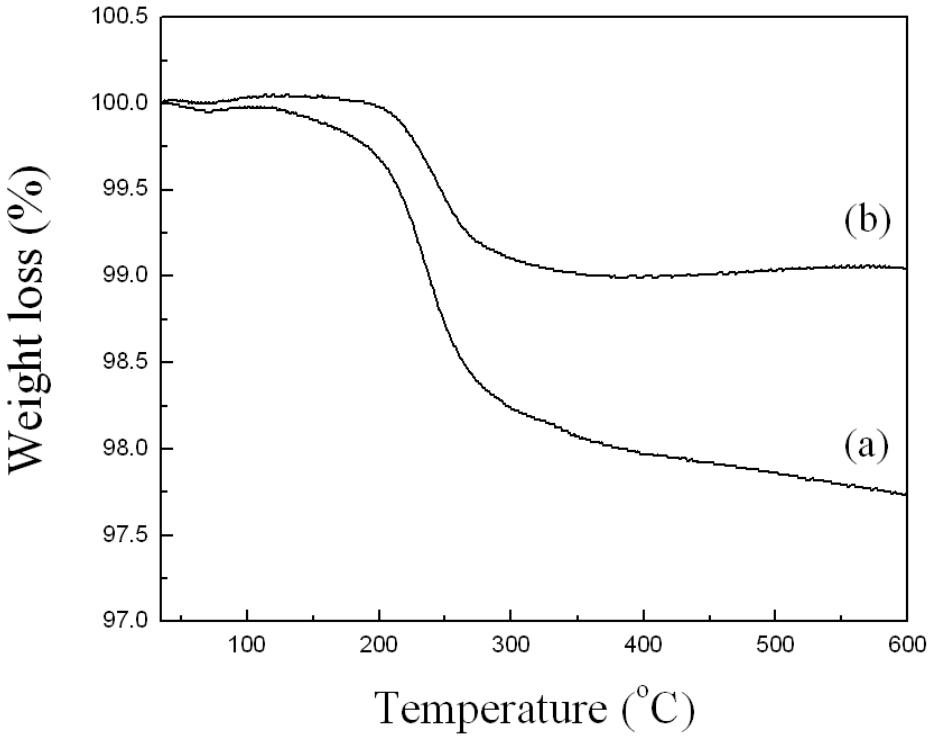

Figure 5-9. TGA curves of the ceria abrasives dried from (a) slurry A and (b) slurry D

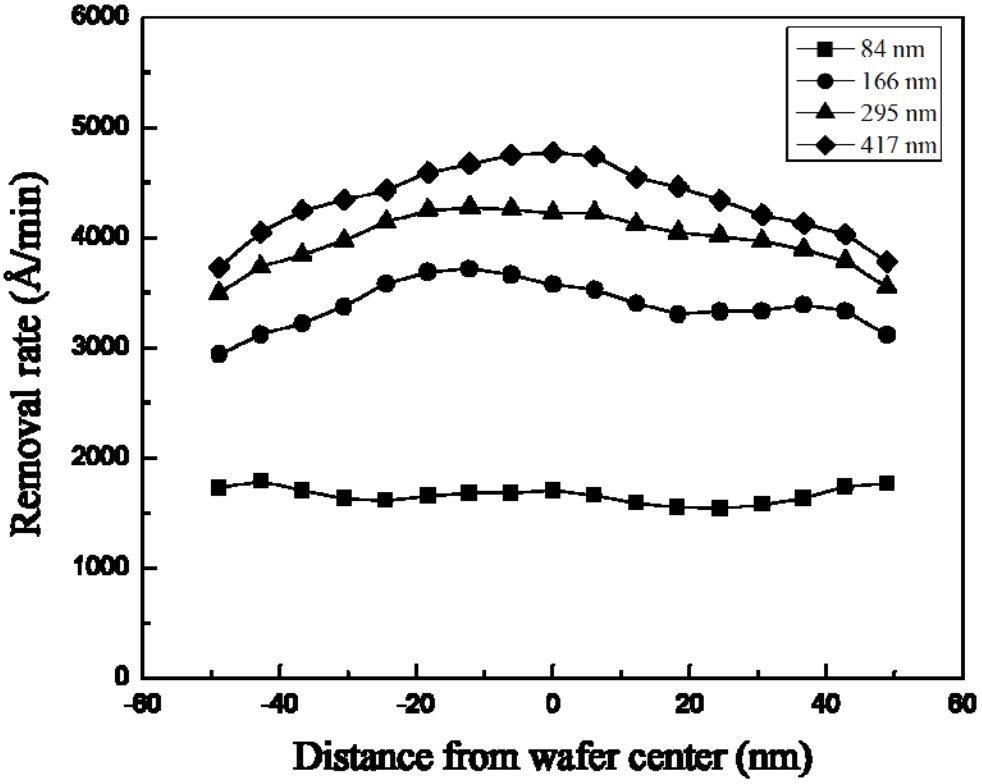

Figure 5-10. Within-wafer non uniformity (WIWNU) of oxide film

Table 5-1. Comparison of slurries used in this study

Samples	Calcination conditions		Primary particle Size (SEM, nm)	Grain size (XRD, nm)	Slurry mean size (UPA, nm)	Surface area (m^2/g)
	Molten salt (wt%)	Temp. (^oC)				
Slurry A	0.5	800	84	38	165	20.53
Slurry B	0.2	850	166	43	278	14.06
Slurry C	0.5	850	295	57	483	12.70
Slurry D	0.5	900	417	88	742	5.58

Table 5-2. The results of the CMP evaluation

Samples	Oxide removal rate (Å/min)	Nitride removal rate (Å/min)	Selectivity	WIWNU of oxide film (%)
Slurry A	1661 ± 77	79 ± 6	21 ± 0.9	7.9
Slurry B	3390 ± 103	117 ± 8	29 ± 1.0	11.0
Slurry C	3989 ±91	127 ± 6	32 ± 1.3	14.6
Slurry D	4343 ±136	155 ± 13	28 ± 1.4	16.7

CHAPTER 6
PREPARATION AND CHARACTERISTICS OF THE CERIA COATED SILICA PARTICLES AND ITS CMP PERFORMANCE

Introduction

This chapter presents studies conducted on synthesis of the ceria coated silica particles and its CMP performance. According to recent reports, the homogeneous precipitation coating method using electrostatic attraction process has been extensively investigated to control the shape and uniformity of particles. In particular, core-shell composites with spherical silica microspheres have been wisely investigated to provide novel properties that are not found in the single metal oxide.[81] Moreover, silica particle as core material offers many advantages such as high specific surface, dispersion stability, narrow particle size distribution, high mechanical strength and controllable size of the particles.[83,84] Therefore, many researchers have investigated methods for producing the ceria coated silica particles. However, in previous works, the synthesized particles experienced severe aggregation due to hydrogen bonding from water during precipitation process.[72] Moreover, the resulting dispersion contains both the ceria coated silica particles and nano-sized ceria particles due to the detachments of ceria coating on the surface of core particles. In addition, in some cases, synthesized particles need post-heat treatment to acquire a well-crystalline ceria coating.[85] However, post-heat treatment often lead to hard aggregation and incomplete coating surface for the particles. Furthermore, the experimental results showing control of the ceria coating thickness not been reported so far.

To overcome these problems, cerium alcoholate complex are proposed as a new precursor of ceria coating on the surface of silica particles in this study. As mentioned in chapter 4, the solvent type used in reaction affected physical properties of ceria

particles.[86] Moreover, nanocrystalline particles produced by alkoxide method shows much more reactivity than those produced by aqueous routes, since the organic solvents of alkoxide act as the dispersant for solid particles during precipitation and prevent from aggregating during drying process.[87]

Therefore, the first objective of this study is to establish a novel synthetic method of preparing monodispersed ceria coated silica particles with precise morphologies and chemical composition. The second objective is to deposit well-crystalline ceria coating on the surface of the silica particles without post-heat treatment. The third objective is to use the synthesized coated particles as abrasives for ceria-based slurry on CMP process. To achieve these purposes, cerium ethanolate solvate complex as a new coating precursor was prepared by alkoxide method, which helps to decrease the colloidal interaction and affects the crystallinity of ceria coating. This study showed that the ceria coated particles prepared by the new precursor were uniformly synthesized without the formation of hard aggregate as compared to those obtained by conventional method. Additionally, the influences of various precipitation conditions on coating characteristics were investigated. Finally, the effect of the synthesized ceria coated silica particles in CMP slurry was investigated on silicon dioxide polishing process.

Materials and Methods

Abrasives

Preparation of monodispersed silica particles

Monodispersed spherical silica particles were synthesized in a semi-batch reactor by modified Stöber method.[84] In a typical preparation, 2 ~ 5 ml of tetraethyl orthosilicate (TEOS) was fed into the reactor, in which a mixture of de-ionized water (1 ~ 3.5 ml), ethanol (10 ~ 80 ml) and ammonia (1 ~ 3.4 ml) was premixed. The size of core silica

particles can be controlled by adjusting different concentration of materials used. The reactants were agitated vigorously by stirring for 3 hours at a constant temperature of 25 ^{o}C. The silica particles were collected and washed repeatedly with ethanol. The particles were then dried at 50 ^{o}C for 24 hours.

Preparation of ceria precursors

To investigate the effects of solvent type on precursor characteristic, two kinds of ceria precursor were prepared via different methods using alcohol-based solvent and water-based solvent. The sufficiently high reactivity of ethanol (as alcohol-based solvent) and water can allow direct reaction between cerium metal and the solvent by heating the suspension under reflux.

Synthesis of cerium ethanolate complex (designated as precursor A). The cerium alcoholate was prepared via alkoxide method. Cerium nitrate hexahydrate ($Ce(NO_3)_2 \cdot 6H_2O$) and potassium hydroxide (KOH) were used as the starting materials. Cerium nitrate hexahydrate (1 g) and potassium hydroxide (1 g) were separately dissolved in 20 ml ethanol under vigorous stirring for 24 hours at 50 ^{o}C. Hydrogen peroxide (30 % H_2O_2, 0.05 ml) was added to mixing solution as the oxidizing agent. Eqn. 6-1 describes the chemical reaction:

$$Ce(NO_3)_2 \cdot 6H_2O + 2(CH_3CH_2OH) + 2KOH \xrightarrow{reflux} Ce(OCH_3CH_2)_2 + 2KNO_3 + 8H_2O \quad (6\text{-}1)$$

The precipitated ceria precursor was separated via centrifugation. The supernatant solution obtained from the centrifugation was discarded and the 1 g of the precipitate was redispersed in 20 ml distilled water under continuous stirring. The pH of the suspension solution was adjusted to 0.1 by adding concentrated nitric acid (HNO_3). Nitric acid was used to obtain peptized ceria sol. Finally, the solution was heated to 40

^{o}C and kept at this temperature for 2 hours. The transparent light yellow solution obtained was cooled down to room temperature.

Synthesis of cerium hydroxide complex (designated as precursor B). The cerium hydroxide was prepared via precipitation method. Cerium nitrate hexahydrate ($Ce(NO_3)_2 \cdot 6H_2O$) and potassium hydroxide (KOH) were used as the starting materials. Cerium nitrate hexahydrate (1 g) and potassium hydroxide (1 g) were separately dissolved in 20 ml distilled water under vigorous stirring for 24 hours at 50 ^{o}C. Hydrogen peroxide (30 % H_2O_2, 0.05 ml) was added to mixing solution as the oxidizing agent. Eqn. 6-2 describes the chemical reaction:

$$Ce(NO_3)_2 \cdot 6H_2O + 2(H_2O) + 2KOH \xrightarrow{reflux} Ce(OH)_2 + 2KNO_3 + 8H_2O \quad (6\text{-}2)$$

The precipitated ceria precursor was separated via centrifugation. The supernatant solution obtained from the centrifugation was discarded and the 1 g of the precipitate was redispersed in 20 ml distilled water under continuous stirring. The pH of the suspension solution was adjusted to 0.1 by adding concentrated nitric acid (HNO_3). Nitric acid was used to obtain peptized ceria sol. Finally, the solution was heated to 40 ^{o}C and kept at this temperature for 2 hours. The transparent light yellow solution obtained was cooled down to room temperature.

Preparation of ceria coated silica particles

For the synthesis of silica particles coated with ceria, 0.1 g of the silica particles was dispersed in 30 ml distilled water. 1.0 ~ 8.0 ml of ceria precursor was added to the solution. After stirring for 30 min, the pH of the solution was adjusted to 3.0 ~ 10.0 by adding 0.5 mol/L ammonium hydroxide (NH_4OH) solution. The final mixed solution was stirred for 4 hours at a temperature of 60 ^{o}C. The coated particles were washed through

several decantation and redispersion cycles by centrifugation. The resulting particles were then dried at 50 ^{o}C for 24 hours. In order to compare with ceria particles, the precipitated ceria precursor was washed with distilled water three times by repeated centrifugation. After washing, the precipitate was dried at 90 ^{o}C.

Preparation of Ceria-bases Slurry

Different slurries were formulated by dispersing the synthesized ceria coated silica particles in deionized water containing an anionic organic polymer (Poly acrylic acid, PAA; Aldrich Mw: 50,000) as dispersant. The PAA was 0.5 wt% based on the total weight of the used abrasives. The pH was adjusted to 3.0 ~ 9.0 by adding ammonium hydroxide (NH_4OH). The solid loading of the used abrasives was fixed to 2.0 wt%.

CMP Evaluation

Silica (SiO_2) wafer for all experiments have a nominal thickness of 2 μm. Plasma enhanced chemical vapor deposition (PECVD) is used to the deposit the oxide layers on 1 mm thick, p-type silicon substrates with (001) orientation. A small sample (0.8 in × 0.8 in) is cut from the silica wafer and then is mounted on the stainless steel cylinder with a plastic adhesive. The silica wafers will be obtained from Silicon Quest International.

Polishing experiments is performed on a Struers® Rotopol 31 and TegraPol 35 tabletop polishers. The TegraPol 35 polisher allows control of platen velocity and pressure down to 3 ~ 7 psi. The ceria polishing slurry is delivered by a Struers® Multidoser unit that is connected to the polisher. The head and platen speed is 60 rpm and the center of the sample to be polished is placed at a distance of 8.9 cm from the center of the table. An IC 1000/Suba IV stacked pads (Rodel Inc.) is used for all polishing tests. During polishing, the slurry is continuously stirred by a magnetic bar,

and pumped to the pad-wafer interface at a flow rate of 100 mL/min by the Multidoser unit. The pad is conditioned before each polishing run with a grid-abrade diamond pad conditioner manufactured by TBW®. The diamond conditioner minimizes pad glazing and ensures reproducible pad conditions for each polish run.

Characterization

Ceria coated silica abrasives. The morphology and the size of the silica particles coated with ceria were examined by field emission scanning electric microscope (FESEM) at an accelerating voltage of 15 kV and high resolution transmission electron microscope (HRTEM) at an accelerating voltage of 120 kV. The average particle size of the silica particles coated with ceria was calculated by measuring ca. 100 particles from FESEM micrographs. The crystal structure of the particles was determined by x-ray diffraction (XRD) using CuKα (1.54 Å) radiation. The X-ray photoelectron spectroscopy (XPS) measurements were performed with a non-monochromatic MgKα source at a base pressure of 5×10^{-1} mbar. For consistency, all binding energies are reported with reference to the C 1s transition at 284.6 eV. The electrophoresis measurements were performed to obtain the electrophoretic mobility and the isoelectric point (IEP) of the prepared particles. The electrophoretic mobility of the particles was determined as a function of the pH.

Slurry stability. The abrasive size distribution of slurry was measured using light scattering method (UPA 150, Microtrac Inc.) as a function of pH of suspension.

Polished wafer. The film thickness on the wafers before and after CMP was measured using Filmetrics F20 (Filmetrics Inc.) to calculate the removal rate. In this experiment, the WIWNU was defined as the standard deviation of remaining thickness

divided by the average of the remaining thickness after the CMP process. The average polishing data for removal rate was carried by performing the same tests more than three times in order to support the validity of the results from the statistical viewpoint.

Results and Discussion

Ceria Coated Silica Particles

Morphology

Fig. 6-1 presents the FESEM micrographs of the silica core particles. It can be seen from the Fig. 6-1 that the uncoated silica particles have a monodispersed spherical shape and a very smooth surface.

Fig. 6-2(a) shows the FESEM micrograph of the ceria coated silica particles prepared using the 1.0 ml of precursor A at pH 6.8. As shown in Fig. 6-2(a), the coated particles have rough surface in contrast with the smooth surface of silica core particles. To better visualize the nature of ceria coating, a HRTEM micrograph of the ceria coated silica particles is presented in Fig. 6-2 (b). It can be found from the Fig. 6-2(b) that ceria coating with a thickness about 3 ~ 8 nm was deposited on the surface of silica particles. Moreover, as shown in Fig. 6-2 (c) and (d), the difference in morphology between two specimens prepared with precursor A and B are very interesting. The coated particles obtained from the precursor B (Fig. 6-2(c)) were severely aggregated. It appears that this result is mainly due to the bridging of adjacent particles with water by hydrogen bonding and subsequent high capillary forces during the drying process.[86] On the other hand, the coated particles synthesized from ceria precursor were monodispersed without hard aggregates (see Fig. 6-2(d)). This is attributed to the fact that the particles prepared by the alkoxide method generally show much higher reactivity than those via aqueous routes because organic solvent used in alkoxide method act as a dispersant

for particles during precipitation and prevent them from aggregating during drying. This result is consistent with the study reported by Ikegami et al.[87], which shows that the $Al(OH)_3$ and $Y(OH)_3$ wet precipitates show better dispersity in alcohols. In our work too, alcohol helps to decrease the colloidal attraction forces between particle surfaces during precipitation process and hence increase the dispersity of the ceria coated silica particles.

Crystalline phase

XRD patterns of the bare silica particles and ceria coated silica particles synthesized from the two precursors are shown in Fig. 6-3. The curve (a) represents the XRD spectra of the bare silica particles while curve (b) and (c) show XRD pattern of the coated silica particles obtained from precursor A and B, respectively. As shown in Fig. 6-3, the major reflections associated with fluorite structure of ceria coating can be observed from curve (b) and (c) in Fig. 6-3. The characteristic peaks corresponding to (111), (220), and (311) planes are located at 2θ = 28.53 47.47 and 56.22 respectively. They show very close to the ones with cubic fluorite structure of ceria crystal in JCPDS database. However, the ceria coating synthesized from precursor A show higher peak intensity as compared to that prepared by precursor B. It is interesting to note that the ceria coating synthesized by using ceria precursor shows better crystallinity in spite of the processing temperature being same as used in the conventional precipitation method. Additionally, the XRD analysis of the coated particles shows very broad peaks of ceria fluorite structure due to a thickness of ceria layer being below 10 nm and ceria coating was formed on the amorphous silica core.

XPS spectra of the ceria coating on silica particles

To further confirm the existence of ceria coating on the surface of silica particles, XPS analysis was carried out. The silica particles coated with ceria were prepared using 2.0 ml of ceria precursor at pH 6.8. Fig. 6-4 shows the XPS survey spectrum of the ceria coated silica particles obtained. It can be found that the sample contains Ce, Si, C and O elements. The photoelectron peaks for Si 2P, Si 2S, Ce $3d_{5/2}$, and Ce $3d_{3/2}$ are detected at 104.4 eV, 164.2 eV, and 860 eV ~ 920 eV with reference to the C 1s transition at 284.6 eV, respectively.

XPS analysis was also used to determine the oxidation state of cerium ions coated on the surface of silica particles. The O 1s core spectra are very informative in terms of structural details of the ceria coating. O 1s spectra of core silica particles and the coated particles are shown in Fig. 6-5. The binding energy of O 1s peaks for pure silica is 533.0 eV. As seen from the Fig. 6-5, it is clear that O 1s peak can be deconvoluted into two peaks associated with silica and ceria. For the silica particles coated with ceria, there are two mixed O 1s peaks at 532.4 eV and 534.8 eV, respectively. According to the data published by National Institute of Standards and Technology of USA, the peak at 532.4 eV is attributed to oxygen in silica particles. Whereas, the other peak at 534.8 eV is associated with the ceria coating on silica surface. After ceria coating, the binding energy of oxygen for the silica was slightly downward shifted. The chemical shift of O 1s peak can be explained by the insertion of Ce^{4+} cations into the tetrahedral sites of the silica network to form Ce-O-Si bonds and the greater electronegativity of Si^{4+} to that of Ce^{4+}. This indicates that the ceria coating layer and core silica particle is connected through the Ce-O-Si chemical bonding at the interface.

To confirm the purity of ceria coating deposited on silica particles, the XPS Ce 3d multiplex is shown in Fig. 5. The Ce 3d peak consists of two main features in the range of 870 ~ 930 eV, corresponding to the Ce $3d_{3/2}$ and $3d_{5/2}$ components due to the spin-orbit coupling. In previous works,[88,89] both Ce(III) and Ce(IV) show the $3d_{5/2}$ and $3d_{3/2}$ multiplexes. However, Ce(III) shows only two peaks (P1 and P2) for each component ($3d_{5/2}$ and $3d_{3/2}$) whereas Ce(IV) shows three peaks (P1, P2 and P3) associated with the initial state of tetravalent cerium. In our work the presence of the initial state of tetravalent cerium is further substantiated by the evidence of an third peak at a binding energy of 918 eV. The presence of three structures (P1, P2 and P3) confirms the coating of ceria on the surface of silica particles.

Electrokinetic behavior

Fig. 6-7 shows the FESEM micrographs of the ceria coated silica particles prepared using the 1.0 ml of precursor A at different pH. At pH 3.2, the ceria layer was not observed on the surface of silica particles (Fig. 6-7(a)). This indicates that the ceria coating was not formed on the surface of silica particles. At pH 6.8, the coated particles were observed and the ceria layer was uniformly deposited on the surface of silica particles (Fig. 6-7(b)). It is found that this pH condition is favorable for the chemical bond formation between the ceria precursor and silica particles. At pH 9.7, the prepared particles were covered with a massive ceria layers (Fig. 6-7(c)). This is attributed to the fact that at pH 9.7, ceria precursor becomes unstable and ceria precipitates. Additionally, the pH is near the ceria precipitate IEP leading to formation of ceria particle aggregates. In Fig. 6-8, curves show the variation of zeta potential with pH value for the silica particles and the precipitated precursor A, respectively. As shown by the curve (c), the precipitated precursor A has the IEP at pH 8 ~ 10. In our work coating process for the

ceria coated silica particles include three steps; the formation of gel by ceria sol, the formation of gel-like layer on the core particles and crystallization of ceria in this layer.[90,91] This coating behavior is qualitatively influenced by the pH value of reaction medium due to variation in the electrostatic forces between ceria precursor and silica core particles as shown in Fig. 6-9. At pH 3.2, the ceria layer was not deposited on the surface of silica particles because of the weak electrostatic attraction between ceria sol and core particles. Besides, participating anions (OH^-) cause the precipitation of ceria particles in liquid phase reaction,[72,92] it is probable that the formation of the gel was not induced in spite of adding ammonium hydroxide due to the acidic condition at pH 3.2. On the other hand, at pH 6.8, silica particles have a negative surface charge and the precipitated ceria precursor has a positive surface charge with a significant difference in magnitude of charge between the two materials as shown in Fig. 6-8. This indicates that the precipitated ceria precursor would be expected to experience a strong electrostatic attraction towards the negatively changed surface of silica particles leading to deposition of ceria layer on the surface of silica particles. Further, at pH 9.7, the pH of ceria precursor solution is near the IEP of precipitated precursor A. Under these conditions, ceria particles aggregate to form thick layer due to unstable conditions and weak interaction between the ceria precipitate and the silica particles. Moreover, in Fig. 6-8, curve (b) shows the variations of zeta-potential with pH values for the ceria coated silica particles. The coated particles were obtained by adding 4 ml of ceria precursor at pH 6.7. As shown in Fig. 6-8, it can be found that the IEP of the coated particles shifted from silica particles toward the similar value of ceria particles and the electrophoretic mobility of the coated particles showed a similar trend with that of ceria particles.

Control of thickness of the ceria coating on silica particles

Fig. 6-10 shows the FESEM micrographs of the ceria coated silica particles prepared with the different concentration of precursor A at pH 6.6 ~ 6.9. The coated particle sizes determined in the FESEM examination gradually increased with the increase in precursor concentration. The variations of the average particle size and the ceria coating thickness with the amount of ceria precursor are shown in Fig. 6-11. The average particle size was 289, 302, 338, and 402 nm for the 0, 1, 2, and 4 ml of the precursor added, respectively. After adding 8 ml precursor, the average particle size could not be calculated, since massive ceria layers were deposited on the surface of silica particles. The average ceria coating thickness was 6.5 nm after adding 1 ml ceria precursor. With increasing the concentration of ceria precursor, the coating thickness gradually increased about 14 nm per additional 1 ml precursor. Therefore, the thickness of ceria coating could be controlled from 6.5 nm to maximum 56.5 nm by changing the concentration of ceria precursor in this system.

Size control of the ceria coating on silica particles

Figure 6-12 shows the FESEM micrographs of the silica particles synthesized by different experiment conditions. It is found that the size of colloidal silica particles could be controlled by adjusting the reaction parameter such as temperature, solvent type, pH, and the concentration of TEOS. In this experiment, the average sizes of silica particles determined by FESEM were 105 nm, 214 nm, 332 nm, and 442 nm, respectively. Figure 6-13 shows the FESEM micrographs of the ceria coated silica particles, which have each different size according to the size of colloidal silica particles used. The average sizes of the synthesized particles determined by FESEM were 146 nm, 256 nm, 334 nm,

and 384 nm, respectively. Therefore, the size of the ceria coated silica particles can be controlled by the size of core silica particles.

CMP Evaluation

To investigate the effects of the ceria coated silica particles on CMP performance, I carried out CMP test with the slurry including the silica particles coated with the coating thickness of 7 ~ 12 nm under the different CMP conditions. Table 6-1 summarizes the quantitative results of the polishing test as a function of suspension pH and down pressure.

Effect of pH

The results for removal rate of the oxide films as a function of suspension pH are shown in Fig 6-14. The downforce was 7 psi. As the pH of ceria-based slurry increased, the slurry had a lower removal rate for the oxide film. This polishing behavior is attributed to electrophoretic mobility and absorption behavior between abrasives and silica film as a function of suspension pH. As shown in Fig. 6-8, the pH at the respective IEP can be identified as the point of zero charge (pH_{pzc}). The pH_{pzc} of ceria abrasives occurs at pH 7 ~ 8. Also, the pH_{pzc} of silica film is at about 1.5 ~ 2.8.[93] This value is close to core silica particles reported in this experiment. At pH values below the pH_{pzc} of ceria abrasives (~ pH 7), the surface of ceria becomes positively charged and the surface of silica film becomes negatively charged, leading to absorption between two materials. However, with the increasing pH of the solution, the ceria surface becomes more negatively charged and the silica surface also has a negative surface charge, leading to repulsion between two materials. It seems that these interaction behaviors affected the removal rate of silica film. Therefore, the removal rate of silica film decreased with the increase in pH of ceria-based slurry.

Effect of down pressure

The results for removal rate of the oxide films as function of CMP pressure are shown in Fig 6-15. For each slurry, pH was adjusted to 2.9 ~ 3.1 by adding ammonium hydroxide. As shown in Fig. 6-15, the removal rate increased with increasing in the pressure during CMP process. This mechanical behavior is explained by Preston's equation. The abrasion/wear-based Preston's equation MRR = K_pP_0V, where MRR is the material removal rate, P_0 the down pressure, V the relative velocity of water, and K_p a constant representing the effect of other remaining parameters, has been widely used in CMP process control and consumable development for integrated circuit (IC) fabrication and manufacturing. It reflects the influence of mechanicals on the material removal rate. From this equation, it is found that the removal rate is proportional to the down pressure (P_0). Therefore, material removal rate of oxide increased with the increase in down pressure.

Wafer roughness (WIWNU)

Fig. 6-16 shows the results for surface uniformity of the oxide films as function of pH. The downforce was 5 psi. As shown in Fig. 6-16, WIWNU decreased with increasing the suspension pH. This polishing behavior is attributed to a broader particle size distribution and the agglomerated particle behavior of ceria slurries as function of suspension pH. The slurry was formulated by dispersing ceria abrasives in DI water containing an anionic organic polymer. Generally, the acidic suspension had greater particle size and broader size distribution of abrasive ceria than those of the neutral or alkaline suspensions.[29] The broader particle size distribution of large abrasives can cause a different removal rate between the center and the edges of the film surface due

to their limited mobility on the wafer surface. Consequently, the surface uniformity deteriorated with the aggregated abrasives during CMP process.

Conclusions

Ceria Coated Silica Particles

Monodispersed ceria coated silica particles were prepared by surface-induced precipitation method using new type of ceria coating precursor. In order to investigate the effects of solvent type on the physical and chemical properties of ceria coating, the cerium ethanolate complex was used as the precursor A and was compared with the precursor B obtained from water-based solvent. The pH of the ceria treatment solution had significantly influence on the formation of the coating on the particles due to the electrostatic attraction between the silica particles and the sol type ceria precursor. The ceria coating was uniformly formed on the surface of silica particles at a pH of about 7.0. The electrophoretic mobility for coated particles proved that the ceria layers were deposited on the surface of silica particles. FESEM and TEM micrographs showed that the resultant coated particles prepared from precursor A exhibited spherical shape without the formation of hard aggregates as compared to that prepared from precursor B. The XRD analysis of the coated particles revealed that the crystalline ceria coating was formed without post-heat treatment. XRD results also revealed a difference in crystallinity of ceria coating obtained from precursor A and B. The XPS investigation for the O 1s and Ce 3d photoelectron lines showed the pure ceria (Ce(IV) oxide) coating on the silica particles which was chemically bonded with the silica particles as evidenced by the additional peak at a binding energy of 918 eV. The coating thickness of particles was controlled by adjusting the amount of ceria coating precursor. As the precursor concentration was increased, the coating thickness gradually increased from 6.5 to 56.5

nm (maximum thickness). Additionally, the size of the ceria coated silica particles could be easily controlled by the size of core silica particles. This means that abrasive size can be controlled according to CMP process conditions without mechanical milling process and filteration system.

CMP Evaluation

In this study, the resultant particles were used as CMP abrasives for ceria-based slurry to investigate the effects of the ceria coated silica particles on polishing performance during oxide CMP. The primary particle size was controlled about 146 nm without mechanical milling process by depositing the ceria coating on the surface of colloidal silica particles with size 135 nm. The removal rate of silicon dioxide film strongly depended upon suspension pH. With increasing suspension pH, the removal rate of silica film decreased. On the other hand, surface uniformity deteriorated as the suspension pH decreases. These polishing behaviors were related to electrophoretic mobility of abrasives for silica film to be polished, since surface charge of the abrasives can be changed by suspension pH. Thus, it means that absorption/repulsion behavior between abrasives and materials to be polished plays an important role in polishing performance during CMP process. Additionally, the removal rate of silica film increased with increasing down pressure in terms of mechanical aspect for CMP condition.

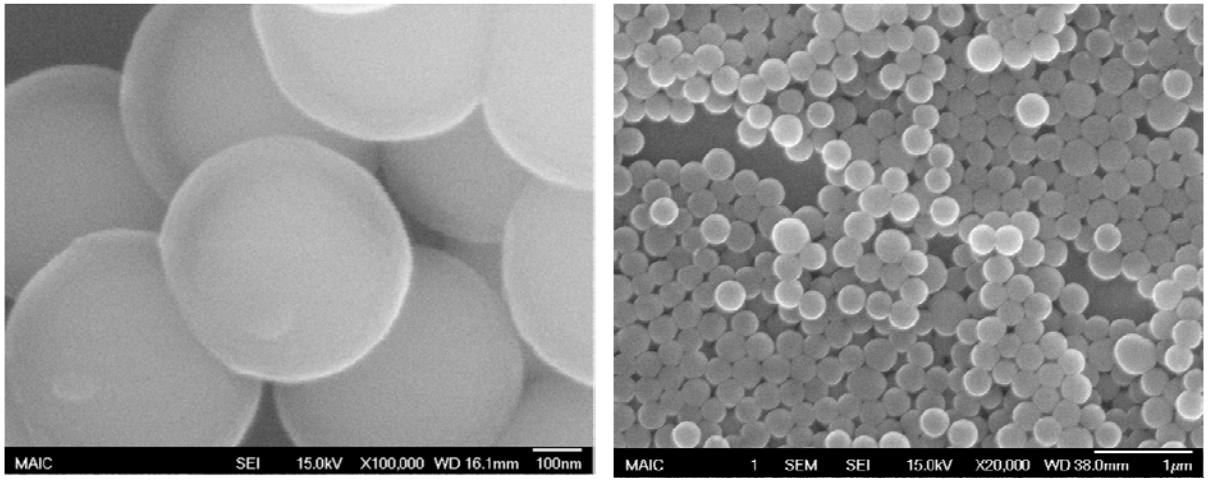

Figure 6-1. FESEM images of silica core particles obtained by modified Stöber method

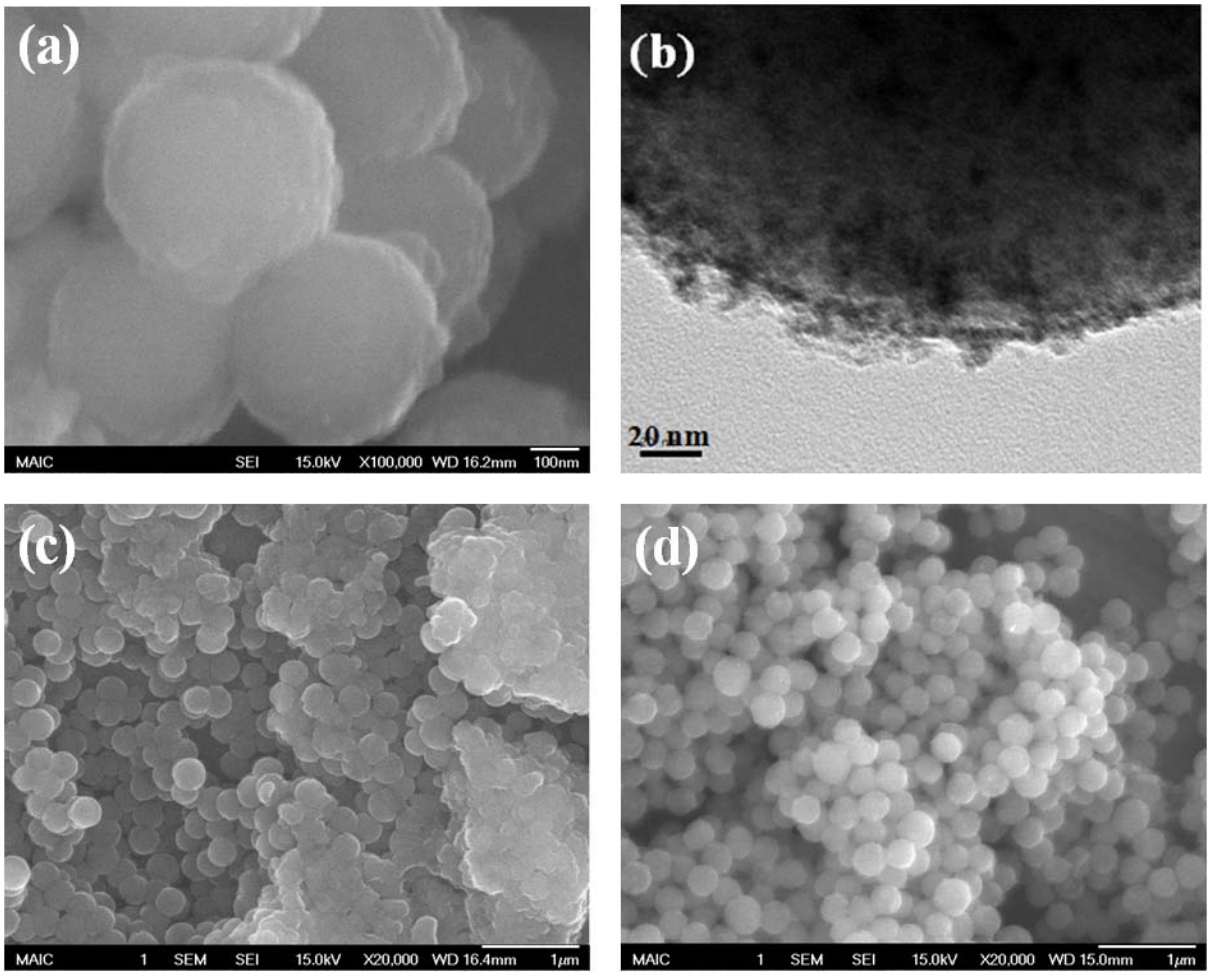

Figure 6-2. (a) FESEM and (b) HRTEM micrographs for the surface condition of coated particle and FESEM micrographs for ceria coated silica particles prepared by (c) precursor B and (d) precursor A, respectively

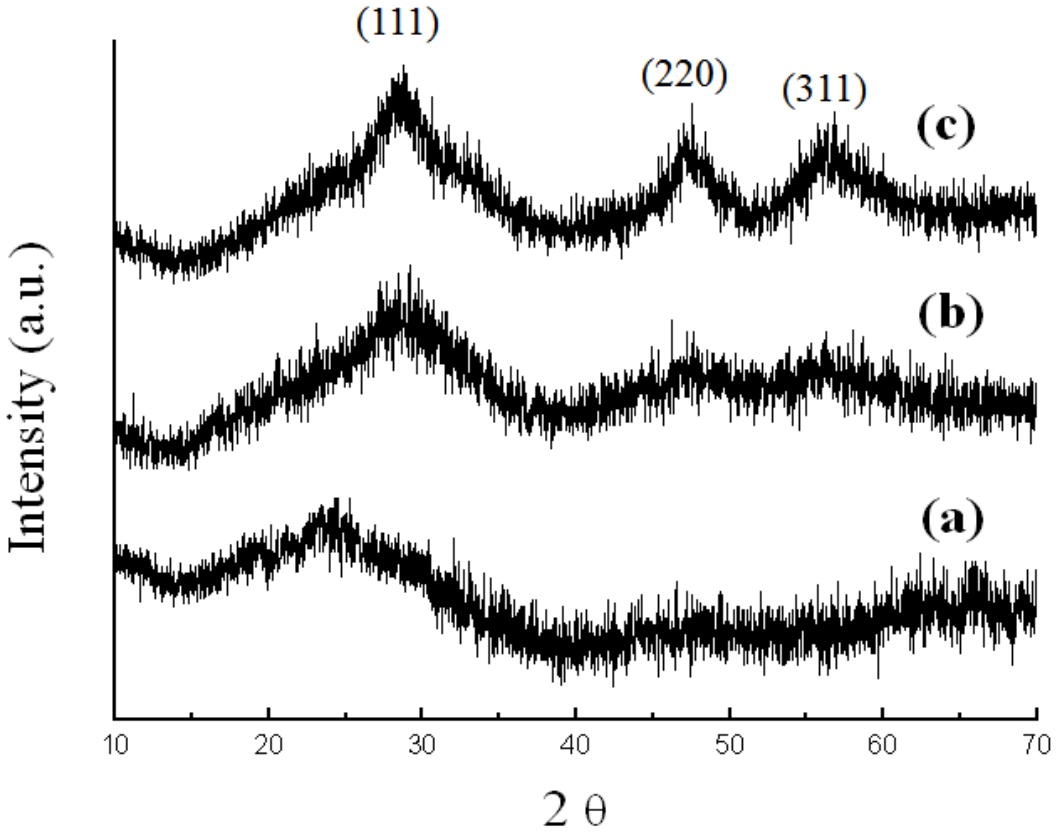

Figure 6-3. XRD patterns of the synthesized particles; (a) bare silica particles, (b) ceria coated silica particles prepared by precursor B, and (c) precursor A

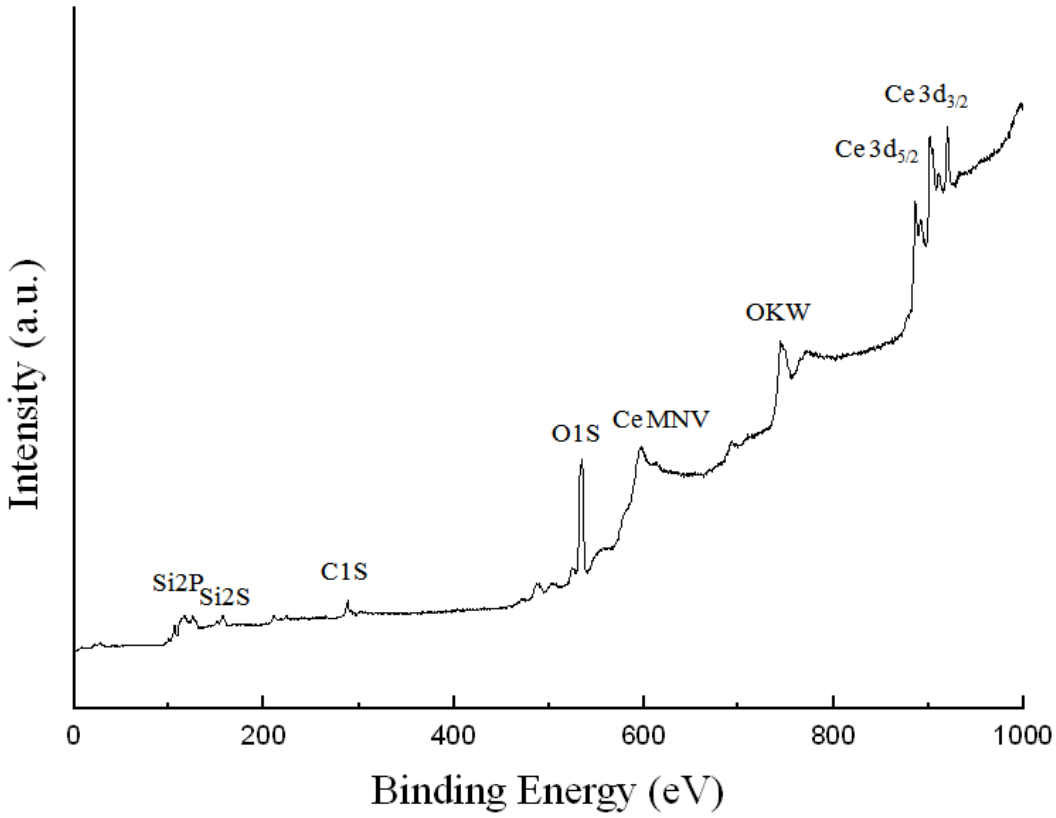

Figure 6-4. XPS survey spectrum of ceria coated silica particles

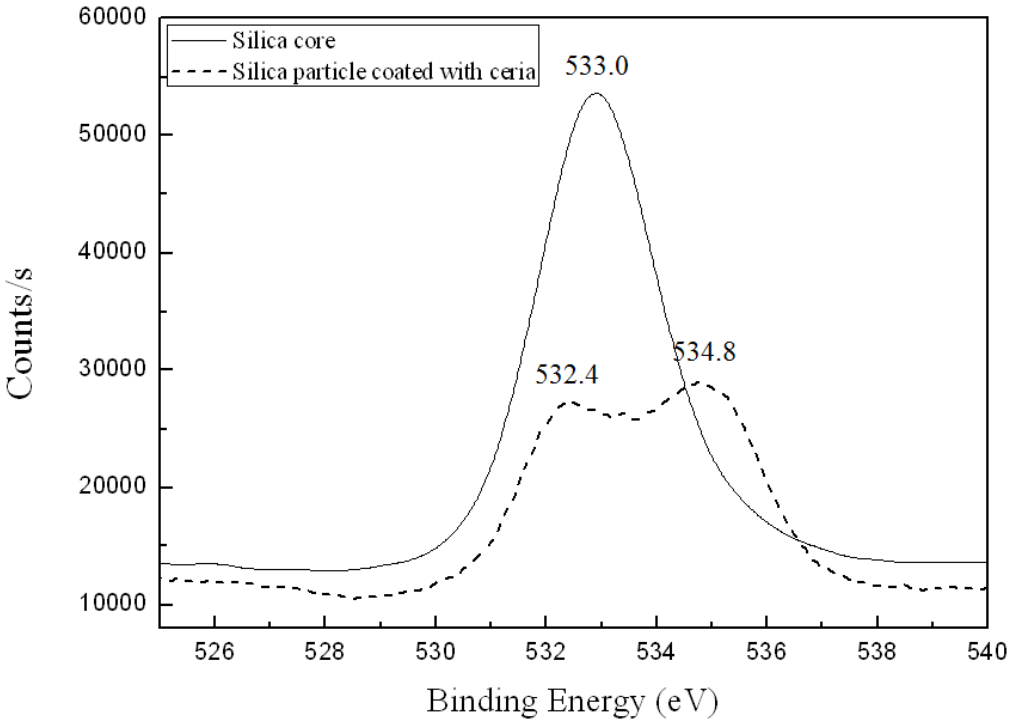

Figure 6-5. XPS spectra of O 1s peaks of ceria coated silica particles

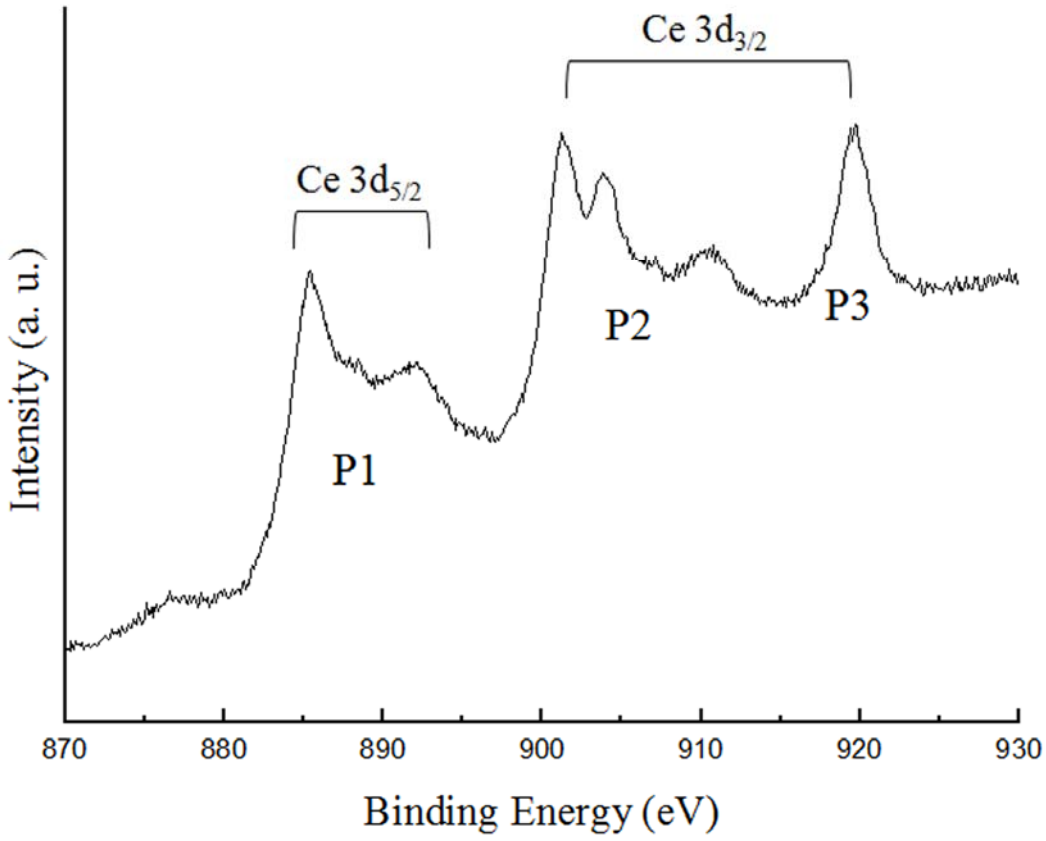

Figure 6-6. XPS Ce 3d multiplex of ceria coated silica particles

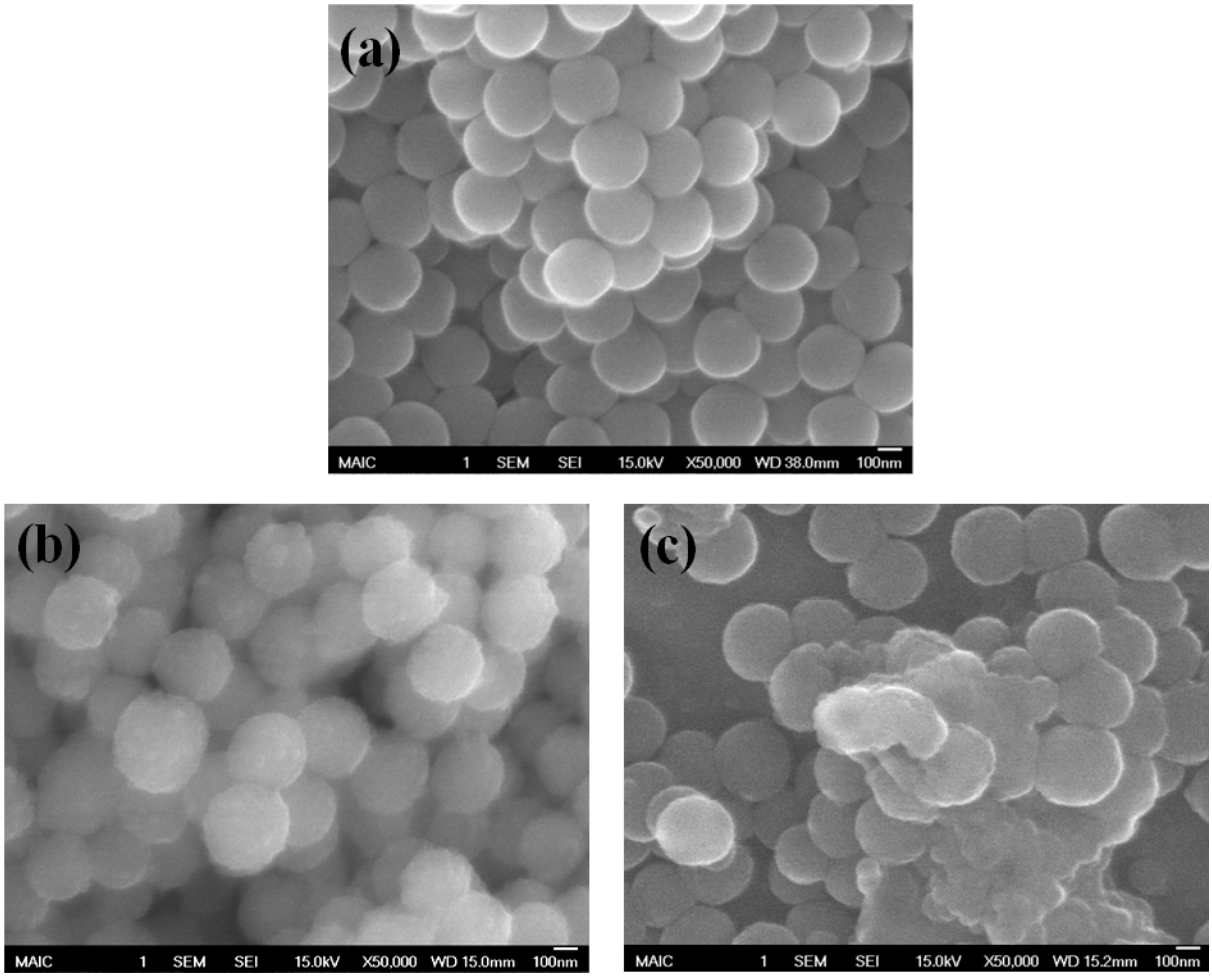

Figure 6-7. FESEM photographs for ceria coated silica particles prepared at different pH (a) 3.2, (b) 6.8 and (c) 9.7

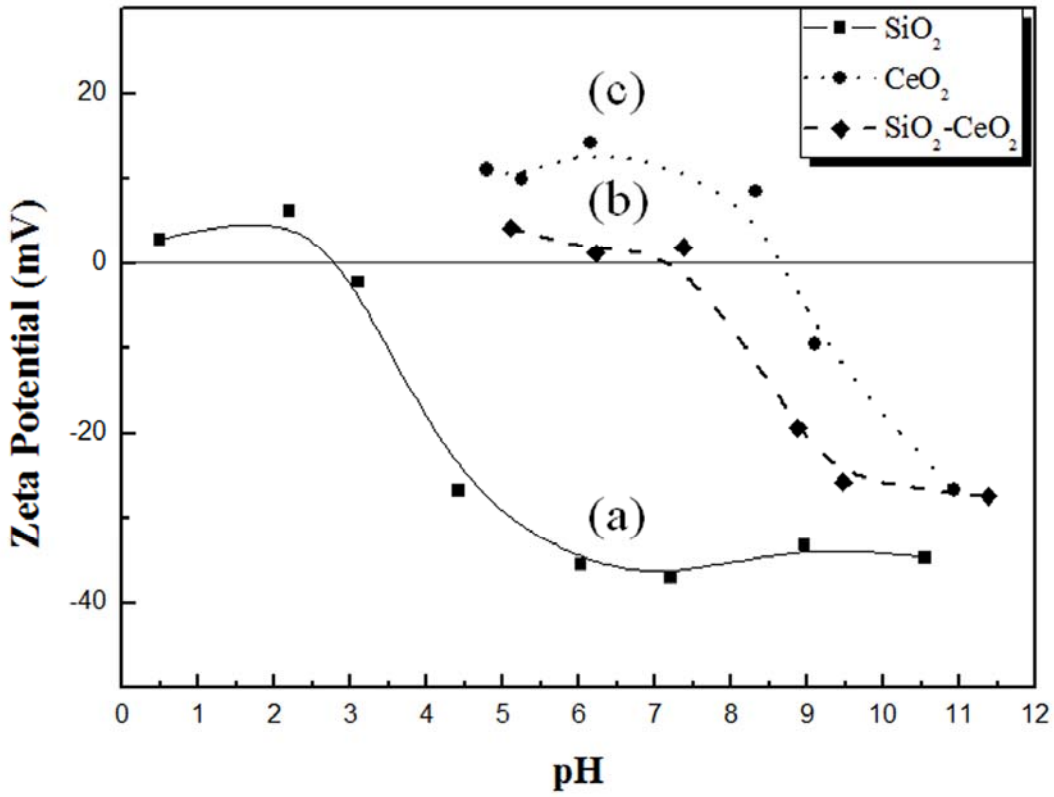

Figure 6-8. Electrophoretic mobility for (a) silica particles (b) ceria coated silica particles and (c) ceria particles

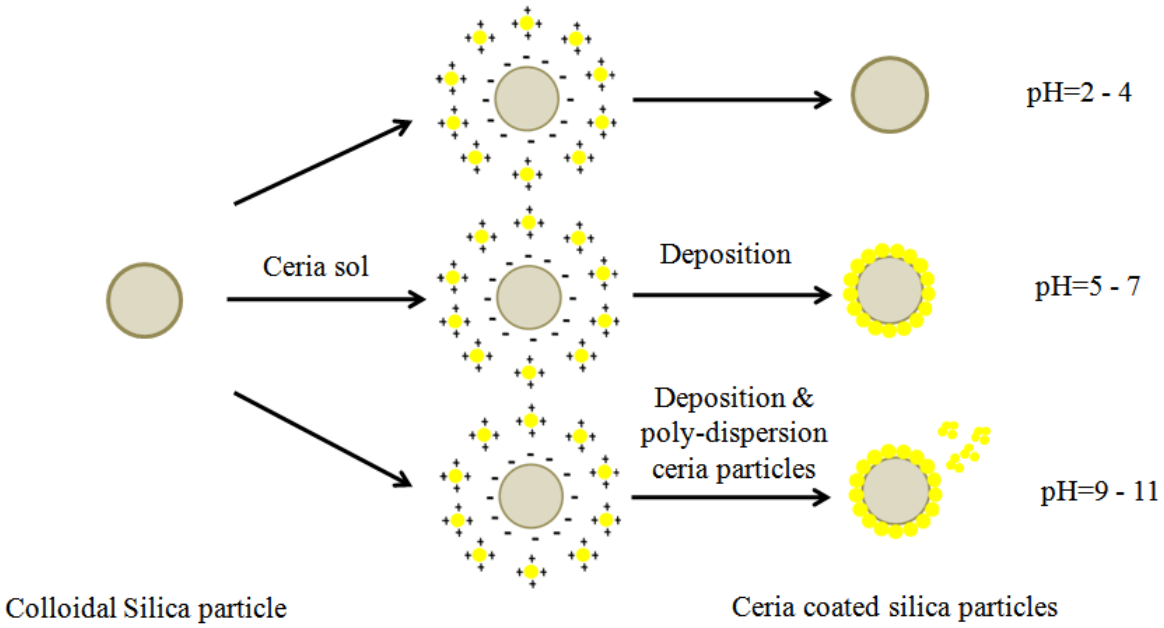

Figure 6-9. Scheme of the formation mechanism of ceria coated silica particles at different pH

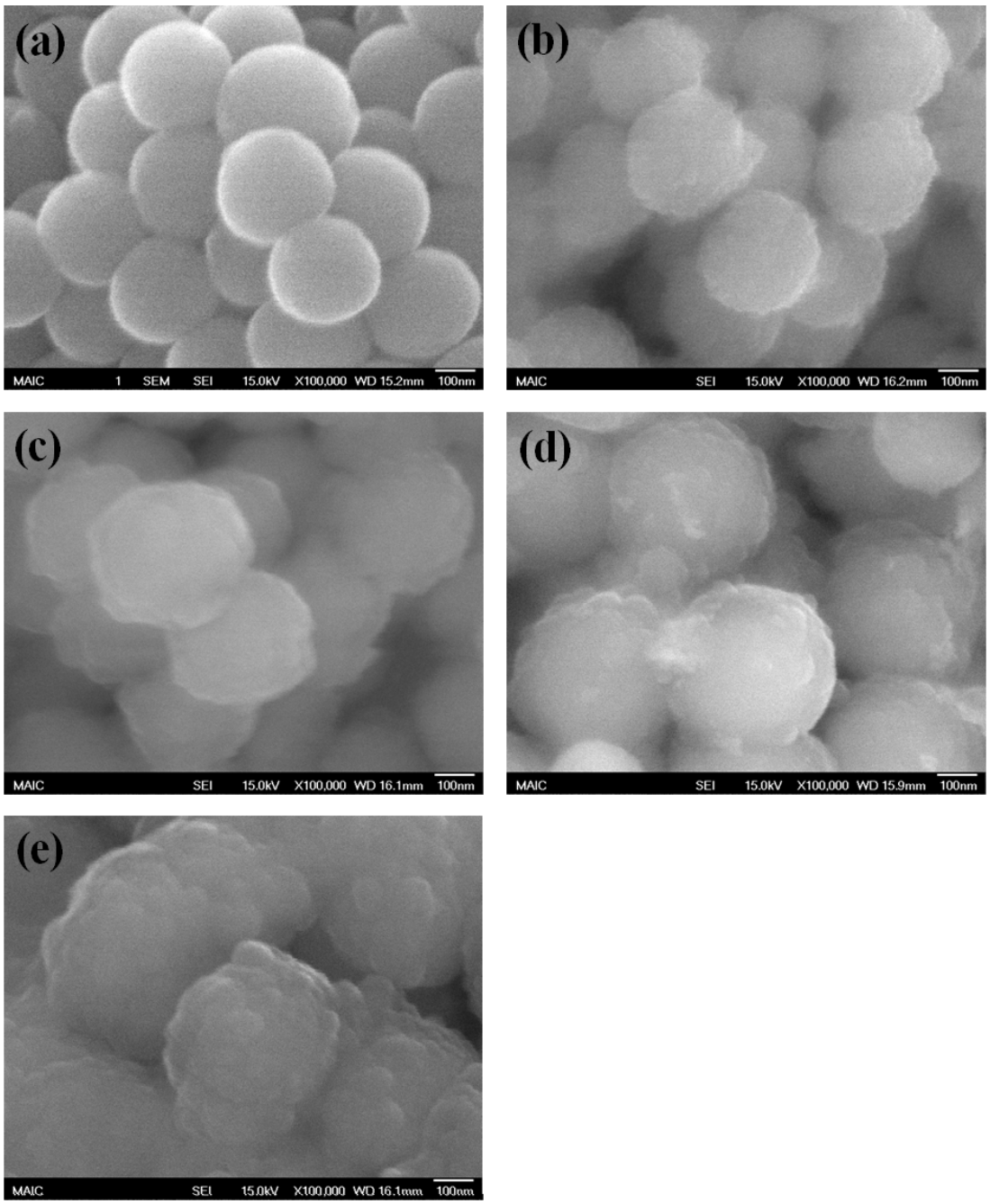

Figure 6-10. FESEM micrographs of ceria coated silica particles prepared by different concentration of ceria precursors (a) 0.0 ml, (b) 1.0 ml, (c) 2.0 ml, (d) 4.0 ml and (e) 8.0 ml

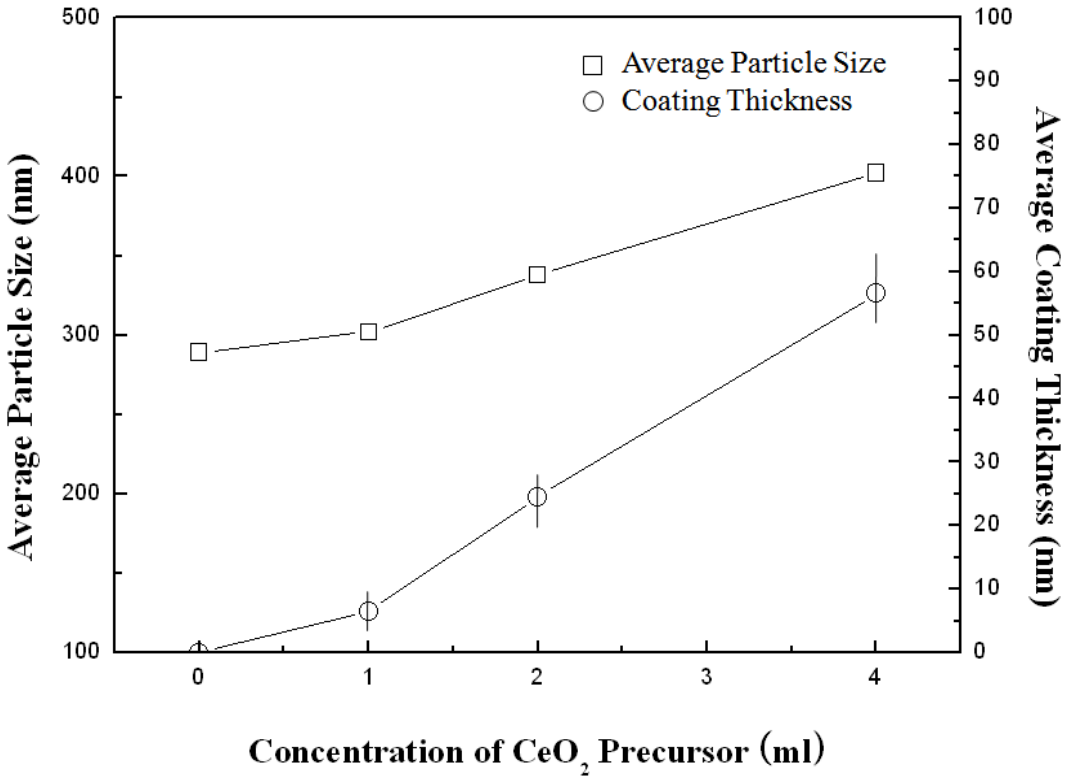

Figure 6-11. The variations of (a) coating thickness and (b) average particle size for samples obtained by changing the concentration of ceria precursors

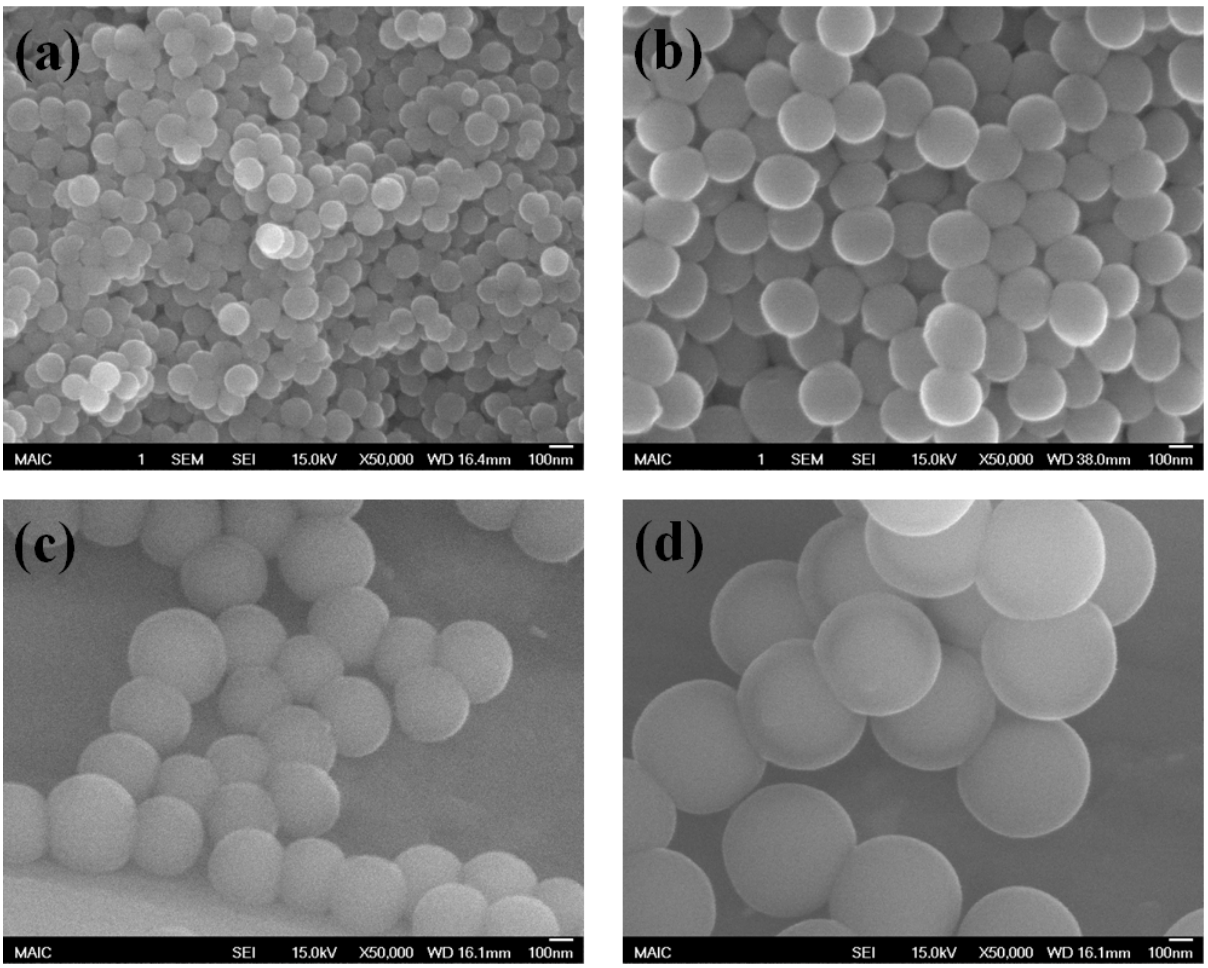

Figure 6-12. FESEM micrographs of the silica particles with different size; (a) 105 nm, (b) 214 nm, (c) 332 nm, and (d) 442 nm

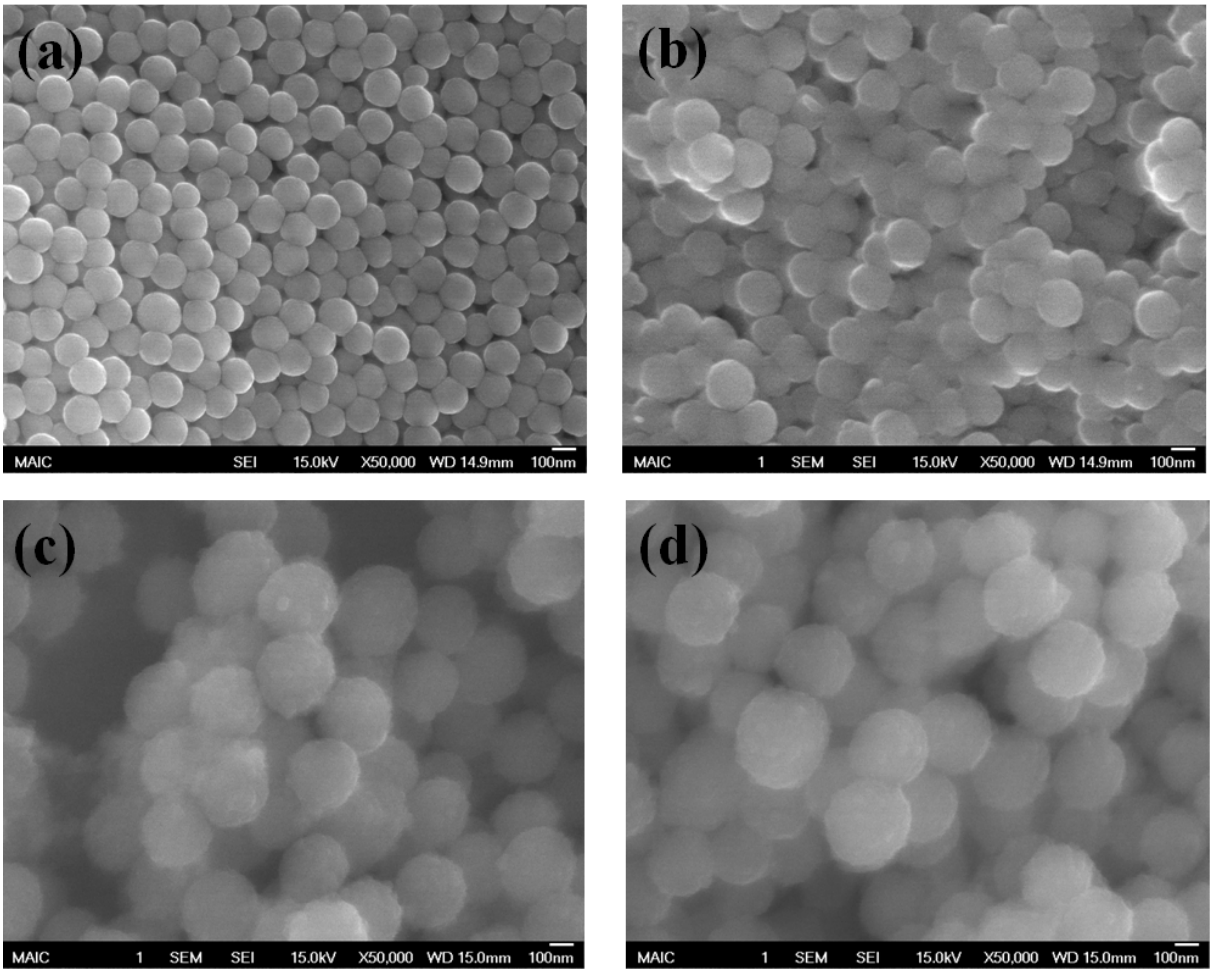

Figure 6-13. FESEM micrographs of the ceria coated silica particles obtained from different core silica particles with different size; (a) 146 nm, (b) 256 nm, (c) 334 nm, and (d) 384 nm

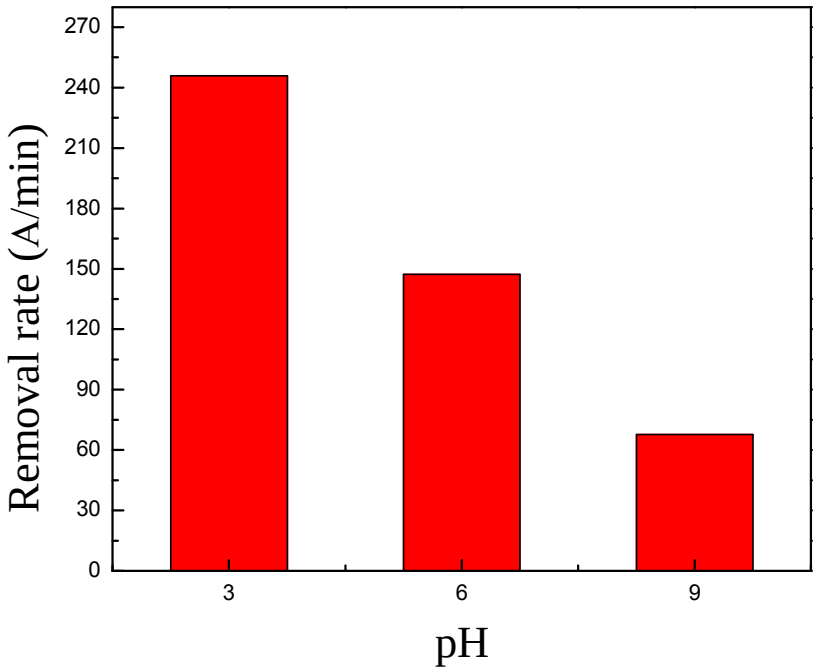

Figure 6-14. Results of CMP field evaluation for removal rate as function of pH

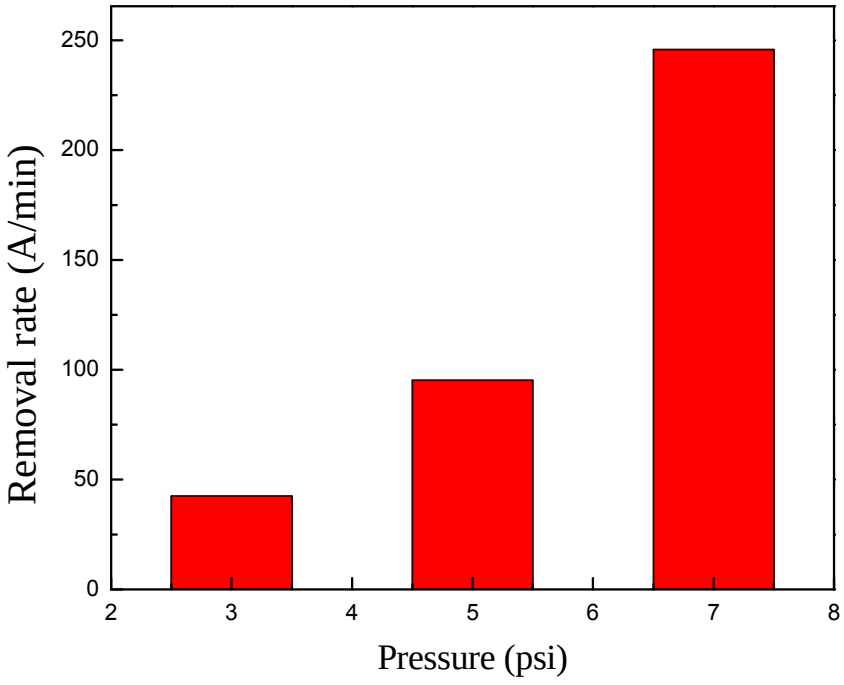

Figure 6-15. Results of CMP field evaluation for removal rate as function of CMP pressure

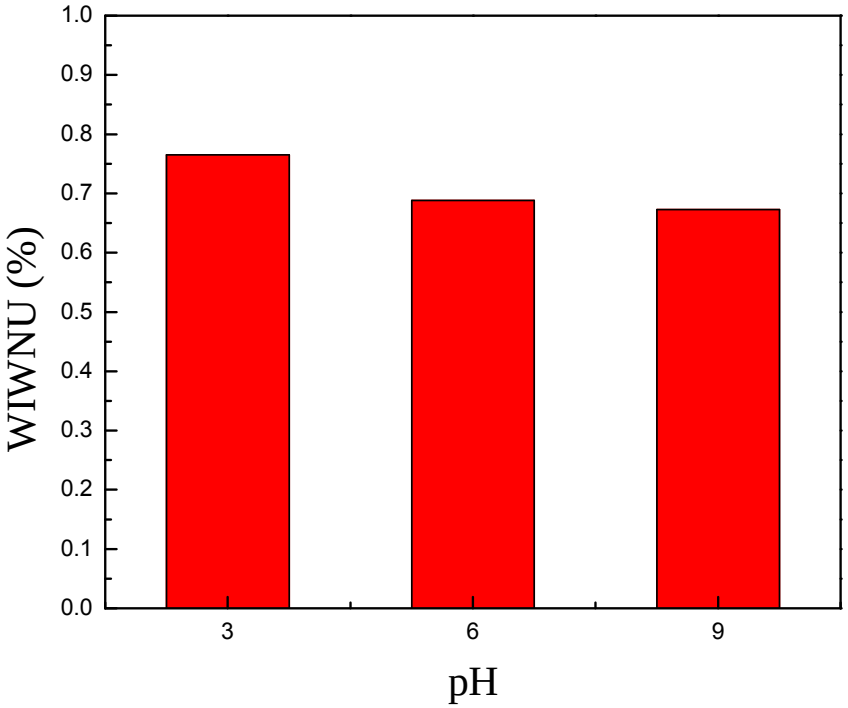

Figure 6-16. The result for within-wafer non uniformity (WIWNU) of oxide film

Table 6-1. The results of the removal rate for the ceria coated silica particles

Pressure (psi)	pH9 (Å/min)	pH6(Å/min)	pH3(Å/min)
3	16.6	24.2	42.4
5	46.4	63.0	95.2
7	67.6	147.2	245.8

CHAPTER 7
SYNTHESIS OF SPHERICAL CERIA PARTICLES BY THERMAL DECOMPOSITION METHOD AND ITS CMP PERFORMANCE

Introduction

The shape-controlled synthesis of nanomaterials has been considered as important research subject in numerous applications, such as in ceramics, catalysis, additive in paint, recording materials, and many others. The change in morphology of nanocrystalline materials will alter the properties which were formerly thought to be constant for given materials. As mentioned in chapter 4 and 5, commercial ceria abrasives is commonly prepared by thermal decomposition method. Although the ceria abrasives obtained from thermal decomposition have a higher porosity leading to softness and high chemical reactivity to oxide films, the size and the shape of the ceria abrasives are very limited since particle growth is difficult to control during calcination process. Therefore, a new method which can control the morphological properties of ceria particle should be proposed.

In chapter 4, solvent effects on the shape, size, and crystalline phase for ceria particles under hydrothermal precipitation condition had been investigated. Also, many research results have been reported that the morphology of solid particles is influenced by the dielectric properties of alcohols as solvent in view of the thermodynamics of reaction system, nucleation kinetics, and particle interaction potentials.[64,65] Therefore, the advantage of the use of organic solvent lies in that it can adjust the growth habit of the ceria particles, leading to the formation of final products with desirable morphology and change the micro-environment of the reaction.

Considering the framework of precursors or starting cerium salt tends to remain immediately after the thermal decomposition,[94] cerium carbonate as precursor is

expected to affect the shape and size of ceria particles after heat treatment. If monodispersed spherical cerium carbonate particles are prepared, ceria particles obtained from the cerium carbonates should have the following properties: (1) spherical shape, (2) narrow particle size distribution, (3) mechanical softness with lager surface area, and (4) chemical properties. From these concepts, in this chapter, spherical ceria particles were prepared by thermal decomposition method using spherical cerium carbonate as as-prepared particles. I have developed a two-step procedure to synthesize ceria crystallites. A cerium carbonate precursor was first prepared via simple precipitation method using alcohol/water mixed solvent, and ceria particles was obtained by subsequent thermal decomposition of the precursor. The resultant particles were used as abrasives of ceria-based slurry. In order to investigate the size effects of ceria abrasives on CMP performance, the size of cerium carbonate particles were modulated by changing the volume ratio of alcohol to water of mixed solvent and the dielectric constant of solvent. For CMP performance evaluation, the effect of spherical ceria abrasives on the removal rate, the oxide-nitride removal selectivity and the within-wafer non uniformity (WIWNU) was investigated.

Materials and Methods

Preparation of Spherical Ceria Abrasives

Cerium (III) nitrate hexahydrate ($Ce(NO_3)_3 \cdot 6H_2O$) and ammonium carbonate ($(NH_4)_2CO_3$) were used as the starting materials for ceria particles. Both regents were of analytical grade purity and were used without further purification. Cerium nitrate and ammonium carbonate were separately dissolved in distilled water. The concentration of both chemicals was adjusted to 5 M. This aqueous solution was then mixed with alcohols to adjust the volume ratio of alcohol to water to 0, 1, 3, and 5. The final

concentration of both chemicals was 1 mol/L, respectively. Alcohols, including methanol (CH_3OH), ethanol (C_2H_5OH), 2-propanol (C_3H_8O), and 1, 4-butandiol ($C_4H_{10}O_2$) were used to investigate the influence of the properties of solvent. The cerium carbonate particles were obtained by dripping the cerium nitride solution into ammonium carbonate solution. The carbonate precipitation was carried out at a temperature of 75 ^oC for 24 hour with magnetic stirring. After the precipitation reaction, the precipitates were washed with distilled water three times by repeated centrifugation and then dried at room temperature with flowing nitrogen. The dried particles were calcined in for 90 min at 500 - 800^oC temperature to obtain ceria particles.

CMP Evaluation

Preparation of ceria-based slurries

Different ceria-based slurries were formulated by dispersing abrasives each with different primary particle size in DI water containing an anionic organic polymer (Poly acrylic acid, PAA; Mw 4000, LG Chem.) as dispersant. 2 wt% of PAA based on the total weight of the ceria abrasives was added. For each slurry, pH was adjusted to 3 ~ 9 by adding ammonium hydroxide (NH_4OH). The solid loading of ceria abrasives was fixed to 2.0 wt%.

CMP tools and consumables

Silicon dioxide film of 2 μm thick was grown on a 5-in. p-type silicon substrates with (001) orientation by plasma enhanced chemical vapor deposition (PECVD). The silicon nitride films were deposited by using low-pressure chemical vapor deposition (LPCVD). Polishing tests were performed on a rotary type CMP machine (GNP POLI 400, G&P technology) for one minute with each of the ceria-based slurries. IC 1000/SUBA IV stacked pads (supplied by Rodel Inc.) were utilized as CMP pads. The

downforce was 4 psi and the rotation speed between the pad and the wafer was 100 rpm. The slurry flow rate was 100 mL/min.

Characterization

Abrasives

The crystal structure and grain size was identified by x-ray diffraction (XRD) using CuKα radiation. The grain size was estimated by the Scherrer equation according to the formula $D = 0.9 \lambda / (\beta \cos \theta)$, where D is the grain size, λ is the wavelength of x-rays, β is the half-width of the diffraction peaks, and θ is the diffraction angle. The broadening of the reflection from the (111) plane was used to calculate the grain size. The morphology and size of the precipitate particles were examined by high resolution transmission electron microscope (HRTEM) and field emission scanning electron microscope (FESEM). The average primary particle size was calculated by measuring ca. 100 particles from FESEM micrographs. The specific surface area (SSA) of the ceria abrasives was determined by Brunauer-Emmett-Teller (BET) method using nitrogen adsorption/desorption at 77 K.

Ceria-based slurry

The abrasive size distribution of slurry was measured using light scattering method (UPA 150, Microtrac Inc.).

CMP performance

The film thickness on the wafers before and after CMP was measured using spectroscopic reflectometry (Nanospec 6100, Nanometrics) to calculate the removal rate. In this experiment, the WIWNU was defined as the standard deviation of remaining thickness divided by the average of the remaining thickness after the CMP process. The average polishing data for removal rate was carried by performing the same tests more

than three times in order to support the validity of the results from the statistical viewpoint.

Results and Discussion

Properties of Spherical Cerium Carbonate Precursor

Influence of solvent type on particle morphology

Figure 7-1 shows the XRD patterns of cerium carbonate compounds synthesized at 75 ^{o}C with different kinds of solvents. All except the particle obtained by using isopropanol as solvent exhibited a pure orthorhombic $CeOHCO_3$ structure with variable crystallinity in JCPDS database (a=5.015, b=8.565, c=7.337 Å, symmetry group *Pmcn*). On the other hand, the particles obtained from isopropanol consisted of a mixture of products including CeO_2 and $CeOHCO_3$, the former being responsible for the stronger peaks. This solvent type has a significant effect on the phase formation with different affinities for water. It is well-known that, physicochemical solvent properties, such as polarity, viscosity, dielectric properties, and softness, will strong influence the solubility and transport behavior of the precursors.

Under various experimental conditions, the microstructures of cerium carbonate compounds can be changed to different shape such as spherical, oval and spindle-shape. Figure 7-2 shows FESEM micrographs of cerium carbonate obtained from water-based solvent. As shown in Fig. 7-2, the cerium carbonate compounds are composed of oval-like particles with the size of 300 ~ 500 nm. On the other hand, the cerium carbonate compounds obtained by using mixed solvent are composed of spherical agglomerates with uniform size distribution as shown in Fig. 7-3. This difference in morphology of the resultant particles indicates that the colloidal stability of the precipitation particles in the mixed solvent is different from that pure water solvent.

This result can be understood by considering the parameters determining the colloidal stability.[95-97] Generally, the maximum repulsive force can be estimated from the eq. 7-1 for electrostatically stabilized particles.

$$F_r = 2\pi\varepsilon_0\varepsilon_r\kappa\alpha\Psi^2 \quad (7\text{-}1)$$

where ε_0 is the permittivity in free space, ε_r is the dielectric constant of the continuous phase, κ is the Debye-Huckel parameter, α is the particle diameter, Ψ is the particle surface potential.[98,99] Under the constant ionic strength of the solvent, the maximum repulsive force depends on the particle surface potential, the dielectric constant and the particle surface potential. According to DLVO (Derjaquin Landau Verwey Overbeek) theory, the energy barrier between each particle which inhibit agglomeration can be also expressed as

$$V_b = -\frac{A\kappa\alpha}{12} + 2\pi\varepsilon_0\varepsilon_r\kappa\alpha\Psi^2 \quad (7\text{-}2)$$

where A is the effective Hamaker constant. The effective Hamaker constant depends on the dispersion medium. Considering that the mixed solvent is composed of water and alcohol, the mixed solvent may not greatly influence the effective Hamaker constant. Therefore, the ionic strength is supposed to be constant in the solvent. From these conditions, the magnitude of repulsive force and the barrier energy is determined by the dielectric constant, the surface potential and particle size.

Additionally, Figure 7-3 shows the morphologies of cerium carbonate compounds prepared from different mixed solvent. The precipitates obtained from mixed solvents are composed of spherical secondary agglomerates with small primary particles of nanometer scale. From these results, it is thought that the particle is grown by the aggregation of fine primary particle in mixed solvents. It is interesting to note that the

size of the resultant particles was varied by the kinds of solvents. Generally, the primary particles nucleated from solutions are known to grow by aggregation or molecular addition with small sub-units. The particle growth after nucleation can be also affected by the types of solvents, because the particle interaction potential is different in each solvent. Thus, the secondary particles are composed of the aggregation of sub-unit particles with fine size. In this experiment, the size of the secondary particles increased as the number of carbon in alcohol used as mixed solvent increased.

Effect of dielectric constant on particle morphology

Table 7-1 summarized the dielectric constants of mixed solvent using ethanol and water and the zeta potentials and the morphologies of particles obtained from each solvent. The dielectric constants and the zeta potentials decrease as the ratio of ethanol to water increases.[67,68] For the pure water, the dielectric constant of water and the zeta potential of the synthesized particles are very high. According to Eq. 7-2, the potential energy barrier is relatively high. Under this condition, primary particles may be relatively stable against the aggregation. On the other hand, in the case of the mixed solvent with a higher ratio of 3 ~ 5, the zeta potential and the dielectric constant are low. So, the zeta potential of the synthesized particles and the dielectric constant of mixed solvent are very low. The precipitated cerium carbonate compounds have a low potential energy barrier and maximum repulsive force. For this condition, primary particles may be relatively unstable as the nucleation occurs. However, the colloidal stability of the precipitates increases as the size of the aggregates increases because the potential barrier and the maximum repulsive force increases with the increase in particle size. Figure 7-4 shows the FESEM micrographs of the precipitates prepared using mixed solvent of ethanol and water as a function of the ratio of ethanol to water. The resulting

particles are composed of small and well-defined particles with spherical shape. These results indicate that the composition of the mixed solvent affects the morphology of particles, which is changed by the dielectric properties of solvent.

CMP Materials

Preparation of ceria abrasives

Figure 7-5 shows the XRD pattern of as-prepared particles of ceria abrasives (cerium carbonate particles) and ceria abrasives obtained from thermal decomposition of the cerium carbonate particles at 700 ^{o}C. The as-prepared particles were synthesized by using mixed solvent of ethanol and water and the ratio of the solvent was 3. As shown in curve (b), the characteristic peaks corresponding to (111), (200), (220), (311), and (222) planes are located at 2θ = 28.54, 33.12, 47.45, 56.32, and 59.02^{o}, respectively. They show very close to the ones with cubic fluorite structure of cerium oxide in JCPDS database. It implies that the cerium carbonate compounds are completely transformed into a pure crystalline cerium oxide at 700 ^{o}C.

Figure 7-6 shows the FESEM micrographs of as-prepared particles of ceria abrasives (cerium carbonate particles) and ceria abrasives obtained from thermal decomposition of the cerium carbonate particles at 700 ^{o}C. As shown in Fig. 7-5, the as-prepared particles exhibits a rough surface and a spherical shape with diameter of 50 ~ 300 nm. After thermal decomposition, the resultant particles show spherical shape regardless of the crystallization to oxide by heat treatment. On the other hand, the surface of particles was rougher due to emission of the resultant gases such as carbon dioxide, ammonia, nitride, etc.

Figure 7-7 shows the relationship between surface area and crystalline size of ceria abrasives as a function of the calcination temperature. The overall trend reveals

that the surface area of ceria abrasives was reduced and the crystalline size was enhanced with increasing in calcination temperature. This result attributes to the fact that the sintering mechanisms generally lead to bonding and growth of necks between each particle, so the strength of the particles compact increases during sintering.[100] This result corresponds to the result for BET and crystalline size of ceria abrasives mentioned in chapter 5.

Characteristics of ceria-base slurry

The electrokinetic behaviors of the ceria particles and ceria particles with PAA as a function of pH were investigated to identify the polishing behavior in oxide CMP. These results are shown in Fig. 7-8. The electrokinetic behavior of each particle is reflected in the interaction between the ceria-based slurry and the silica wafer. The electrophoretic mobility of all components is strongly dependent on the suspension pH. The electrophoretic mobility of silica is negative above pH = 2.2, which is the isoelectric point (pH_{IEP}) of silica. The electrophoretic mobility of silica decreases with increasing suspension pH. This is attributed to a compression of the electrical double layer due to both the dissolution of the Si ion, resulting in an increase of ionic silicate species in solution, and the presence of alkaline ionic species.[93] For ceria abrasives, the pH_{IEP} is at about pH 7, and a slightly positive-charged surface below this pH region. However, the pH_{IEP} of the ceria abrasives shifted toward the acidic pH region with additive polymer (PAA). There are two reasons for this behavior. First, the ionization of near-surface segments partially screens the charge on the particles, thereby decreasing the shear plane potential. Second, the presence of polymer chains may disturb the hydrodynamic plane of shear, shifting it further out from the particle surface. Because the potential decreases exponentially with distance,[102] the modified shear plane will

experience a lower potential. Above the pH_{IEP}, the electrophoretic mobility of ceria abrasives increased with suspension pH up to the saturation point. Saturation occurs in the pH region of 6–8, resulting in a negatively charged particle whose electrokinetic behavior is essentially no longer dependent on the suspension pH.

Figure 7-9 shows the changes in particle size distribution of ceria-based slurry as a function of suspension pH. As shown in Fig. 7-9, the acidic suspension had broader size distribution of ceria particles and bigger particle size than those of the alkaline or neutral suspensions. Ceria-based slurry in acidic condition became unstable because of lower electrostatic repulsive forces. On the other hand, it is observed that the ceria-based slurry have a better dispersion stability in neutral and alkaline suspension due to higher surface potential.

CMP Evaluation

Effects of calcination temperature on physical properties of ceria abrasives

Figure 7-10 shows the results for removal rate of oxide and nitride blanket wafers. To evaluate the effects of calcination temperature on CMP performance, four kinds of ceria abrasives were prepared by calcination at 500 ~ 800 ^{o}C temperature. The suspension pH of all slurries were adjusted at 6.8 ~ 7.1. As shown in Fig. 7-10(a), it is observed that the ceria-based slurry had a higher removal rate for the silica wafer as the calcination temperature increased. Especially, the removal rate of oxide film rapidly increased in high calcination temperature above 700 ^{o}C. On the other hand, the removal rate of nitride film increased slightly and did not vary much with increasing the calcination temperature as shown in Fig. 7-10(b).

Figure 7-11 summarizes the quantitative results of the polishing test as a function of calcination temperature. The removal rate of oxide film is mainly affected by its

chemical interaction with the ceria abrasives, and by physical parameters including the physical properties of the particles and the mechanical grinding factor. The surface of silica film is soluble in neutral and alkaline pH solutions due to the dissolution of Si ions. Interaction between the ceria abrasives and the surface of oxide film occurs in this pH region and Si–O–Ce bonds are formed on the surface of oxide film during polishing. As a consequence, the Si-O-Ce bonds can be rapidly removed by the mechanical force generated by pressed pad and abrasives, and this physicochemical reaction lead to the high removal rate of oxide film. In this experiment, the suspension pH was maintained constant for all slurries. Therefore, it seems that the increase in the removal rate of oxide film is relate to the mechanical factors rather that to the effect of the chemical interaction. These mechanical factors are influenced by several physical parameters of the CMP process, such as morphological aspects of the abrasives, crystallite size of the abrasives and the CMP conditions. As seen from Fig. 7-7, the crystalline size of ceria abrasives increased as the calcination temperature increased. The removal rate can be significantly affected by the crystalline size of ceria abrasives because indentation is related to the mechanical properties of abrasive hardness and abrasive size.

The removal rate of nitride film is affected by the physical properties of ceria-based slurry systems and the amount of surfactant adsorbed on the film surface.[5] The surface of the nitride film during polishing is passivated with an anionic acrylic polymer in the slurry, which prevents the ceria abrasives from contacting the film surface. In this study, the amount of the polymer was also maintained constant for all slurry. Therefore, it seems that the increase in the removal rate of nitride film is relate to the mechanical

factors rather that to the effect of passivation layer of the polymer absorbed on the film surface.

The removal selectivity can be calculated by comparing the removal rate between oxide and nitride film. As shown in Fig. 7-11, the removal selectivity increases with calcination temperature, from 27.8 at 500 ^{o}C to 37.4 at 800 ^{o}C. This behavior was different with the CMP results for removal selectivity shown in chapters 4 and 5. In chapters 4 and 5, the removal selectivity showed a transition behavior and the existence of optimum abrasive size in slurry. This result attributes that the ceria abrasives used in this experiment have a relatively high surface area in spite of high calcination temperature. For nitride removal rate, passivation layer might be insufficiently formed on the nitride film surface due to a largely adsorbed polymer on the particle surface. This adsorption behavior for additive polymer leads to the steady increase in removal rate of nitride. Moreover, the removal rate of oxide film rapidly increased in high calcination temperature. Therefore, in this experiment, the removal selectivity increased as calcination temperature increased.

Effects of suspension pH on oxide and nitride CMP

Figure 7-12 shows the results for removal rate of oxide and nitride and Table 7-2 summarizes the quantitative results of the polishing test as a function of suspension pH. The ceria-based slurries were prepared by using ceria abrasives calcined at 700 ^{o}C. As shown in Fig. 7-12, it is observed that the ceria abrasives dispersed in neutral and alkaline conditions had high removal rates for silicon dioxide layer and low within-wafer nonuniformity (WIWNU). It is well known that the removal rate of oxide film is dependent on two CMP parameters, the mechanical grinding and the chemical interaction. The surface of the oxide film is soluble in alkaline pH solutions due to the instability of the

silica at this pH. As mentioned in previous section, the interaction between the ceria abrasives and the oxide film occurs during the polishing of the silica blanket wafer, and then Si–O–Ce bonds are formed on the film surface. Si–O–Ce bonding on the surface is reported to be the dominant mechanism in the chemical interaction between silica film and the ceria abrasives.[12] Mechanical removal of the Si–O–Si bonds causes O-Si-O or Si-$(OH)_4$ monomer to be removed as a lump, which is released by the ceria abrasives during CMP process. Therefore, the removal rate of oxide film showed higher value at alkaline region of pH 9 ~ 10 because silicon on the oxide film dissolved, which caused the oxide film to become softer.

The reduction in the removal rate of oxide film at the acidic region is related to the chemical solubility, a decrease in the frictional interactions, and lubrication by polymer adsorption. The dissolution process of silica film in aqueous solution is mainly due to the hydrolysis of Si–O–Si bonds. However, at acidic region, the Si ions on the silica film seldom dissolve, which results in the low chemical solubility of the film surface. Thus, the removal rate of oxide film in acidic suspension was lower than in other conditions. Additionally, as shown in Fig. 7-9, broader particle size distribution in slurry was observed in the acidic slurry because of lower surface potential of ceria abrasives. The presence of agglomerated particles leads to a decrease in the contact area between the oxide film to be polished and the ceria abrasives. Furthermore, the frictional force between the oxide film and the ceria abrasives is decreased due to the presence of the agglomerated particles because the frictional force is directly proportional to the contact area. Therefore, the removal rate of oxide film decreased with acidic ceria-based slurry.

The slurry shows a higher WIWNU for the oxide film with acidic ceria-based slurry as shown in Fig. 7-12. This polishing behavior is attributed to a broader particle size distribution of the slurry. The distribution data in Fig. 7-9 shows that the particle size distribution broadens with the decrease in suspension pH. The inhomogeneous distribution in acidic pH region leads to local frictional interactions of the agglomerated particles, causing different removal rates between the center and the edge of the wafer due to their limited mobility on the wafer surface. Therefore, it seems that surface uniformity of oxide film is related to the particle uniformity of the ceria-based slurry.

Conclusions

Synthesis of Cerium Carbonates

Spherical cerium carbonate compounds were synthesized by using mixed solvent of alcohol and water. The obtained results indicated that physicochemical solvent properties had a significant effect on the crystalline phase, microstructures and morphological properties of the resultant particles. FESEM results revealed the morphology of cerium carbonates could be changed by the type of solvent. In this experiment, the particles obtained from pure water were composed of oval-like particles with the size of 300 ~ 500 nm. In contrast, the particles prepared by using alcohols had a spherical shape with uniform size distribution. FESEM analysis also showed that the size of the cerium carbonates increased as the number of carbon in alcohol used as mixed solvent increased. Moreover, the size of the precipitants decreased with the increase in the ratio of ethanol to water.

Synthesis of Ceria Abrasives

Spherical ceria abrasives were prepared by thermal decomposition of the synthesized spherical cerium carbonates at 700 ^{o}C. XRD result revealed that the cerium

carbonates were completely transformed into a pure crystalline cerium oxide at 700 ^{o}C. From FESEM analysis, ceria particles after calcination process exhibited spherical shape regardless of the crystallization to oxide by heat treatment. On the other hand, the surface of particles was rougher due to emission of the resultant gases such as carbon dioxide, ammonia, nitride, etc. BET and XRD results showed that the surface area of ceria abrasives was reduced and the crystalline size was enhanced with increasing in calcination temperature.

Preparation of Ceria-based Slurry

Ceria-base slurries were prepared by dispersing the synthesized particles and additive polymer into DI water. The obtained results showed that the pH_{IEP} of ceria abrasives shifted toward the acidic pH region with additive polymer. Moreover, the acidic suspension had broader size distribution of ceria particles and bigger particle size than those of the alkaline or neutral suspensions in terms of electrostatic repulsive forces.

CMP Evaluation

In this study, the effect of the calcination temperature on the physical properties of synthesized ceria particles and suspension pH on CMP performance were investigated. The CMP results revealed that the ceria-based slurry had a higher removal rate for the silica and nitride wafer as the calcination temperature increased. Moreover, the removal selectivity increased as calcination temperature increased. For suspension pH, the ceria abrasives dispersed in neutral and alkaline conditions had high removal rates for silicon dioxide layer because the surface of the oxide film is soluble in alkaline and neutral pH solutions. In addition, the surface uniformity deteriorated at acidic pH solution because of a broader particle size distribution of the ceria abrasives in the slurry and the

presence of agglomerated abrasives. Furthermore, the surface uniformity deteriorated with acidic pH solution due to inhomogeneous distribution leading to local frictional interactions of the agglomerated particles.

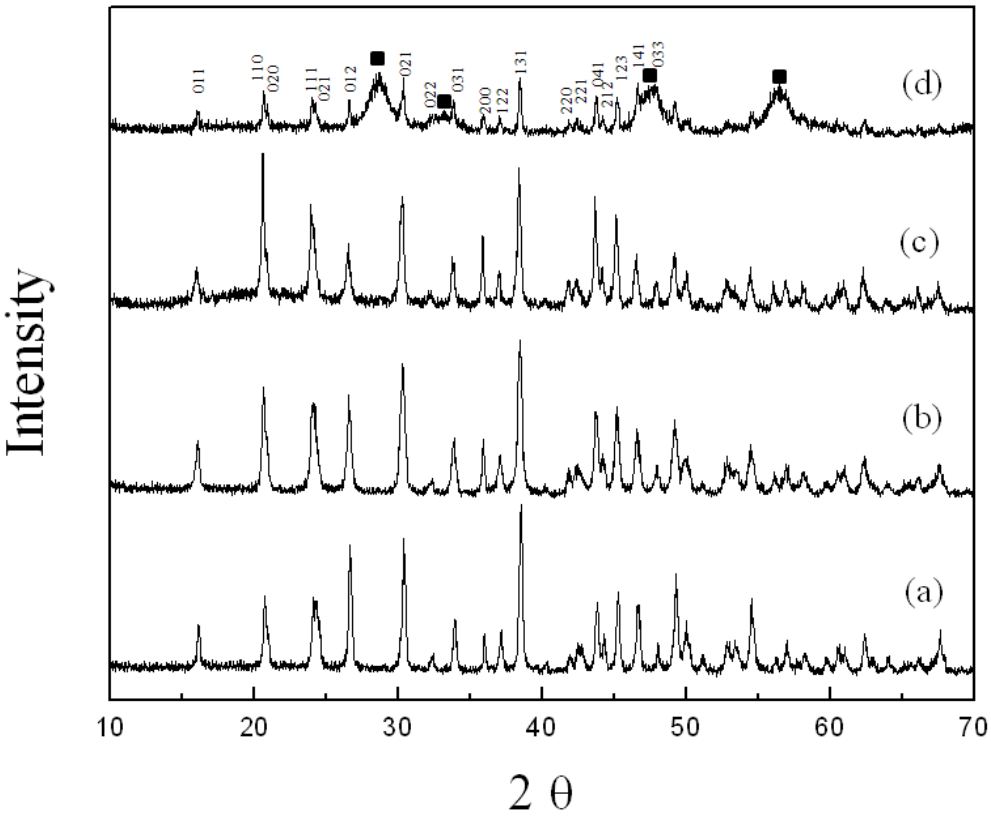

Figure 7-1. XRD patterns of cerium compositions produced under precipitation conditions with different solvent

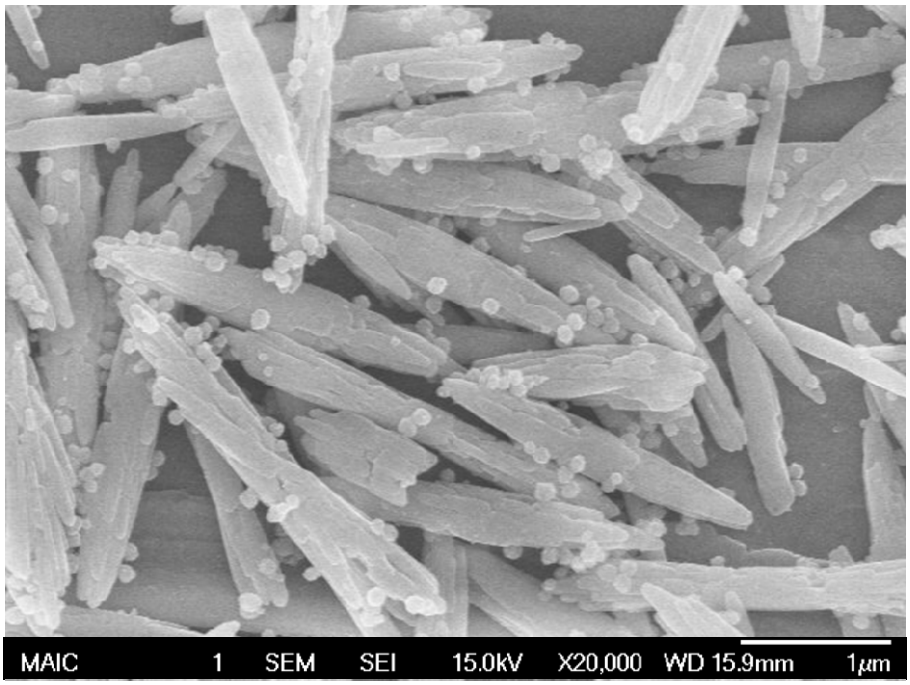

Figure 7-2. FESEM micrographs of cerium carbonate compounds obtained by using pure water as solvent

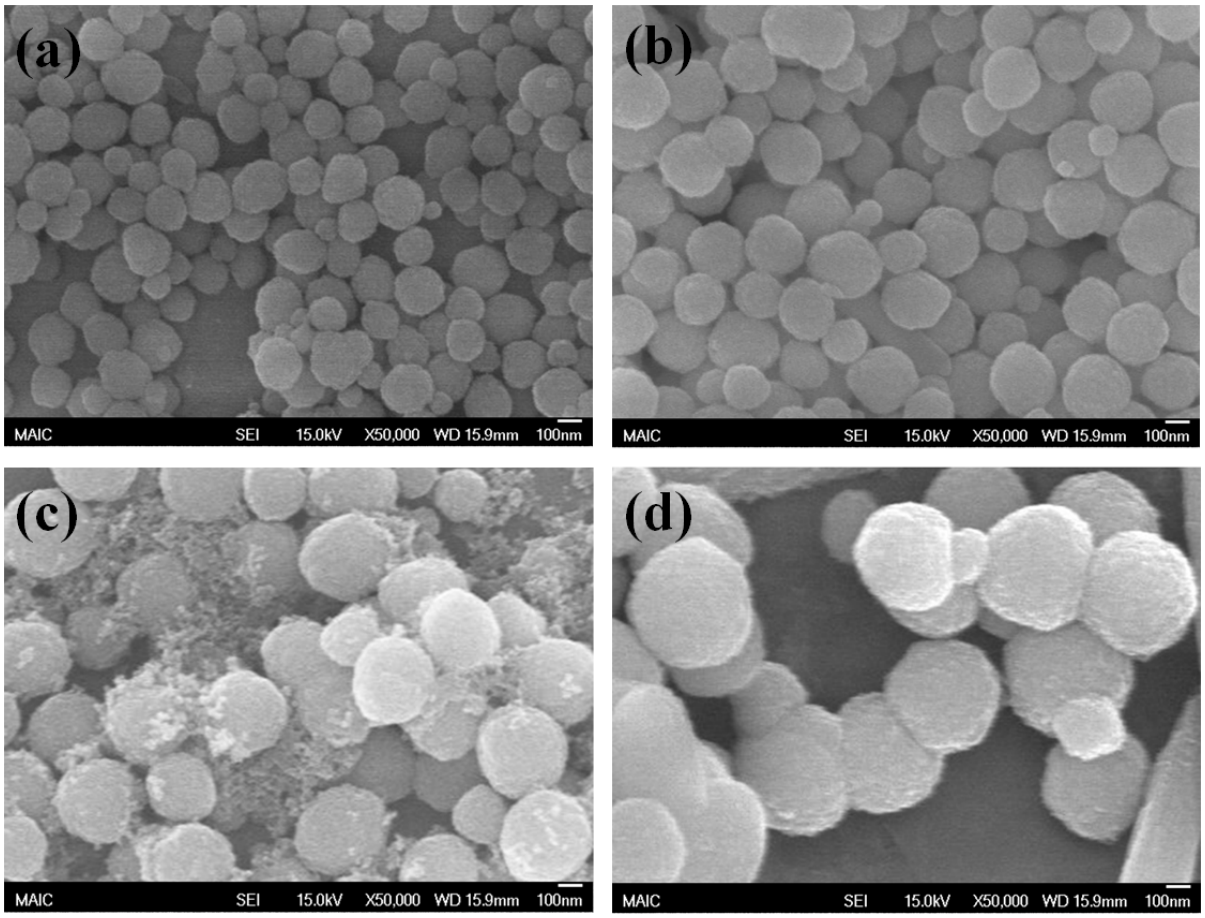

Figure 7-3. FESEM micrographs of spherical cerium carbonate particles prepared from the mixture of water and different alcohols; (a) methanol (CH_3OH), (b) ethanol (C_2H_5OH), (c) 2-propanol (C_3H_8O), and (d) 1, 4-butandiol ($C_4H_{10}O_2$)

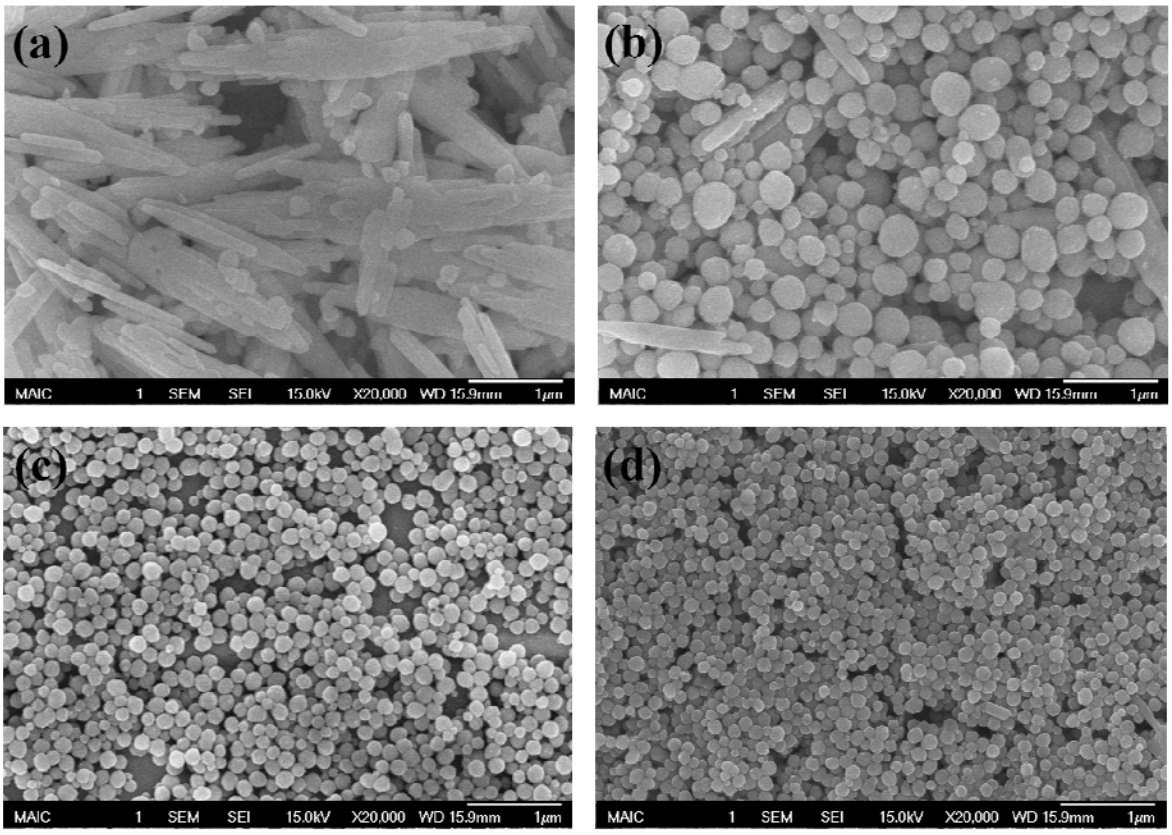

Figure 7-4. FESEM micrographs of cerium carbonate compounds prepared by various ratio of ethanol to water: (a) 0, (b) 1, (c) 3, and (d) 5

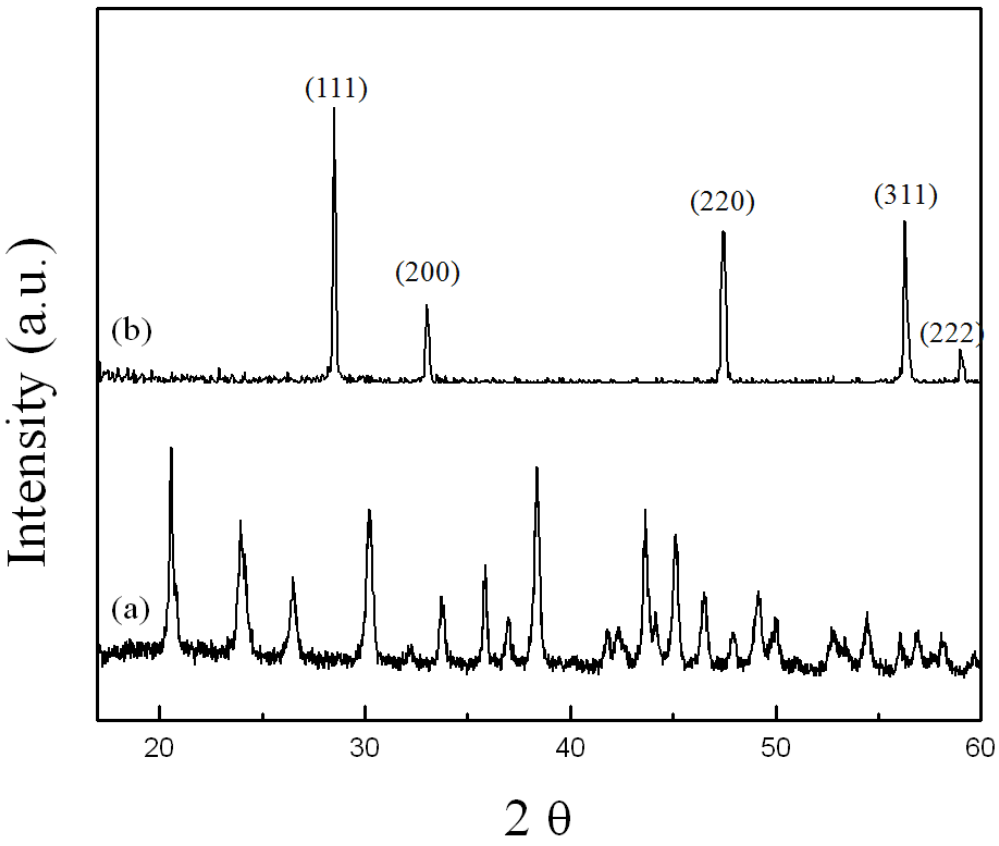

Figure 7-5. The XRD pattern of (a) cerium carbonate prepared by using mixed solvent of ethanol and water and (b) ceria abrasives obtained from thermal decomposition of the cerium carbonate at 700 ^{o}C

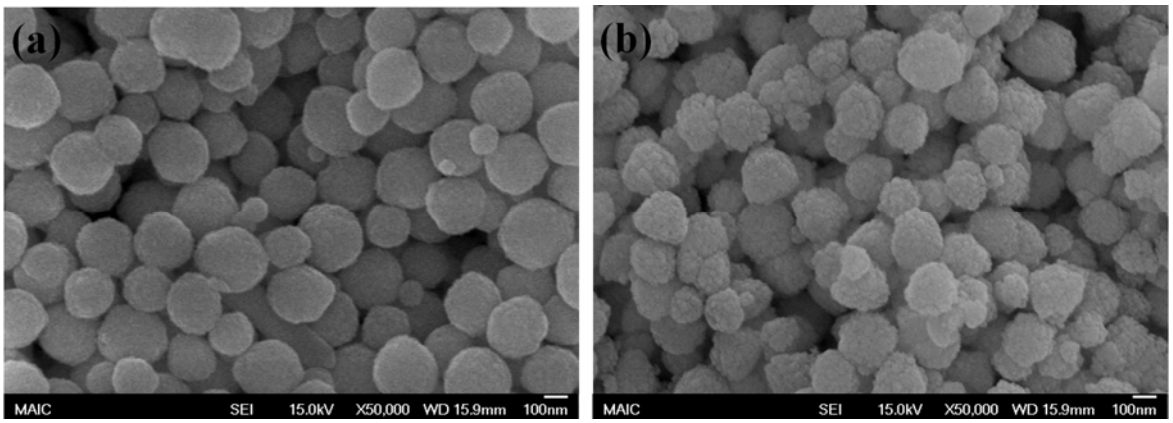

Figure 7-6. FESEM micrographs of (a) as-prepared particles of ceria abrasives and (b) ceria abrasives obtained from thermal decomposition at 700 ^{o}C

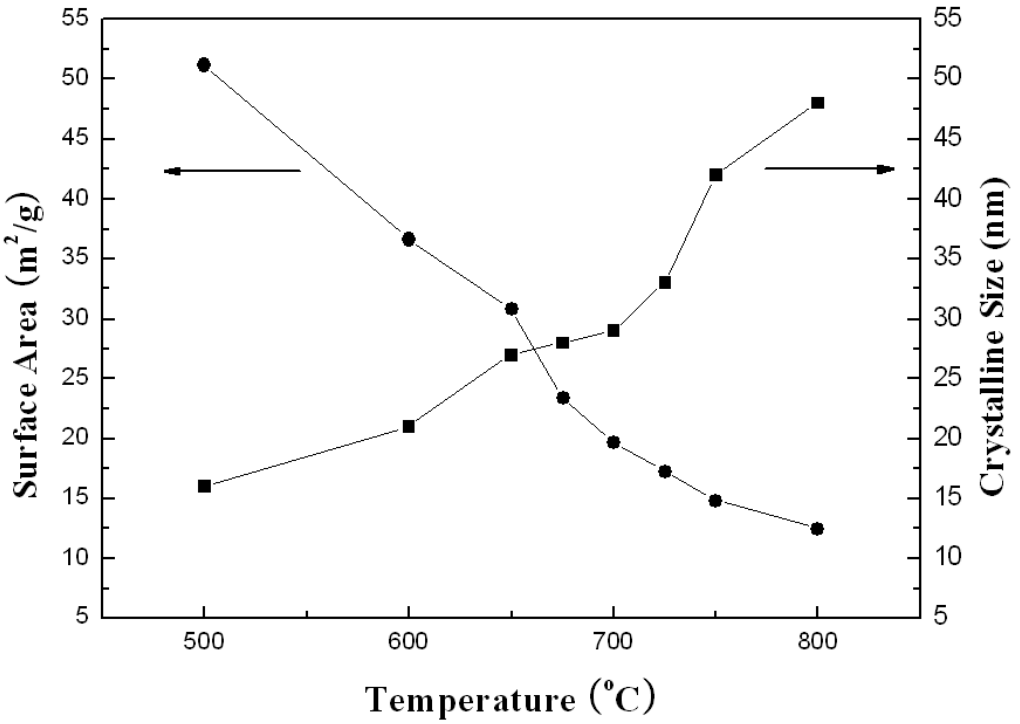

Figure 7-7. Relationship between surface area and crystalline size of ceria abrasives as a function of calcination temperature

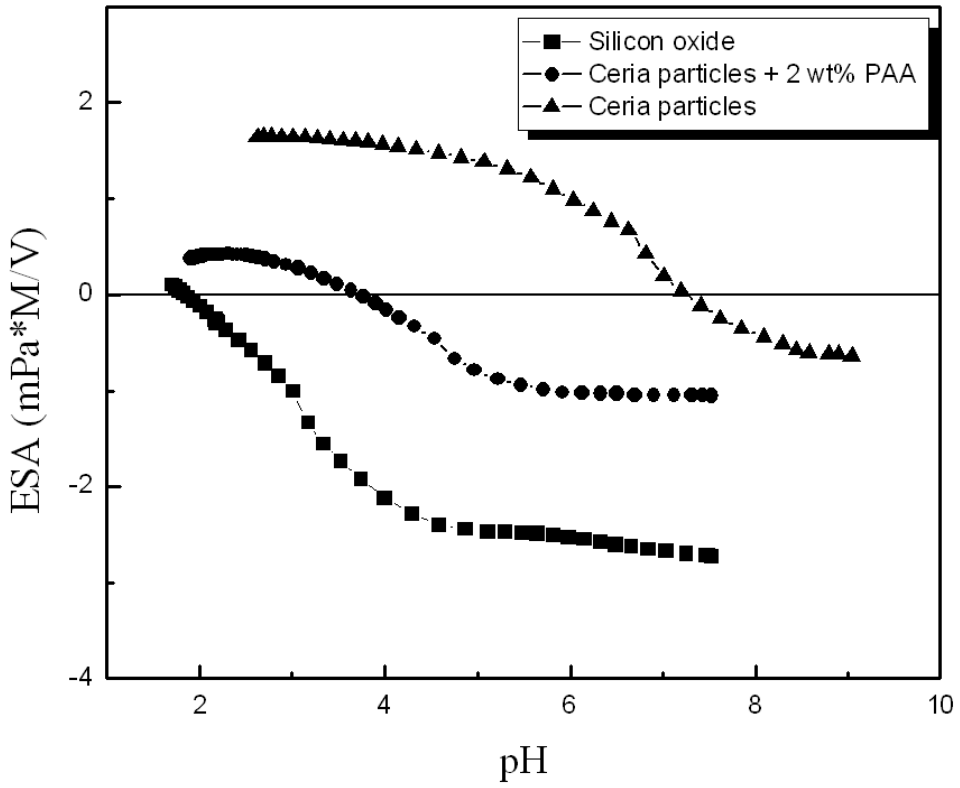

Figure 7-8. Electrokinetic behavior of silica, ceria and ceria with surface active agent added as a function of suspension pH

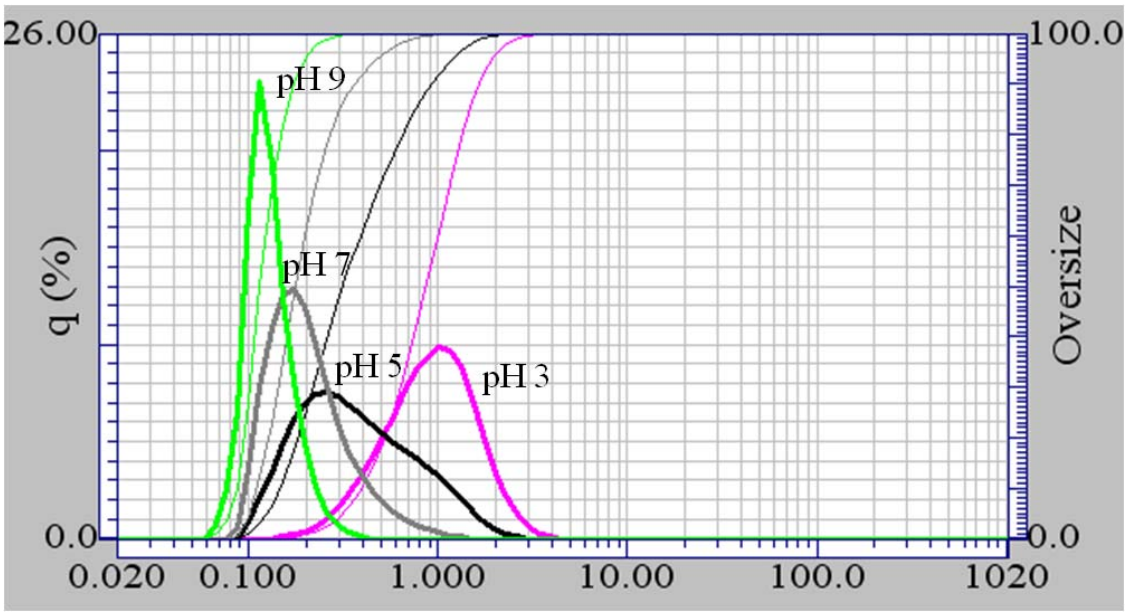

Figure 7-9. The changes in particle size distribution of ceria-based solvent as a function of suspension pH

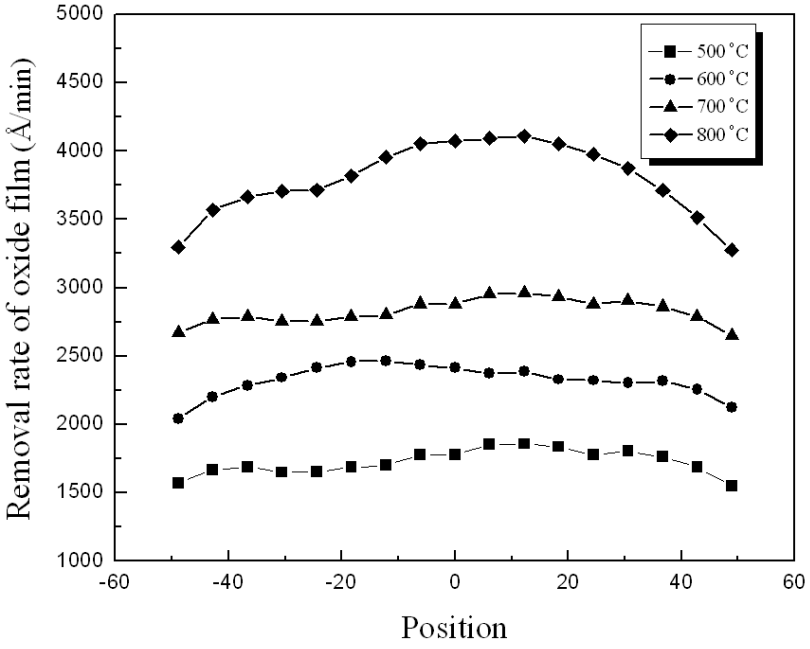

(a)

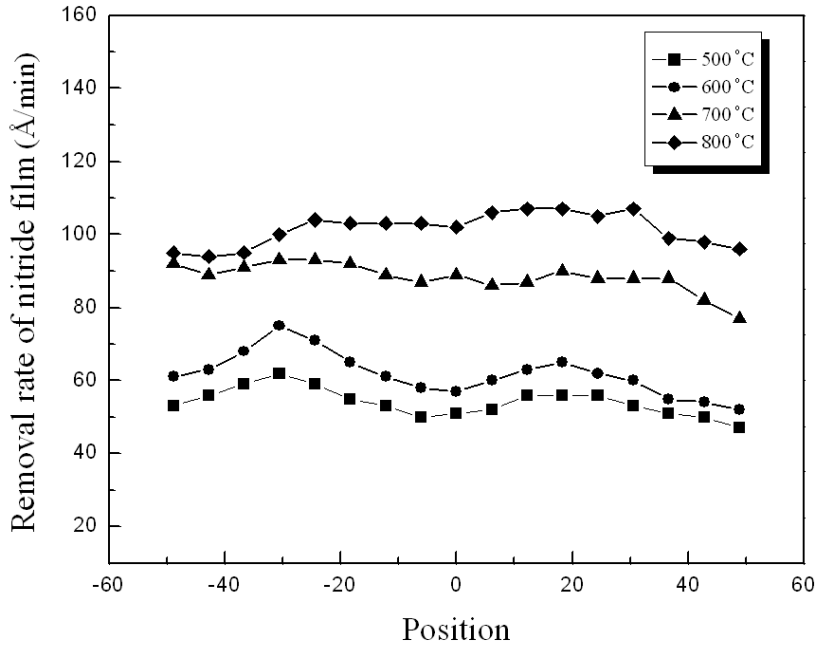

(b)

Figure 7-10. The CMP evaluation for removal rate of oxide and nitride films as a function of calcination temperature

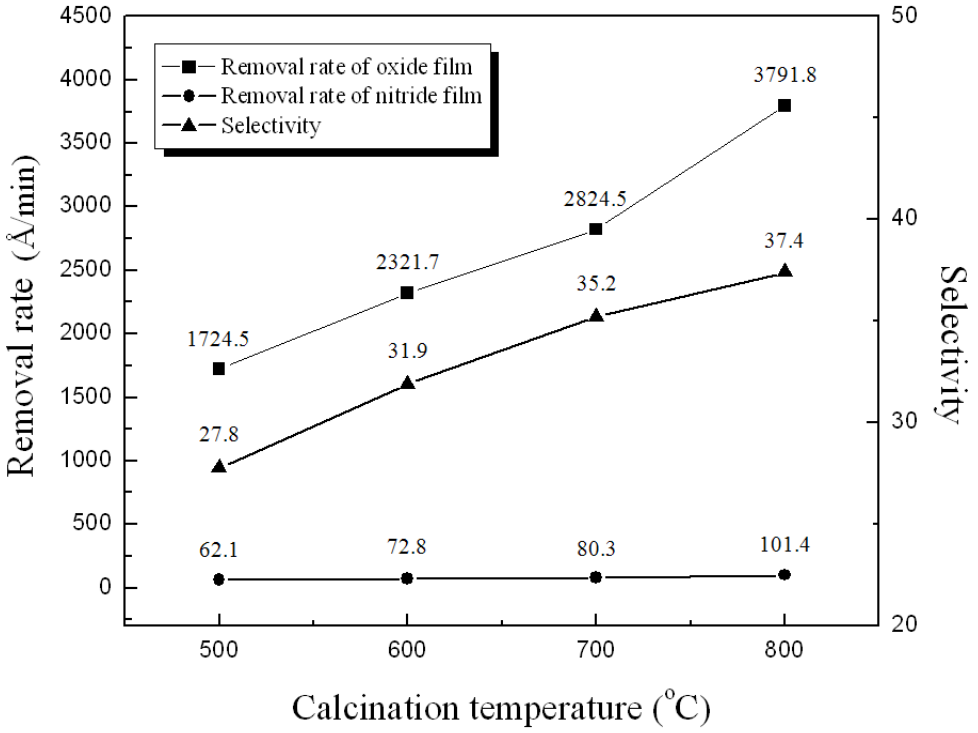

Figure 7-11. Results of CMP field evaluation for removal rate and selectivity

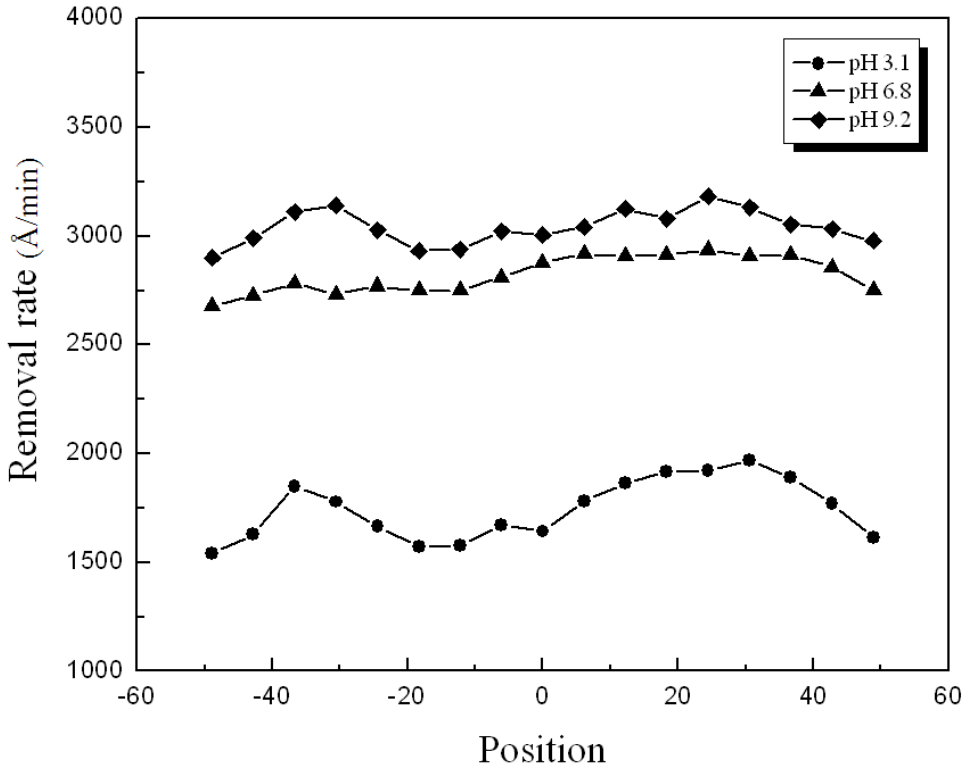

Figure 7-12. The CMP evaluation for removal rate of silicon oxide wafer as a function of suspension pH

Table 7-1. Dielectric constants of mixed solvent, zeta potentials and morphologies of cerium carbonate compounds with the ratio of ethanol to water[22,23]

Ratio of ethanol to water at 20 °C	Dielectric constant of solvent at 20 °C	Zeta potential at 20 °C	Morphology
0	80.01	18.3	Spindle and spherical
1	56.53	11.2	Spindle and spherical
3	49.50	4.8	Spherical
5	42.46	3.6	Spherical

CHAPTER 8
A COMPARISION OF CMP PERFORMANCE IN THE CERIA ABRASIVES SYNTHESIZED VIA VARIOUS METHODS

Introduction

As shown in previous chapters, there are many methods to manufacture ceria particles. Most of methods introduced in this paper give rise to spherical ceria particles because it is thought that slurries formulated using such particles will be required for future CMP technology in order to meet the ever more challenging defectivity requirements. On the other hands, certain methods lead to ceria particles with irregular shape due to its cubic crystalline structure. However, there is no substantive evidence that the round particles are superior to the irregular particles in effective CMP slurry. Although the slurries containing spherical particles are promoting, it has not been possible to convincingly tie in morphology with removal rate or defectivity. In fact, surface chemistry or particle size distribution of ceria abrasives may appear to be more important than morphological properties considering the polishing mechanism for removal rate of oxide and nitride layer.

In this chapter, I intend to investigate the effects of abrasive material properties on polishing removal rate and wafer defectivity by using different kinds of ceria particles obtained from previous chapters.

Materials and Methods

Sample Preparation

Preparation of ceria abrasives

Four types of ceria particles obtained from different methods, including solution growth method (hydrothermal method), grain control method (flux method), core-shell composition method (surface-induced precipitation method), and solid state method

(thermal decomposition method), were used as abrasives for ceria-based slurry at pH 6 ~ 7. The size ceria abrasive with diameter of 140 ~ 170 nm was controlled by adjust the reaction parameters of each method.

Preparation of ceria-based slurries

Different ceria-based slurries were formulated by dispersing abrasives each with different primary particle size in DI water containing an anionic organic polymer (Poly acrylic acid, PAA; Mw 4000, LG Chem.) as dispersant. 2 wt% of PAA based on the total weight of the ceria abrasives was added. For each slurry, pH was adjusted to 6 ~ 7 by adding ammonium hydroxide (NH_4OH). The solid loading of ceria abrasives was fixed to 2.0 wt%.

CMP tools and consumables

Silicon dioxide film of 2 μm thick was grown on a 5-in. p-type silicon substrates with (001) orientation by plasma enhanced chemical vapor deposition (PECVD). The silicon nitride films were deposited by using low-pressure chemical vapor deposition (LPCVD). Polishing tests were performed on a rotary type CMP machine (GNP POLI 400, G&P technology) for one minute with each of the ceria-based slurries. IC 1000/SUBA IV stacked pads (supplied by Rodel Inc.) were utilized as CMP pads. The downforce was 4 psi and the rotation speed between the pad and the wafer was 100 rpm. The slurry flow rate was 100 mL/min.

Characterization

Abrasives

The crystal structure and grain size was identified by x-ray diffraction (XRD) using CuKα radiation. The grain size was estimated by the Scherrer equation according to the formula $D = 0.9 \lambda / (\beta \cos \theta)$, where D is the grain size, λ is the wavelength of x-rays, β

is the half-width of the diffraction peaks, and θ is the diffraction angle. The broadening of the reflection from the (111) plane was used to calculate the grain size. The morphology and size of the precipitate particles were examined by field emission scanning electron microscope (FESEM). The average primary particle size was calculated by measuring ca. 100 particles from FESEM micrographs. The specific surface area (SSA) of the ceria abrasives was determined by Brunauer-Emmett-Teller (BET) method using nitrogen adsorption/desorption at 77 K.

Ceria-based slurry

The abrasive size distribution of slurry was measured using light scattering method (UPA 150, Microtrac Inc.).

CMP performance

The film thickness on the wafers before and after CMP was measured using spectroscopic reflectometry (Nanospec 6100, Nanometrics) to calculate the removal rate. Defectivity of wafer after CMP was measured by using a KLA-Tencor® puma 91XX. This system uses a UV/visible light source to illuminate defect types. The average polishing data for removal rate was carried by performing the same tests more than three times in order to support the validity of the results from the statistical viewpoint.

Results and Discussion

Comparison in Polishing Removal Rate

Fig. 8-1 shows FESEM micrographs of the four types of ceria abrasives prepared from various methods as described in Table 8-1. The size of ceria particles was controlled by adjusting the reaction parameters of each method. As shown in Fig. 8-1, all abrasives except sample A have a round shape with diameter of 140 ~ 170. The sample A shows irregular morphology possessing shape edges and wide size variations

between each particle. In the case of sample C, the grain size of particles could be not measured by Scherrer equation because the particles compose of core/shell composites.

Table 8-2 summarizes the quantitative results of removal rate and WIWNU of oxide wafer after CMP process. For oxide removal rate, the slurries including sample B and D showed higher removal rare than other slurries. This result attributes to the fact that the ceria particles obtained from solid state method are brittle and easily broken-down by applied pressure and shear force during CMP process. As mentioned previously, the physicochemical reaction by Si-O-Ce bonding leads to the high removal rate of oxide film. At this point, it is thought that the broken fragments of ceria abrasives promote more Si-O-Ce bonds onto oxide film and increase contact area between abrasives and wafer surface. Thus, the oxide layer can be more rapidly removed by the brittle behavior of ceria abrasives. In chapter 5 and 7, they were commonly synthesized via thermal pyrolysis (calcination), leading to softness and high chemical reactivity to oxide film. Moreover, using FESEM results in Fig. 4-12 and 5-7, we could confirm that the ceria abrasives obtained from solid state method are easily broken-down by applied pressure and shear force during polishing, while the ceria abrasives synthesized from solution state method are less brittle and don't fracture upon applied pressure during polishing. Therefore, it was found that the removal rate of oxide film is dependent on synthesis method of ceria abrasives. It seems that the brittle behavior of ceria abrasives plays an important role in the physicochemical reaction mechanism for oxide CMP.

Comparison in WIWNU

For WIWNU, the slurries including sample C and D showed a lower WIWNU for the oxide film. This result is related to particle size distribution of the slurry. Fig. 8-2

shows the particle size distribution of the ceria abrasives used in this experiment. Although the size of four types of ceria abrasives were similarly controlled to diameter of 140 ~ 170 nm, there was difference in the particle size distribution of slurries as shown in Fig. 8-1 and 8-2. Sample C and D have a narrow particles size distribution, while sample A and B have a relatively boarder particle size distribution. The slurry with narrow particle size distribution and uniform particle size can uniformly impose interaction force of ceria abrasives over the whole wafer surface. This can enhance wafer uniformity after CMP process. On the other hand, the broader particle size distribution of large abrasives can cause different removal rates between the center and the edge of the wafer due to their limited mobility on the wafer surface. This result is also consistent with the WIWNU results of chapter 4 and 5. Therefore, uniformity of ceria abrasives and narrow particle size distribution should be optimized to realize the global planarization.

Abrasive Effects on Defectivity

Fig. 8-3 shows a comparison on total scratch defect after polishing in CMP process using various ceria abrasives. As shown in Fig. 8-3, the ceria abrasives obtained from solid state method exhibit superior defect performance over the ceria abrasives prepared from solution state method. It seems that this result is related to the morphological properties and crystalline structure of ceria abrasives. As mentioned previously, the ceria-base slurry with non-uniform particle size distribution not only created surface deformation but also changed the polishing removal rate. For solution growth ceria, the sharp edge of the abrasives can be regarded as another factor for roughness of wafer. The film abraded by the sharp edge has a higher local pressure to generate more friction force during polishing. This behavior can induce serious defects

by pit formation on the wafer surface. Moreover, the ceria abrasives are not easily broken and don't fracture upon applied pressure during CMP process. This means that the particles have a higher hardness leading to the scratch defects on the wafer surface. On the other hand, the abrasives obtained from solid state method have brittle properties on wafer surface to be polished. It is thought that this brittle behavior induces the reduction in the number of scratch defect on wafer surface. Therefore, it seems that surface defectivity of oxide film is related to the mechanical factors (crystalline structure) and morphological properties of ceria abrasives used during CMP.

Conclusion

To compare the polishing properties of ceria abrasives according to synthesis method, CMP tests for four types of ceria-based slurry were preformed. The synthesis methods were classified by solution state method, including hydrothermal method and surface-induced precipitation method, and solid state method, including thermal decomposition method and flux method. For oxide removal rate, the result showed that the brittle behavior of ceria abrasives plays an important role in the physicochemical reaction mechanism for oxide CMP. This brittle behavior also affected the reduction in defectivity of wafer surface. The result for WIWNU showed that the slurry with narrow particle size distribution and uniform particle size help to improve wafer uniformity after CMP process.

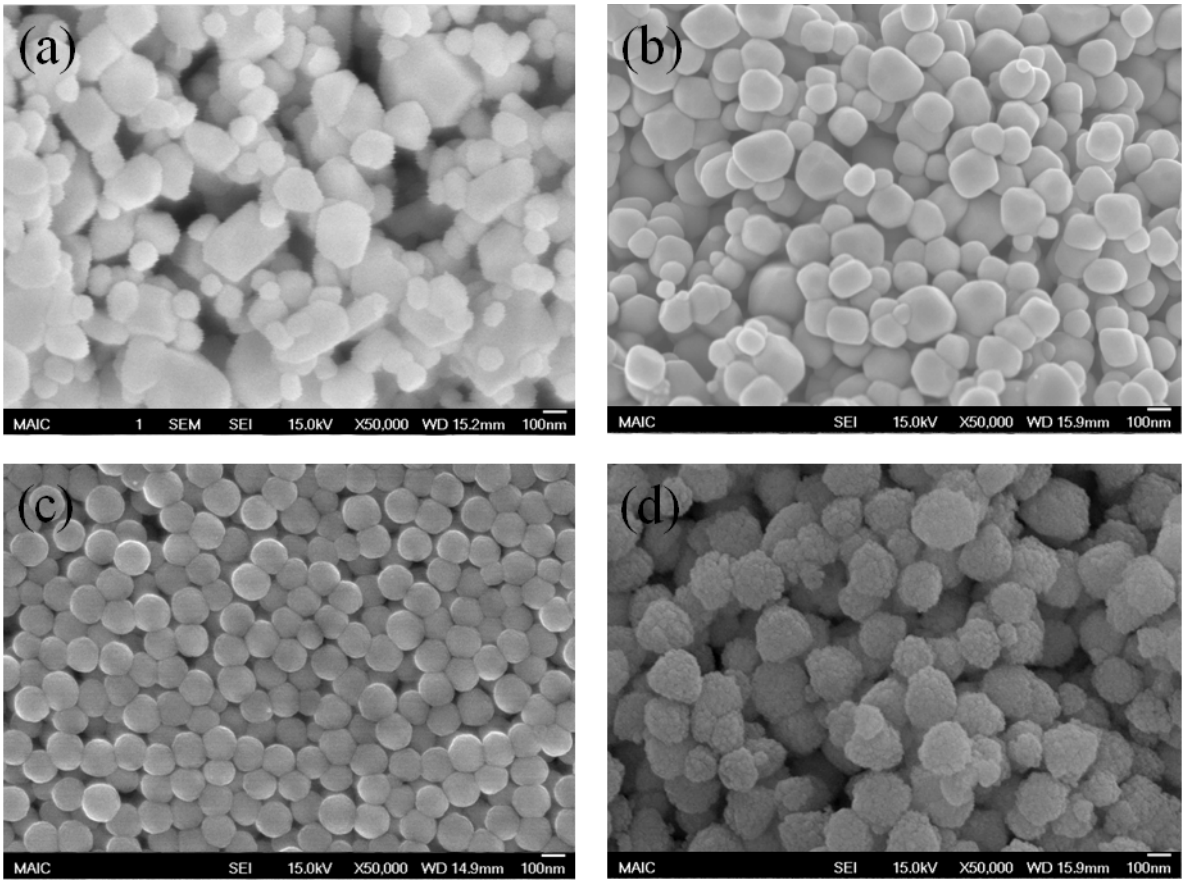

Figure 8-1. FESEM micrographs of various kinds of spherical ceria abrasives synthesized by variety methods; (a) hydrothermal method, (b) flux method, (c) surface-induced precipitation method, and (d) thermal decomposition

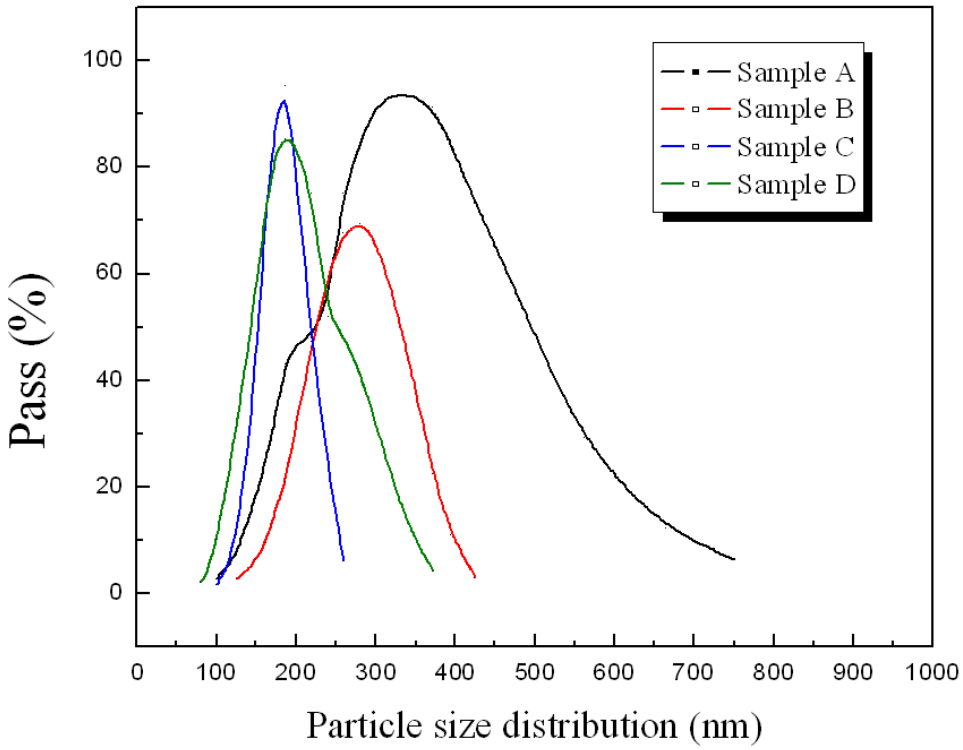

Figure 8-2. Particle size distribution of ceria-based slurries

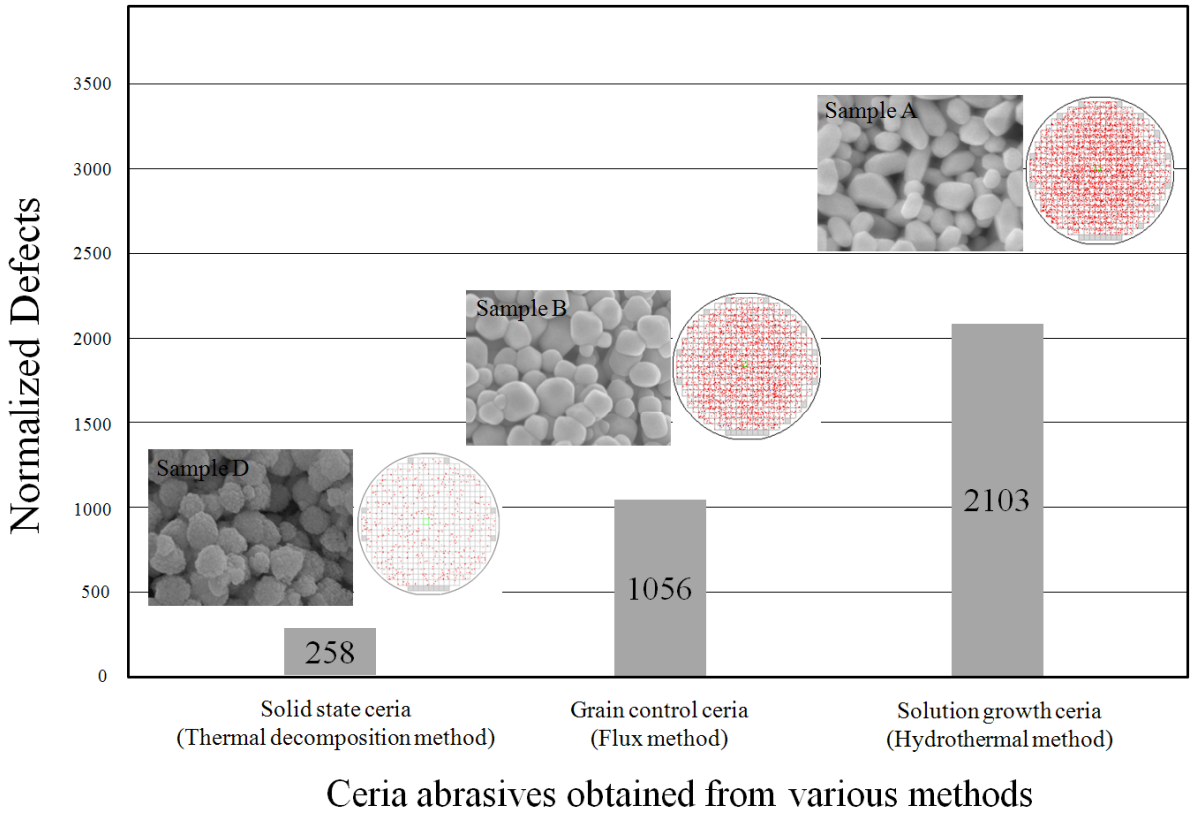

Figure 8-3. Comparison of different ceria abrasives on surface defectivity

Table 8-1. Comparison of ceria abrasives used in this study

Sample	Synthesis method	Primary particle Size (SEM, nm)	Grain size (XRD, nm)	Slurry mean size (UPA, nm)	Surface area (m^2/g)
A	Hydrothermal (Solution state reaction)	163	45	326	11.14
B	Flux (Solid state reaction)	166	43	278	14.06
C	Precipitation coating (Solution state reaction)	146	-	198	37.63
D	thermal decomposition (Solid state reaction)	158	29	242	22.02

Table 8-2. The results of the CMP evaluation

Samples	Oxide removal rate (Å/min)	WIWNU of oxide film (%)
Slurry A	2369.4	10.1
Slurry B	3390.9	11.0
Slurry C	245.8	0.765
Slurry D	2824.5	6.02

CHAPTER 9
CONCLUSIONS

Ceria abrasive particles are becoming more widely used in a variety of CMP applications for multilevel IC manufacture. However, only a few years ago, most facilities traditionally used silica particles for all IC applications, mainly to remove deposited oxide topography for bulk oxide removal for ILD and STI applications. Chemical additives in CMP slurries were formulated with fumed or colloidal silica particles in order to improve the removal selectivity in STI CMP. As the device design rule decreased, ceria particles have been used instead of silica particles, since ceria-based slurries address many of the issues resulting from the use of silica-based slurries. Recently, the ceria-based slurries are being introduced not only in ILD but also STI CMP step in order to improve removal rate, chip uniformity, and selectivity.

In spite of its advantages, ceria particles usually induce higher scratch level than silica particles due to its cubic crystalline structure, irregular shape, and poor dispersion stability in slurry. Especially, flash memory devices such as NAND or NOR type are more sensitive to CMP scratch than conventional DRAM devices because of the lack of their redundancy. Therefore, it is very important in CMP process to reduce CMP scratch level and increase device yield. Additionally, although an understanding of nature of mechanical interaction between ceria particles and substrates to be polished is essential to maintain the strict process requirements for manufacturing current and future generation IC devices, the fundamental knowledge of its mechanical behaviors on planarization performance is not clear.

To accomplish this aim, this research developed novel ceria particles for CMP abrasives and introduced novel technology to synthesize these particles. Furthermore,

this article was intended to provide a fundamental basis for the directions of ceria particles needed for present-day and next generation CMP technologies.

Solution Growth Abrasives

Well-crystalline ceria particles were synthesized by heating peptized ceria sol as precursor under hydrothermal conditions. The morphology and the crystallites size of ceria particles were controlled by varying the dielectric property of solvent used in preparation of the ceria precursor. The synthesized particles exhibit cubic fluorite structure with size ranged from 20 to 400 nm without the formation of hard aggregates. In this work, the relationships between dielectric property of the solvent and particle size were discussed in terms of the supersaturation of solute. In addition, the influences of precipitation participating anions (OH^-) and acidic hydrothermal medium on crystallites size of ceria particles were investigated.

For CMP performance evaluation, the effects of single crystalline ceria abrasives in CMP slurries were investigated for silicon dioxide and silicon nitride CMP process. The size of ceria abrasives was controlled by varying hydrothermal reaction conditions. Polishing removal rate was measured with four slurries, with different mean primary particle size of 62 nm, 116 nm, 163 nm and 232 nm. The polishing results showed that the single crystalline ceria abrasives were not easily broken-down by mechanical force during CMP process. It was found that the removal rate of oxide and nitride film strongly depend upon abrasive size, whereas the surface uniformity deteriorates as abrasive size increases. The observed polishing results confirmed that there exists an optimum abrasive size (163 nm) for maximum removal selectivity between oxide and nitride films. The polishing behavior of the single crystalline ceria abrasives was discussed in terms of morphological properties of the abrasive particle.

Grain Control Abrasives

The effects of spherical ceria abrasives in CMP slurries were investigated on silicon dioxide and silicon nitride polishing process. The ceria abrasives were prepared by the flux method, using potassium hydroxide as the grain growth accelerator. The primary particle size of the ceria abrasives was controlled in the range of ~ 84 - 417 nm by changing the concentration of potassium hydroxide and the calcination temperature without mechanical milling process. The removal rate of silicon dioxide film strongly depended upon abrasive size up to an optimum abrasive size (295 nm) after CMP process. However, the surface uniformity deteriorated as abrasive size increases. The observed polishing results confirmed that there exists an optimum abrasive size (295 nm) for maximum removal selectivity between oxide and nitride films. In this study, polishing behaviors of the spherical ceria abrasives were discussed in terms of morphological characteristics.

Core/shell Composite Abrasives

Monodispersed ceria coated silica particles were prepared using a peptized ceria sol as coating precursor. The ceria coating precursor was synthesized by alkoxide method, which employs ethanol as solvent. The resulting particles were characterized with scanning electron microscopy (SEM), transmission electron microscopy (TEM), X-ray photoelectron spectroscopy (XPS), X-ray diffraction (XRD) and zeta potential measurements. It was found that crystalline ceria coating was formed on the surface of silica particles at temperature of 60 ^{o}C without requirement for the post-heat treatment. The thickness of ceria coating was controlled by changing the concentration of the coating precursor. The influence of solution pH on the formation of ceria coating was investigated in terms of electrostatic attraction mechanism. The apparent surface

coverage was estimated using an isoelectric point (IEP) data. In this study, the resultant particles were used as CMP abrasives for ceria-based slurry to investigate the effects of the ceria coated silica particles on polishing performance during oxide CMP. The primary particle size was controlled about 146 nm without mechanical milling process by depositing the ceria coating on the surface of colloidal silica particles with size 135 nm. The removal rate of silicon dioxide film strongly depended upon suspension pH. With increasing suspension pH, the removal rate of silica film decreased. On the other hand, surface uniformity deteriorated as the suspension pH decreases. These polishing behaviors were related to electrophoretic mobility of abrasives for silica film to be polished, since surface charge of the abrasives can be changed by suspension pH. Thus, it means that absorption/repulsion behavior between abrasives and materials to be polished plays an important role in polishing performance during CMP process. Additionally, the removal rate of silica film increased with increasing down pressure in terms of mechanical aspect for CMP condition.

Solid State Abrasives

The ceria abrasives were developed via two-step procedure; simple precipitation method using mixed solvent and thermal decomposition method using spherical cerium carbonate compounds. In the first step, spherical cerium carbonate compounds were synthesized by using mixed solvent of alcohol and water. The obtained results indicated that physicochemical solvent properties had a significant effect on the crystalline phase, microstructures and morphological properties of the resultant particles. FESEM results revealed the morphology of cerium carbonates could be changed by the type of solvent. In this experiment, the particles obtained from pure water were composed of oval-like particles with the size of 300 ~ 500 nm. In contrast, the particles prepared by using

alcohols had a spherical shape with uniform size distribution. FESEM analysis also showed that the size of the cerium carbonates increased as the number of carbon in alcohol used as mixed solvent increased. Moreover, the size of the precipitants decreased with the increase in the ratio of ethanol to water. In the second step, spherical ceria abrasives were prepared by thermal decomposition of the synthesized spherical cerium carbonates at 700 ^{o}C. XRD result revealed that the cerium carbonates were completely transformed into a pure crystalline cerium oxide at 700 ^{o}C. From FESEM analysis, ceria particles after calcination process exhibited spherical shape regardless of the crystallization to oxide by heat treatment. On the other hand, the surface of particles was rougher due to emission of the resultant gases such as carbon dioxide, ammonia, nitride, etc. BET and XRD results showed that the surface area of ceria abrasives was reduced and the crystalline size was enhanced with increasing in calcination temperature.

In CMP test, the effect of the calcination temperature on the physical properties of synthesized ceria particles and suspension pH on CMP performance were investigated. The CMP results revealed that the ceria-based slurry had a higher removal rate for the silica and nitride wafer as the calcination temperature increased. Moreover, the removal selectivity increased as calcination temperature increased. For suspension pH, the ceria abrasives dispersed in neutral and alkaline conditions had high removal rates for silicon dioxide layer because the surface of the oxide film is soluble in alkaline and neutral pH solutions. In addition, the surface uniformity deteriorated at acidic pH solution because of a broader particle size distribution of the ceria abrasives in the slurry and the presence of agglomerated abrasives. Furthermore, the surface uniformity deteriorated

with acidic pH solution due to inhomogeneous distribution leading to local frictional interactions of the agglomerated particles.

Comparison of Polishing Behavior

To compare the polishing properties of ceria abrasives according to synthesis method, CMP tests for four types of ceria-based slurry were preformed. The synthesis methods were classified by solution state method, including hydrothermal method and surface-induced precipitation method, and solid state method, including thermal decomposition method and flux method. For oxide removal rate, the result showed that the brittle behavior of ceria abrasives plays an important role in the physicochemical reaction mechanism for oxide CMP. This brittle behavior also affected the reduction in defectivity of wafer surface. The result for WIWNU showed that the slurry with narrow particle size distribution and uniform particle size help to improve wafer uniformity after CMP process.

APPENDIX A
DIELECTRIC CONSTANTS OF MIXED SOLUTION OF SOME ORGANIC SOLVENT AND WATER AT ROOM TEMPERATURE

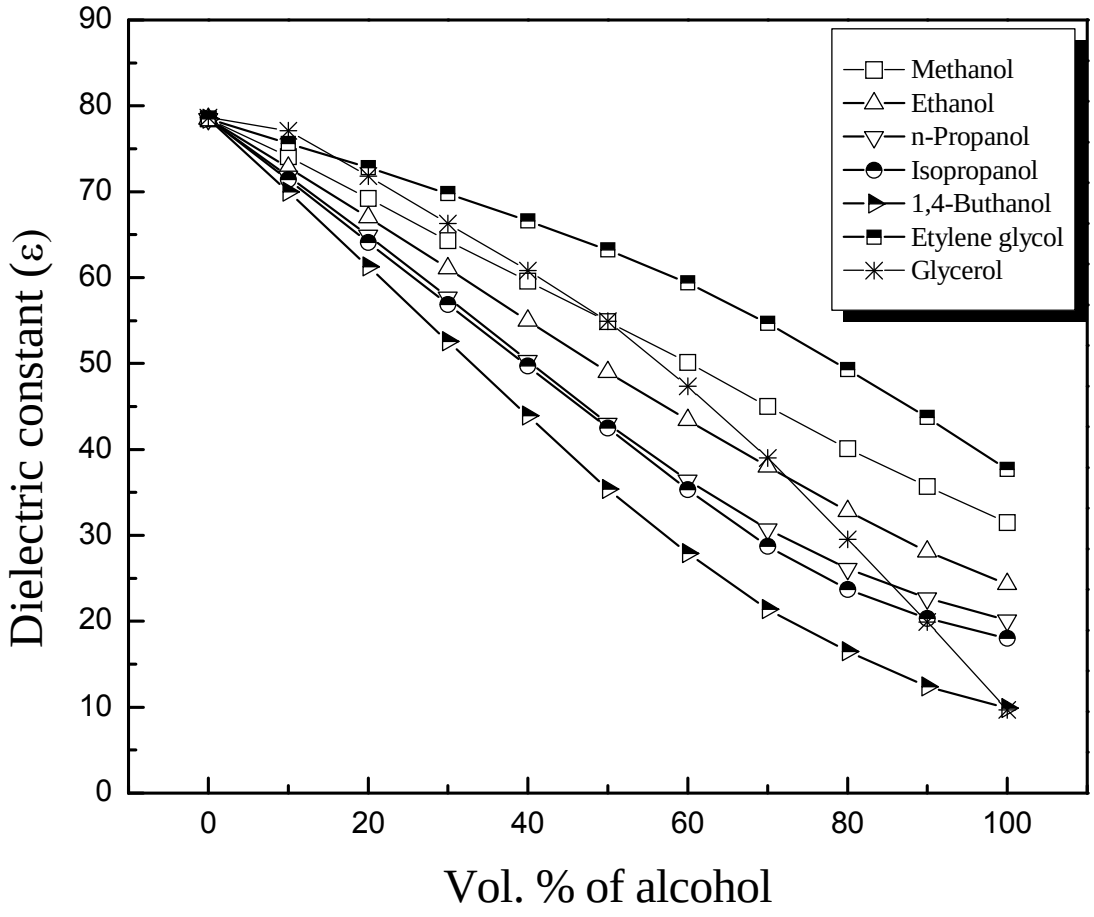

Figure A-1. The dependence of dielectric constant on the composition of different alcohols and water.[68]

LIST OF REFERENCES

1. J. M. Steigerwald, S. P. Murarka, and R. J. Gutmann, *Chemical Mechanical Planarization of Microelectric Materials*, John Wiley & Sons. INC., New York (1997).

2. C. F. Lin, W. T. Tseng, and M. S. Feng, *J. Electrochem. Soc*., **146**, 1984 (1999).

3. K. D. Beyer, *IBM Micronews*, **5**, 40 (1999).

4. W. Choi, J. Abiade, S. Lee, and R. K. Singh, *J. Electrochem. Soc*., **151(8)**, G512 (2004).

5. H. -G. Kang, H. -S. Park, U. Paik, T. Katoh, and J. -G. Park, *J. Mater. Res.,* **22(3)**, 777 (2007).

6. J. H. So, D. J. Lee, Y.-J. Cho, M.-H, Ahn, I.-Y. Lee, S.-J. Jeon, S. Kim, and S.-M. Yang, in *Proceedings of the Korean CMP-UGM Conference*, The Korean Institute of Electrical and Electronic Material Engineers, Paper 2 (2005).

7. S. –K. Kim, Y. –H. Kim, U. Paik, T. Katoh, and J. -G. Park, *J. Electrochem. Soc.,* **154(7)**, H642 (2007).

8. P. Janos, M. Petrak, Preparation of ceria-based polishing powders from carbonates, J. Mater. Sci. 26 (1991) 4062-4066.

9. Y. N. Prasad and S. Ramanathan, *J. Electrochem. Soc*., **9(12)**, G337 (1999).

10. R. K. Singh, S. M. Lee, K. S. Choi, G. B. Basim, W. Choi, Z. Chen, and B. M. Moudgil, *Mater. Res. Bull*., **27**, 752 (2002).

11. M. J. Cumbo, D. Fairhurst, S. D. Jacobs, and B. E. Puchebner, *Applied Optics*, **34**, 3743 (1995).

12. L.M. Cook, J. Non-Cryst. Solids, **120**, 152 (1990).

13. R. Jairath, M. Desai, M. Stell, R. Tolles, and D. Scherber-Brewer, *Mater. Res. Soc. Symp. Proc.*, **337**, 121(1994).

14. Y. Xie and B. Bhushan, *Wear*, **200**, 281 (1996).

15. T. Izumitani, *Polishing lapping and diamond grinding of optical glasses* in *Treaise on Material Science and Technology,* M. Tomozawa and R. Dorrmus, Editors, p. 115, Academic Press, New York (1979).

16. U. Mahajan, M. Bielmann, and R. K. Singh, *Mater. Res. Soc. Symp. Proc*., **566**, 27 **(**1999).

17. M. Bielmann, Masters Thesis, University of Florida, Gainesville, FL (1998).

18. S. D. Kim, I. S. Hwang, H. M. Park, J. K. Rhee, and C. W. Nam, *J. Vac. Sci. Technol. B,* **20**, 918 (2002).

19. J. W. Lee, B. U. Yoon, S. Hah, and J. T. Moon, Mater. *Res. Soc. Symp. Proc.,* **671**, M5.3.1 (2001).

20. O. Kubaschewski, E. Evans, and C. Alcock, *Metallurgical Thermochemistry*, Pergamon Press, Oxford (1967).

21. K. Osseo-Asare, *J. Electrochem. Soc*., **149**, G651 (2002).

22. M. Jiang, N. O. Wood, and R. Komanduri, *J. Eng. Mater. Technol.,* **120**, 30 (1998).

23. H. Zhu, A. B. Tessarotto, V. A. Greenhut, D. E. Niesz, and R. Sabia, *Ceram. Trans*., **102**, 259 (1999).

24. P. W. Carterz and T. P. Johns, *Electrochem Solid-State Lett.,* **8(8)**, G218 (2005).

25. L. Bergstrom and E. Bostedt, *Colloids Surf*., **49**, 183 (1990).

26. S. Mezzasalma and D. Baldovino, *J. Colloid Interface Sci*., **180**, 413 (1996).

27. C. Galassi, F. Bertoni, S. Ardizzone, and C. L. Bianchi, *J. Mater. Res*., **15**, 155 (2000).

28. E. Laarz, B. V. Zhmud, and L. Bergstrom, *J. Am. Ceram. Soc*., **83**, 2394 (2000).

29. S. K. Kim, S. Lee, U. Paik, T. Katoh, and J. G. Park, *J. Mater. Res.,* **18**, 2163 (2003).

30. W. G. America and S. V. Babu, *Electrochem. Solid-State Lett.,* **7**, G327 (2004).

31. L. Wang, W. M. Sigmund, and F. Aldinger, *J. Am. Ceram. Soc.,* **83**, 697 (2000).

32. A. Philipossian and M. Hanazono, Tribology and fluid dynamics characterization of cerium oxide slurries, *www.innovativeplanarization.com*. (2001).

33. S. K. Kim, P. H. Yoon, U. Paik, T. Katoh, and J. G. Park, *Jpn. J. Appl. Phys.,* **43**, 7427 (2004).

34. Y.Z. Hu, R.J. Gutmann, and T.P. Chow, *J. Electrochem. Soc.,* **145,** 3919 (1998).

35. S. D. Kim, I. S. Hwang, and H. M. Park, *J. Vac. Sci. Technol. B,* **20,** 918 (2002).

36. Y. Zhuang, D. King, T. Kido, and A. Philipossian, *Jpn. J. Appl. Phys.,* **44**, 30 (2005).

37. M. Jun, S. Atsushi, Y. Masato, H. Keizou, A. Toranosuke, and O. Yuuto, US patent 6615499 (2003).

38. H. G. Kang, T. Katoh, D. H. Kim, U. Paik, and J. G. Park, *Jpn. J. Appl. Phys.* **44**, 238

(2005).

39. M. Jun, S. Atsushi, Y. Masato, H. Keizou, A. Toranosuke, O. Yuuto, US patent 6615499 (2003).

40. Y. Masato, A. Toranosuke, T. Hiroki, K. Yasushi, M. Jun, T. Kiyohito, and O. Yuuto, US patent 6863700 (2005).

41. E. Remsen, S. Anjur, D. Boldrige, M. Kamiti, S. Li, T. Johns, and C. Dowell, J. Electrochem. Soc., **153(5)**, G453 (2006).

42. E. Matjevic, and W. Hsu, J. Colloid. Interface Sci., **118**, 506 (1987).

43. M. Hirano, Y. Fukuda, H. Iwata, y. Hotta, and M. Inagaki, J. Am. Ceram. Soc., **83**, 1287 (2000).

44. M. Hirano, and E. Kato, J. Am. Ceram. Soc., **79**, 777 (1996).

45. M. Hirano, and E. Kato, J. Am. Ceram. Soc., **82**, 786 (1999).

46. X. Chu, W. Chung, and L. D. Schmidt, J. Am. Ceram. Soc., **76**, 2115 (1993).

47. Y. Zhow, R. J. Philips, and J. A. Switzer, J. Am. Ceram. Soc., **78**, 981 (1995).

48. J. H. Park, H. Cui, S. H. Yi, and J. G. Park, J. Mater. Res., **23(12)**, 3323 (2008).

49. F. Preston, *J. Soc. Grass Technol*., **11**, 214, (1927).

50. J. Luo and D. A. Dornfeld, *IEEE Trans. Semicond. Manuf*., **14(2)**, 112 (2001).

51. J. Luo and D. A. Dornfeld, *IEEE Trans. Semicond. Manuf*., **16(1)**, 45 (2003).

52. Y. Moon, Ph.D. Thesis, University of California Berkeley, CA (1999).

53. T. Detzel, S. Hosali, A. Sethuraman, J. F. Wang, and L. Cook, in Proceedings of the CMP-MIC Conference, IMIC, 2007, p. 202.

54. G. B. Basim, J. J. Adler, U. Mahajan, R. K. Singh, and B. M. Moudgil, J. Electrochem. Soc., **147**, 3523 (2000).

55. T. L. Neo, E. S. Y. Shang, and C. M. Chong, in Proceedings of the International Symposium on Semiconductor Manufacturing, IEEE, 2001, p. 321.

56. Y. J. Seo, G. U. Kim, and W. S. Lee, Microelectron. Eng., **71**, 209 (2004).

57. D. Boning, B. Lee, C. Oji, D. Ouma, T. Park, T. Smith, and T. Tugbawa, Mater. *Res. Soc. Symp. Proc.,* **566**, P5.5, (2000).

58. R. J. Hunter, *Foundations of colloid science*, Oxford University Press, (2001).

59. I. D. Morrison and S. Ross, *Colloidal suspensions: Suspensions, Emulsions, and Foams*, John Wiley and Sins, New York, (2002).

60. H. Ota, M. Hachiya, Y. Ichiyasu,, and T. Kurenuma, *Hitachi Review*, **55(2)**, 78 (2006).

61. http://www.testwafer.com/PDF/skw1-200_spec.pdf

62. S.H. Lee, Z.L. Lu, S.V. Babu, and E. Matijevic, *J. Mater. Res*., **17(10)**, 2744 (2002). 2744-2749.

63. N.C. Wu, E.W. Shi, Y.Q. Zheng, W.J. Li, *J. Am. Ceram. Soc*., **85(10),** 2462 (2002).

64. H. K. Park, D. K. Kim, C. H. Kim, *J. Am. Ceram. Soc*., **80,** 743 (1997).

65. C. S. Fang and Y. W. Chen, Mater. Chem. Phys., **78,** 739 (2003).

66. M.Z.C. Hu, E. A. Payzaut, C.H. Byers, J. Colloid. Interface. Sci., **222** 20 (2000).

67. D. R. Lide, *CRC handbook of Chemistry and Physics, 87th edn*., CRC press, New York (2007).

68. G. Akerlof, *J. Am. Chem. Soc*., **54**, 4125 (1932).

69. J. N. Israelachvili, *Intermolecular and Surface Forces, 2nd edn*., Academic press, London (1992).

70. J. W. Mullin, *Crystallization, 3rd edn*., Butterworth-Heinemann, London (1992).

71. P. L. Chen and I. W. Chen, *J. Am. Ceram. Soc*., **76**, 1577 (1993).

72. J. G. Li, T. Ikegami, J. H. Lee, and T. Mori, *Acta Mater*., **49**, 419 (2001).

73. X. D. Zhou, W. Huebner, and H. U. Anderson, *Appl. Phys. Lett*., **80**, 3814 (2002).

74. N. C. Wu, E. W. Shi, Y. Q. Zheng, and W. J. Li, *J. Am. Ceram. Soc*., **85**, 2462 (2002).

75. T. Allen, Particle size measurement, Vol. 1, 5th ed., Chapman and Hall, New-York (1997).

76. Y.H. Kim, S.K. Kim, N.S. Kim, J.G. Park, and U. Paik, *Ultramicroscopy*, **108**, 1292 (2008).

77. A. R. West, *Solid State Chemistry and its Applications*, Wiley, New York (1995).

78. F. Bondioli, A. Bonamartini Corradi, C. Leonelli, and T. Manfredini, *Mater. Res. Bull*., **34**, 2159 (1999).

79. C. Kleinlogel and L. J. Gauckler, *Adv. Mater.*, **13(14)**, 1081 (2001).

80. H. Wakita and S. Kinoshita, *Bull. Chem. Soc. Jpn.*, **52(2)**, 428 (1979).

81. U. Mahajan, M. Belmann, and R.K. Singh, *Electrochem. Solid-State Lett.*, **2**, 46 (1999).

82. Y. X. Li, X. Z. Zhou, Y. Wang, and X. Z. You, *Mater. Lett.*, **58**, 245 (2004).

83. A. Yoshida, *The colloidal chemistry of silica, advance in chemistry series, vol. 234,* Oxford Univ. Press, Oxford (1994).

84. W. Stöber, A. Fink, and E. Bohn, *J. Colloid Interface Sci.*, **26**, 62 (1968).

85. X. Song, N. Jiang, Y. Li, D. Xu, and G. Qiu, *Mater. Chem. Phys.*, **110**, 128 (2008).

86. M. S. Kaliszewski and A. H. Heuer, *J. Am. Ceram. Soc.*, **73**, 1504 (1990).

87. T. Ikegami and N. Satio, *J. Ceram. Soc. jpn.*,**104**, 469 (1996).

88. N. Thromat, M. Gautier-Soyer, and G. Bordier, *Suf. Sci.*, **345**, 290 (1996).

89. S. Gavarini, M. J. Guittet, P. Trocellier, M. Gautier-Soyer, F. Carrot, and G. Matzen, *J. Nuclear Mater.*, **322**, 111 (2003).

90. B. Cheng, Li Zhao, J. Yu, and X. Zhao, *Mater. Res. Bull.*, **43**, 714 (2008).

91. J. Yu, Li Zhao, and B. Cheng, *Mater. Chem. Phys.*, **96**, 311 (2006).

92. X.D. Zhou, W. Huebner, and H. U. Anderson, *Appl. Phys. Lett.*, **80(20)**, 3814 (2002).

93. P. Suphantharida and K. Osseo-Asare, *J. Electrochem. Soc.*, **151(10)**, G658 (2004).

94. T. Murata, F.S. Howell, and K. Itatani, *J. Mater. Sci.*, **36**, 1277 (2001).

95. I. S. Seog, C. H. Kim, *J. Mater. Sci.*, **28**, 3277 (1993).

96. Y.T. Moon, H.K. Park, D.K. Kim, I.S. Seog, and C.H. Kim, *J. Am. Ceram. Soc.*, **78**, 1103 (1995).

97. R.J. Hunter, Foundation of colloid science, Vol. 1, p. 443, Clarendon press, Oxford, UK, 1987.

98. J.L. Look, C.F. Zukoski J. Colloid. Interface. Sci. **153** 469 (1992).

99. J.L. Look, C.F. Zukoski, J. Am. Ceram. Soc. **78** 21 (1995).

100. M.N. Rahaman, *Ceramic processing*, CRC Press, New York (2007).

101. V.A. Hackley and S.G. Malghan, *J. Mater. Sci.*, **29**, 4420 (1994).

102. J. Scheutjens and G. J. Fleer, *J. Phys. Chem.*, **83,** 1619 (1979).

BIOGRAPHICAL SKETCH

Oh, Myoung Hwan was born in Suwon, South Korea. In February of 2001, he received Bachelor of Engineering from chemical engineering of Korea University in Seoul, South Korea. He started his graduate study at Korea University in March of 2001, where he pursued Master of Engineering in chemical engineering under the advisory of Professor Kwan-young Lee. In January of 2003, he joined as researcher at chemical mechanical planarization (CMP) team in LG Chem Research Park in Daejeon, South Korea, where he helped develop the ceria-based slurry for STI CMP.

He was accepted to the graduate program in the Department of Materials Science and Engineering (MSE) in August of 2007. He began pursuing his doctorate degree in MSE and joined Dr. Singh's research group in October 2007. His dissertation research focused on synthesis of ceramic powder for CMP slurry and its CMP performance. He graduated from University of Florida with a doctorate degree in MSE with electronic materials in December 2010.